



---

Profiling of target molecules of human astrocytes for selective transduction by  
the Adeno-associated virus variant AAV9P1

---

Amelie Bauer

Dissertation an der Fakultät für Biologie  
der Ludwig-Maximilians-Universität München

München, 15.07.2021

**Profiling of target molecules of human astrocytes for selective transduction by the Adeno-associated virus variant AAV9P1**

Dissertation at the Faculty of Biology, Ludwig Maximilian University Munich

Conducted at the Institute of Virology, Helmholtz Center Munich - German Research Center for Environmental Health, under supervision of Prof. Dr. Ruth Brack-Werner

Submitted by M. Sc. Amelie Bauer from Neuburg an der Donau

First reviewer: Prof. Dr. Ruth Brack-Werner

Second reviewer: Prof. Dr. Benedikt Grothe

Date of submission: 15.07.2021

Date of oral defense: 25.11.2021

# Table of Contents

1	Introduction.....	1
1.1	Glial cells .....	1
1.2	Astrocytes .....	1
1.2.1	Astrocyte subtypes and functions .....	1
1.2.2	Astrocytes in neuropathologies.....	4
1.2.3	Astrocytes as a therapy target.....	6
1.3	Adeno-associated viruses .....	7
1.3.1	Classification .....	7
1.3.2	Genome organization .....	8
1.3.3	Replication cycle .....	9
1.3.4	The cap proteins .....	13
1.3.5	Recombinant AAVs as viral vectors .....	14
1.3.5.1	Characteristics .....	14
1.3.5.2	Advantages of rAAVs as viral vectors .....	15
1.3.5.3	rAAV vectors as research tools.....	16
1.4	Selective astrocyte targeting with rAAV .....	18
1.4.1	rAAV9P1 – a vector for selective targeting of human astrocytes in cell culture.....	20
1.4.2	AAV9 .....	20
1.5	Aim of the thesis .....	22
2	Material and methods .....	23
2.1	Material.....	23
2.1.1	Consumables.....	23
2.1.2	Chemicals and solutions .....	24
2.1.3	Buffers and media.....	26
2.1.4	Kits and reagents .....	28
2.1.5	Oligonucleotides.....	29
2.1.6	Plasmids.....	30
2.1.7	Prokaryotic cells.....	32
2.1.8	Eukaryotic cells .....	33
2.1.9	Antibodies and staining agents .....	33
2.1.10	Software and online tools.....	34
2.2	Cell culture methods and rAAV-virology.....	34
2.2.1	Thawing and freezing of cells .....	34

2.2.2	Cultivation and passaging of cells (except HNSC.100 cells).....	35
2.2.3	Cultivation and passaging of HNSC.100 cells.....	35
2.2.4	Seeding and harvesting of cells .....	36
2.2.5	Differentiation of HNSC.100 .....	37
2.2.6	rAAV vector production by iodixanol gradient.....	37
2.2.7	Transduction with rAAV vectors.....	38
2.2.8	Cell treatment assays.....	39
2.2.9	CellTiter-Blue® (CTB) viability assay.....	39
2.2.10	<i>In vitro</i> rAAV-binding assay (rABA) .....	40
2.2.11	Fluorescence-activated cell sorting (FACS).....	40
2.3	Molecular biology methods .....	41
2.3.1	gDNA isolation .....	41
2.3.2	PCR.....	41
2.3.3	Quickchange PCR.....	41
2.3.4	Agarose gel electrophoresis .....	42
2.3.5	Ligation independent cloning (LIC) for sgRNA expression plasmids.....	42
2.3.6	Transformation of competent bacteria .....	43
2.3.7	Plasmid isolation.....	44
2.3.8	Sanger sequencing.....	44
2.3.9	rAAV lysis .....	44
2.3.10	RNA isolation and complementary DNA (cDNA) synthesis .....	44
2.3.11	qRT-PCR .....	45
2.3.11.1	qRT-PCR from DNA .....	45
2.3.11.2	qRT-PCR from cDNA.....	45
2.3.12	Bicistronic acid (BCA) protein assay .....	46
2.3.13	SDS-PAGE and immunoblot analysis .....	46
2.3.14	CRISPR/Cas9 mediated gene targeting.....	48
2.3.14.1	sgRNA transfection .....	48
2.3.14.2	Limiting dilution and clonal expansion.....	48
2.3.14.3	Genotyping – Miseq .....	48
2.3.15	CRISPR/Cas9 knockout screen .....	50
2.3.15.1	Lentivirus production .....	50
2.3.15.2	Generation of U251MG-Cas9 stable cell line .....	51
2.3.15.3	Lentivirus sgRNA library titration .....	51

2.3.15.4	Generation of U251MG-Cas9-GeCKO cell pool .....	51
2.3.15.5	CRISPR/Cas9 screen .....	52
2.4	<i>In silico</i> modelling and alignments.....	54
2.5	Transmission electron microscopy .....	54
2.6	Statistical analysis .....	54
3	Results .....	55
3.1	rAAV9P1 transduces human astrocytic cell lines more efficiently than rAAV9 and more selectively than rAAV2 .....	55
3.2	The P1 peptide is located on an exposed position in the capsid .....	56
3.3	Subunits of RGD-binding integrins are differentially expressed on astrocytes and neurons .....	60
3.4	rAAV9P1 transduction is prevented by pharmacological inhibition of $\alpha\beta3$ and $\alpha\beta5$ or $\alpha\beta8$ .....	62
3.5	Genetic ablation of integrin subunits $\alpha$ , $\beta8$ , or $\beta3/\beta5$ decreases the transduction efficiency of rAAV9P1 .....	67
3.6	The P1 peptide is not sufficient for efficient astrocyte transduction.....	69
3.7	S263 is an essential amino acid residue for rAAV9P1 transduction.....	70
3.8	rAAV9P1 does not require HSPG, but N-linked glycans with terminal GAL for efficient astrocyte transduction.....	71
3.9	LamR and AAVR are involved in rAAV9P1 transduction .....	75
3.10	Identification of post-entry pathways in astrocytes relevant for rAAV9P1 transduction by genome-wide CRISPR/Cas9 knockout screening .....	76
4	Discussion .....	81
4.1	rAAV9P1 shows a unique transduction behavior for human astrocytes.....	81
4.2	The P1 peptide is likely to be involved in capsid-receptor interactions .....	82
4.3	RGD-binding integrin heterodimers $\alpha\beta8$ and $\alpha\beta3/\alpha\beta5$ are required for astrocyte transduction by rAAV9P1.....	83
4.4	rAAV9P1 requires the AAV9 receptors AAVR, LamR, and N-terminal GAL for efficient transduction.....	87
4.5	The unique rAAV9P1 receptor profile of human astrocytes .....	90
4.6	A CRISPR/Cas9 knockout screen reveals involvement of intra-cellular pathways for astrocyte transduction by rAAV9P1.....	91
4.7	Future perspectives for rAAV9P1.....	94
5	Summary.....	96
6	Appendix.....	97
6.1	Supplementary information.....	97
6.2	Equipment.....	98

7	Abbreviations.....	100
8	References.....	105
9	Acknowledgements.....	119
10	Publications.....	121
11	Eidesstattliche Erklärung.....	122

# 1 Introduction

## 1.1 Glial cells

When Rudolf Virchow published his famous manuscript *Cellular Pathology* in 1858, he was one of the first researchers to acknowledge that the central nervous system (CNS) consists of more parts than just nervous elements. He postulated that there is a tissue that "lies between the proper nervous parts, surrounds them and gives the whole its form and appearance" ([1] p. 316) and that it is impossible to study nervous elements without understanding this interstitial tissue. For the lack of comparable tissues in the body, he created the name *Neuroglia* (Greek for brain glue), implying that it resembles connective tissue and that its primary purpose is the passive physical connection and cohesion of neurons [1].

Today, it is widely known that the group of neuroglial cells consists of four main cell types that take over various crucial functions in the brain apart from just providing structural support to neurons. These main cell types are oligodendrocytes, oligodendrocyte progenitor cells (OPC, also known as NG-2 glia), microglia, and astrocytes. Recent studies suggest that the median proportion of glial cells to neurons in the whole brain is roughly equal to 1, with the distinct fractions of neurons and subtypes of glial cells differing spatially and temporally throughout the brain (reviewed in [2]). In general, NG-2 glia and microglia show high regional variability and are less numerous than oligodendrocytes and astrocytes. Oligodendrocytes are responsible for generating the insulating myelin sheath around the neuronal axons, allowing increased transmission speed of action potentials along the axon. NG2-glia maintain their proliferation ability in the adult brain with their main purpose of differentiating into oligodendrocytes. Microglia are CNS-resident macrophages with phagocytotic abilities that clear the CNS from pathogens, debris and, apoptotic cells while also involved in pruning aberrant synapses during brain development (reviewed in [2]). The fourth and arguably the most versatile type of cells in the CNS are astrocytes, which will be discussed in greater detail in the following paragraphs.

## 1.2 Astrocytes

### 1.2.1 Astrocyte subtypes and functions

Astrocytes, combined with oligodendrocytes, make up the biggest fraction of total glial cells. Although the determination of the total number of astrocytes in the human brain is challenging due to limited sample availability, the comparison of sections from rat and human cerebral cortex revealed a direct correlation between astrocyte to neuron ratio and the evolutionary stage of the organism [3–5]. Astrocytes are versatile both in morphology and functionality and can be divided into two basic

subgroups, protoplasmic and fibrillary astrocytes, with the common characteristic that they express the glial fibrillary acidic protein (GFAP) at varying levels [6, 7]. The most abundant astrocyte cell type in the human brain is the protoplasmic astrocyte that strikes with its unique bushy, star-shaped morphology. Protoplasmic astrocytes are present in the gray matter and form numerous, highly branched processes to connect with nearby neurons. In their connection to neuronal synapses, astrocyte distribution is organized in domains so that one neuronal cell and its synapses are only connected to one single astrocyte, and intercellular connection between astrocytes only happens at domain borders. Estimates claim that one protoplasmic astrocyte can cover up to two million synapses [8–11].

Astrocytes take over many crucial functions in the grey matter that exceed merely providing structural support to neurons and that are depicted in an overview in Figure 1-1. In general, astrocytes are responsible for maintaining environmental conditions for optimal neuronal functioning. They function as a relay station for nutrients taken up from blood vessels and transported to the neurons. Besides, lipid synthesis and glycolytic pathways are very active in astrocytes to provide nearby neurons with source materials for the production of neurotransmitters and energy sources [11]. Modulation of astrocyte metabolic activity by neural activity ensures neuronal nourishment even in states of high nutrient consumption and even hypoglycemia. Astrocytes are closely connected to blood vessels in the CNS and have been shown to induce vaso-contraction and dilatation by secretion of vaso-modulatory factors, thereby influencing blood flow in the CNS [12].

While astrocytes are crucial for the pure survival of neurons, they are also acknowledged to participate actively in different mechanisms involving synapses. Araque et al. were the first to postulate that astrocyte projections ensheath the synaptic space, including the pre- and post-synaptic neuronal terminals, and actively participate in synaptic transmission regulation. This concept is called the tripartite synapse [13]. It was shown that astrocytes closely regulate the ion concentration and pH in the synaptic space by shuttling protons, taking up potassium ions, and maintaining fluid homeostasis via a high molecule density of aquaporine 4 (AQP4) channels. Importantly, astrocytes take up glutamate from the synaptic space via specialized glutamate transporters and recycle it back to the presynaptic terminal as a glutamine intermediate, thereby avoiding neuronal excitotoxicity and providing the source material for excitatory and inhibitory neurotransmitter production [12, 14]. The rate of glutamate uptake is not consistent over time but is rather influenced by overall synaptic activity, allowing tightly regulated availability of neurotransmitters and reduced diffusion to neighboring synapses. Astrocytes can also be directly influenced by the presence of neurotransmitters and neuromodulators via specific receptors. These receptors activate an intracellular calcium signaling cascade that ultimately leads to the release of gliotransmitters such as adenosine triphosphate and D-serine. Gliotransmitter act on the synaptic terminals and can either strengthen or weaken the

respective synaptic connection, therefore influencing overall short and long-term synaptic plasticity [11, 15, 16].

The synaptic connection between neurons is dependent on astrocyte appearance during neural development, indicating the importance of astrocytes or astrocyte-derived factors for synapse development. For excitatory synapses, the time-dependent protein secretion for synapse generation is fairly well investigated and includes molecules for the structural and functional building of the synapses [17, 18]. To counteract excessive synapse formation and emphasize certain synaptic connections, astrocytes are also responsible for the pruning of synapses in an activity-dependent manner. They can either phagocytically eliminate synapses via phagocytic receptors or mark synapses for elimination by microglia cells by introducing complement component 1q (C1q) production in neuronal terminals and their subsequent opsonization [17–21]. The contribution of astrocytes to inhibitory synapse formation is not yet well characterized, but *ex vivo* cell culture experiments indicate astrocyte involvement [18]. Overall, active astrocytes play an important role in learning and memory formation by forming, strengthening, and stabilizing highly active synapses and eliminating weak or excessive synapses. This function is broadly conserved across evolution [22, 23]. Astrocytes also participate in the function of the blood-brain-barrier (BBB) in collaboration with pericytes and endothelial tight junctions, but their concrete contributions to BBB establishment and function are still under investigation [6, 12].

A widely researched function of astrocytes is their contribution to CNS protection after brain and spinal cord injury. Protoplasmic astrocytes react to a compromised CNS by switching to an activated state of astrogliosis, resulting in upregulation of GFAP, hypertrophy of processes, and changes in the gene expression profile. In this state, astrocytes show increased proliferation and formation of borders, the glial scar, to separate injured CNS parts from healthy brain tissue. Simultaneously, neurons are protected by the secretion of neurotrophic factors and anti-inflammatory molecules, and axonal growth to the severed site is inhibited. After glial scar formation, astrocytes promote the development of new synapses and the refinement of neuronal circuits. Overall, reactive astrogliosis is a mechanism to protect neurons and counteract the detrimental physiological changes after brain damage (reviewed in [23]). White matter astrocytes are morphologically and functionally different from their grey matter counterparts. Based on their larger size but fewer branches and straighter processes, these cells are called fibrous astroglia. These astrocytes are characterized by generally higher GFAP expression levels and seem to play an increased role in the metabolic support of axons but are not involved in regulating neuronal activity.

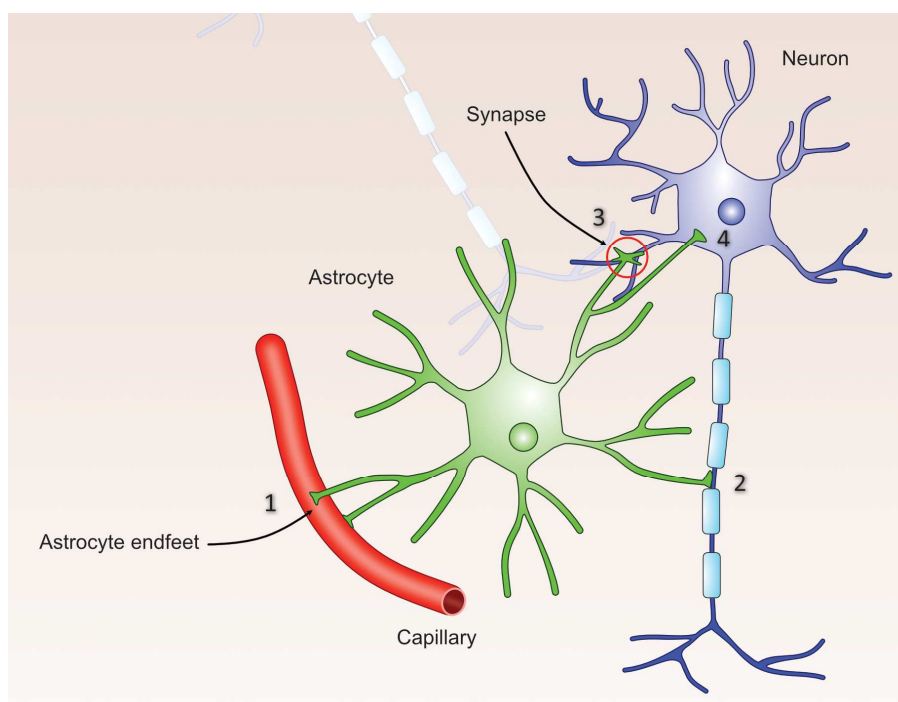


**Figure 1-1 Overview of astrocyte functions in the CNS.** Astrocytes take part in essential functions like (1) formation and maintenance of the BBB and nutrient uptake from blood vessels, (2) myelination of neuronal axons in cooperation with oligodendrocytes, (3) formation of synapses and regulation of synaptic activity and synapse functionality, and (4) maintenance of neuronal homeostasis, including balanced ion and fluidics levels and metabolic support (modified from [24]).

While the two main astrocytic subtypes, protoplasmic and fibrous astrocytes, can be found in organisms of different evolutionary stages, two morphologically distinct forms of astrocytes have been described as primate- or even human-specific, namely interlaminar and varicose projection astrocytes. Because of their exclusivity in higher-order primates, they are very likely involved in long-distance coordination within the brain and even higher cognitive functions. Their distinct functions are still under investigation and reviewed in Vasile et al. and Chung et al. [4, 25].

### 1.2.2 Astrocytes in neuropathologies

In the progress of psychological and somatic neuropathologies, malfunctioning and death of CNS neurons are often observed and accompanied by synapse dysfunction. For decades, the death of neurons was considered the leading underlying cause for CNS pathologies, while effects on astrocyte number or morphology were attributed to the secondary impacts. Given the emerging data on astrocytes' immense influence on brain function and synapse regulation, hypotheses arose whether astrocyte misregulation and malfunctioning could be the cause rather than the symptom of neuropathologies [26]. In most cases, genetic mutations in proteins that contribute to critical astrocytic

functions lead to their incapability to maintain a healthy brain environment. One of these proteins is GFAP, a very prominent astrocytic protein. Although it has been considered an astrocyte-specific marker protein for decades, the exact function of GFAP in astrocytes remains unknown. Together with vimentin, it forms intermediate filaments in the cell and contributes to structure, morphology, and proliferation, and it is highly upregulated in reactive astrocytes after CNS injury. Several studies have shown GFAP involvement in various astrocyte functions, but most of these processes can be accomplished by vimentin alone, or their physiological relevance are in question [27]. In Alexanders' disease, mutations in the GFAP gene lead to an abnormal gain-of-function phenotype in which GFAP aggregates to Rosenthal fibers and leads to a severe neurodegenerative phenotype with loss of myelin sheaths (reviewed in [27]). A similar phenotype of axonal hypomyelination can be observed in the Vanishing-White-Matter disease (VWMD), in which a defect in the translation initiation factor 2B leads to a lack of GFAP expressing astrocytes with abnormal morphology and unusual protein expression patterns. Notably, the generation of other cell types such as oligodendrocytes from VWMD patient progenitor cells is not significantly impaired, suggesting an increased susceptibility of astrocytes and their crucial regulatory role for axon myelination, especially after brain damage, trauma, or inflammation [12, 27–29].

Increased expression of GFAP in astrocytes has also been observed in a variety of other conditions and is usually linked to prolonged reactive gliosis. Astrocytes are activated by the brain's neurodegenerative changes and fail to return to their default state because of ongoing neuronal death. It is unclear to what extent astrocytes contribute to the development of these diseases, but adverse effects of chronic reactive gliosis may lead to aggravated symptoms and worse disease progression. Diseases characterized by reactive gliosis are, among others, amyotrophic lateral sclerosis, Parkinson's, and Alzheimer's disease [30]. Experimental evidence also connects these neurodegenerative diseases to defects in glutamate transporters, leading to glutamate excitotoxicity of neurons due to ineffective clearing of glutamate from the synaptic cleft [31]. Distinct mutations in the Na/K-ATPase on astrocyte endfeet have been associated with lower activity and subsequent facilitation of spreading of migraine attacks, depression, and anxiety-related behavior [32, 33].

Astrocyte function can also be negatively influenced after infection with certain viruses. Infection with human T-lymphotropic virus type 1 leads to a disturbed ability to maintain the glutamate homeostasis in the synaptic cleft by decreased expression of glutamate transporters and misregulation of glutamate-metabolizing enzymes [34]. Astrocytes infected with Zika virus show significant dysregulation of their protein expression profile, subcellular restructuration, and production of pro-inflammatory cytokines [35, 36]. Due to their longevity, astrocytes are promising target cells for the establishment of latency by integrating viruses. Human herpesvirus 6B was shown to establish a persistent nonproductive infection with low integrated DNA levels and absent viral messenger RNA

(mRNA). In cell culture experiments, it did not cause morphological changes of astrocytes but might serve as a virus source in immunocompromised patients suffering from encephalitis [37, 38]. Another example is the human immunodeficiency virus type 1 (HIV-1). Although its primary target cells are cluster of differentiation 4 (CD4) expressing T-lymphocytes, it has been shown early after its discovery that HIV-1 is also found in CNS tissue of symptomatic and asymptomatic patients. After integration into the host cell genome, the HIV-1 provirus is transcriptionally silent but can be reactivated to form infectious particles by pro-inflammatory cytokines or even stochastic events [39]. Data shows that infected astrocytes can be sources for HIV-1 particles that emigrate from the CNS via trafficking immune cells and support systemic infection [40]. Even in the latently infected state, astrocytes are negatively affected by HIV-1 and produce low levels of mRNA and the viral accessory proteins trans-activator of transcription (Tat) and negative regulatory factor (Nef), both of which have been shown to have direct or indirect neurotoxic effects [41].

### **1.2.3 Astrocytes as a therapy target**

As described above, dysregulation of protein expression in astrocytes is attributed to the development or aggravation of neurocognitive disorders. These changes can have different origins, such as genomic mutations, viral infections, or age-related factors. An increasing body of evidence indicates that targeted genetic manipulation of or drug administration to astrocytes may positively influence different CNS-related disorders. For implementing these strategies, tools for selective astrocyte targeting are needed to further understand the fundamental molecular functions of astrocytes in the healthy and diseased CNS and targeted therapeutic delivery (reviewed in [13, 42]). In the process of developing these tools, several aspects of astrocyte biology have emerged as caveats. Astrocytes are an incredibly diverse population across the CNS, both morphologically and physiologically. Targeting all astrocytes or only specific subclasses has to be considered when designing delivery tools and analyzing potential therapy outcomes [32, 43]. Astrocytes are also closely connected to neurons that are very sensitive to physiological changes and can only be regenerated under very limited conditions, increasing the need for high astrocyte selectivity.

Viral vectors have been widely used in investigating basic astrocyte functions and in therapeutic astrocyte modulation *in vitro* and in mice [44]. Frequently used viral vectors include lentiviral (LV) as well as adeno-associated virus (AAV) vectors. LVs are usually known for their very broad tropism and high transduction efficiency when pseudotyped with the glycoprotein of the vesicular stomatitis virus (VSV-G). Interestingly, the local injection of VSV-G LVs results in a mainly neurotropic phenotype with limited transduction of other CNS cell types. Pseudotyping with envelope proteins from other viruses

such as lymphocytic choriomeningitis virus and mokola virus leads to increased transduction of astrocytes after local injection, although further quantifications are needed [45]. In addition, the expression of an immunoglobulin G (IgG) antibody against the glutamate aspartate transporter 1 (GLAST) protein, which is highly expressed in astrocytes, leads to preferential astrocyte targeting [46]. While the long-lasting transgene expression mediated by LVs is useful for certain research questions, e.g. for neurodegenerative models, integration into the host cell genome also poses risks for insertional mutagenesis [47, 48]. So far, AAV-derived vectors are considered the gold standard for gene therapy and will be described in more detail in the following section.

## **1.3 Adeno-associated viruses**

### **1.3.1 Classification**

AAVs were first described by Atchison et al. in 1965 [49]. When performing electron microscopy analysis of adenovirus stocks, they identified virus-like particles that were approximately 24 nm in size and displayed a hexagonal shape. At first, AAVs were considered an incomplete virus since they cannot pursue a productive infection on their own but seem to be dependent on the presence of any adenovirus co-infection [49]. Referring to this dependency, AAVs are classified into the genus Dependovirus and the family of Parvoviridae. They are small, non-enveloped viruses with an icosahedral capsid and carry a linear, single-stranded DNA (ssDNA) genome. Today it is known that AAVs are not defective since they can infect target cells but instead remain in a latent stage without additional harm to the target cell and will only enter the productive life cycle when additional stressors and co-infection with a helper virus appear. Although approximately 80 % of the world population are carrying antibodies against several serotypes, no pathological outcomes have been detected in humans or other species so far [50, 51]. The AAVs known to date can be categorized in serotypes according to the targeting by neutralizing antibodies and into clades according to their phylogenetic relationships. Commonly known serotypes that are serologically separated from one another are AAV1-5 and AAV7-9. Apart from these serotypes, AAV6, AAV10, and AAV11, and more than a hundred poorly characterized human isolates, are known. For lack of good serological characterization, these AAVs are termed AAV variants rather than serotypes. While AAV1-6 were detected as contaminants in adenovirus stocks, AAV7-9 were identified by a targeted polymerase chain reaction (PCR)-based approach in human and primate tissue samples, alongside a plethora of AAV variants [52]. By sequencing the main capsid protein of AAVs from more than 250 human and non-human primate individuals, Gao et al. postulated AAVs' separation into six clades (Clade A-F) and five genetically distinct clones [53]. This analysis sheds light on the potential evolution of AAVs from avian AAVs to

variants with clear human or non-human host tropism. Traces of AAV genomic DNA (gDNA) could be found in various human and non-human primate tissues, indicating diverse tropisms of different AAV variants [53].

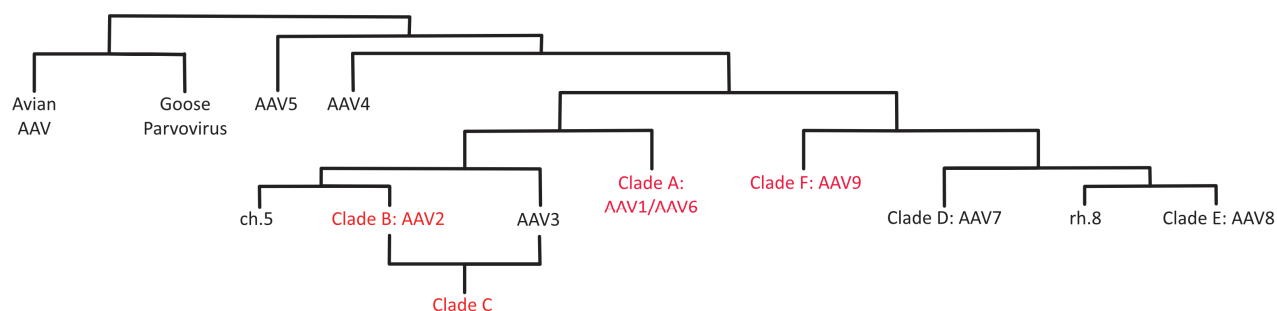


**Figure 1-2 Classification of identified AAV variants into clades and clones.** Each clade contains one representative AAV serotype that is serologically unique and one or more closely related variants. AAV3, AAV4, AAV5, ch.5, and rh.8 are serologically distinct clones with no further clade members. Clades indicated in red only contain AAV variants isolated from humans, clades shown in black include isolates from non-human primates. Variants are clustered based on the phylogenetic relatedness of their cap gene sequences (modified from [53]).

### 1.3.2 Genome organization

The organization of the AAV genome is broadly conserved across AAVs. The AAV genome is approximately 4700 nucleotides (nt) in length and is flanked on both sites by identical inverted terminal repeats (ITRs) with a length of 145 nt. The first 125 nt of each ITR contain palindromic sequences that lead to the formation of T-shaped secondary hairpin structures and have signals for DNA replication and packaging [54, 55]. The genome itself contains the two open reading frames (ORF), *rep* and *cap*. *Rep* encodes four non-structural proteins, Rep78, Rep68, Rep52, and Rep40, that are essential for genome replication and viral packaging and are transcribed from two promoters p5 and p19. Rep78 and Rep52 are encoded by unspliced RNA, and Rep68 and Rep40 coding RNAs are generated by splicing the respective RNA product. The structural proteins VP1, VP2, and VP3 are encoded by the *cap* gene and transcribed via the p40 promoter. While VP1 is generated using an alternative splice site, the *cap* gene contains two additional start codons with different efficiencies, from which VP2 and VP3 are produced. Fairly recently, the existence of an alternative ORF within the *cap* gene called *aap* was described. The transcribed 23 kilodaltons (kDa) assembly-activating protein (AAP) was shown to be essential for capsid assembly next to the cap proteins in several AAVs among all clades [51, 56–58].

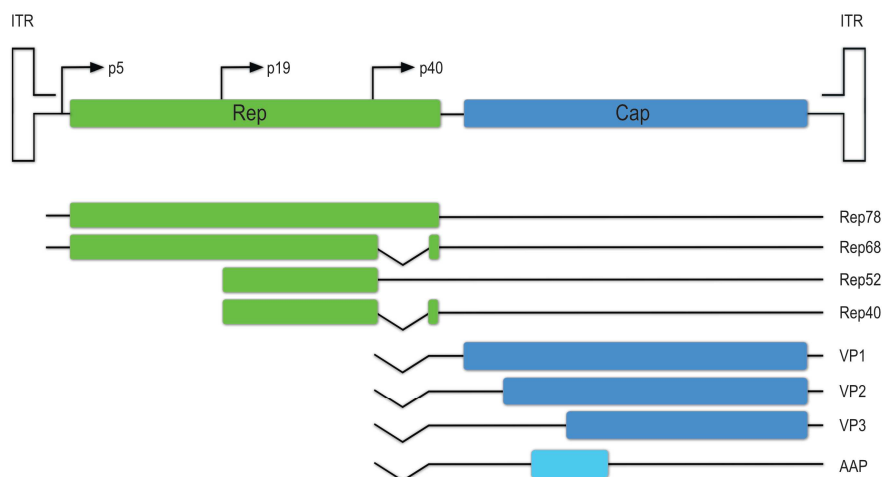


**Figure 1-3 Genome organization of AAV.** The two primary genes, *rep* and *cap*, are framed by two identical inverted terminal repeat (ITR) sequences. The *rep* gene contains all three promoters from which five non-structural and three structural proteins are formed. The p5 and the p19 promoter each result in two non-structural rep proteins, Rep78 and Rep52, by full-length transcription of the rep gene and Rep68 and Rep40 by splicing one intron. Transcription from the p40 promoter results in the three cap proteins VP1, VP2, and VP3 and the non-structural protein AAP. VP1 is generated using an alternative splice site, while VP2, VP3, and AAP contain different start codons with varying efficiencies.

### 1.3.3 Replication cycle

Since AAV infection is not known to cause any disease in its host organism, most studies on the molecular mechanisms of AAV infection and intracellular processing were not conducted *in vivo* or with primary AAV samples but with tissue-culture adapted AAV stocks. Therefore, it is essential to note that conclusions drawn from *in vitro* experiments might not wholly reflect the situation of wildtype (WT) AAVs in their natural host. Also, different AAV serotypes are likely to differ in specific parameters of their replication cycle, for example, the use of entry receptors and necessary factors for intracellular trafficking, uncoating, and DNA replication. Therefore, the general features of the AAV life cycle are described with AAV2 as the example organism and are depicted in Figure 1-4 [51].

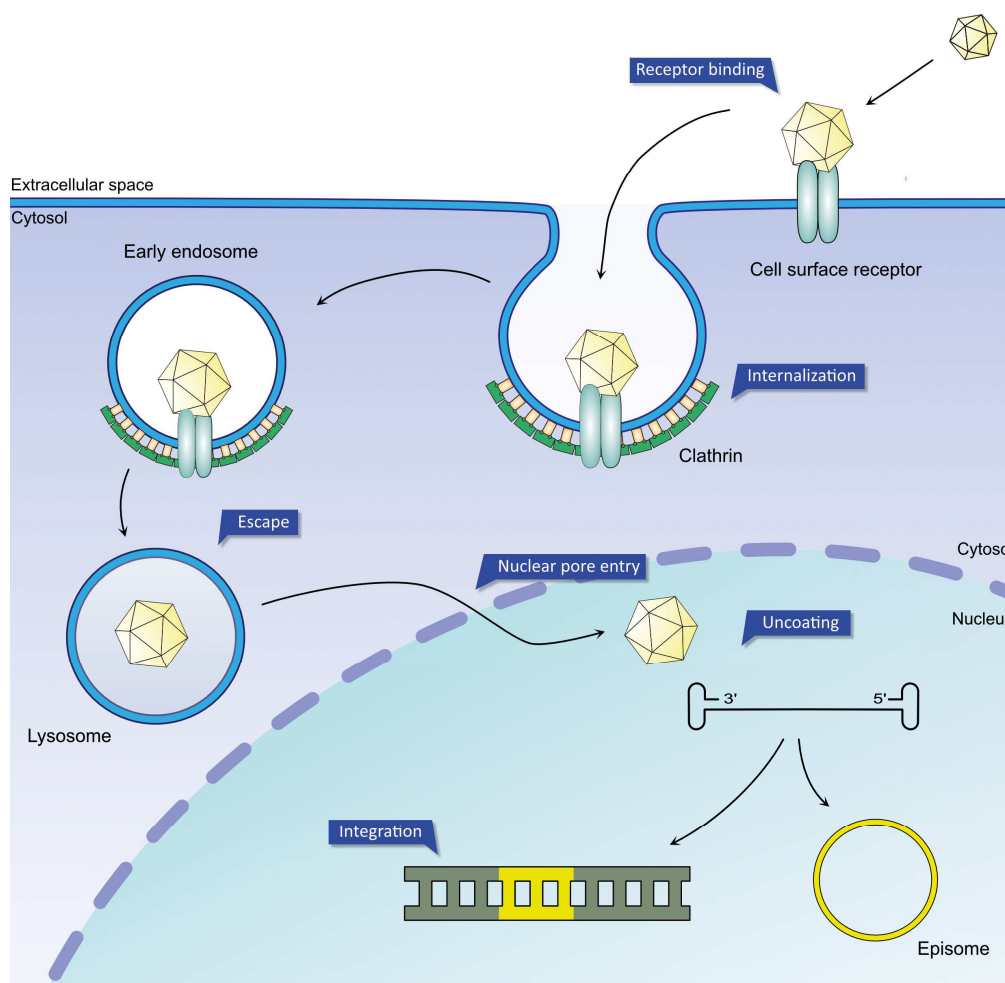


**Figure 1-4 Infection of a target cell by AAV.** Free AAV particles attach to the target cell by interaction with cell surface molecules unique for different AAV serotypes. After binding, AAVs enter the cell via clathrin-mediated endocytosis and remain in clathrin-coated early endosomes. Upon development of the early endosome into the endolysosome and subsequent pH changes, AAV escapes the endolysosome by an unknown mechanism and presumably enters the nucleus via the nuclear pore complex. In the nucleus, uncoating of the virus takes place. In the absence of a helper virus, the AAV genome undergoes targeted integration into the host cell genome or remains in an episomal state within the nucleus (modified from [59]).

The first step of the AAV infectious cycle is the attachment of viral particles to the host cell via specific receptors. Different AAV serotypes and variants were shown to use different surface molecules as binding partners and will be discussed in more detail below. After cell surface binding, AAV particles are taken up by clathrin-mediated endocytosis and remain intracellularly in early endosomes. Here, the data suggest that intact AAV particles escape the early endosome or lysosome through conformational changes of the capsid induced by pH alteration, travel through the cytosol, and enter the nucleus via the nuclear pore complex after the reorganization of the capsid structure to some extent or even partial uncoating [60, 61]. It is also possible to assume that the route of AAV intracellular

trafficking is dependent on the presence and identity of helper viruses [62]. However, the exact process of how viral DNA eventually ends up in the nucleus for DNA replication is still subject to investigation.

In case of helper virus absence, AAVs establish a latent infection in the host cell. AAV DNA is either present in a circular, episomal state or integrates into the host cell genome. With the help of the Rep78 protein, AAV performs a site-specific integration of its genome into the AAVS1 locus on chromosome 19. Latently infected host cells do not show any impairments morphologically or physiologically [63, 64]. After co-infection with a helper virus, AAV enters its lytic life cycle by Rep-mediated rescue of the integrated or episomal DNA genome.

To produce new AAV particles, the excised AAV genome needs to undergo replication, as depicted in Figure 1-5. In the first step of DNA replication, the single-stranded (ss) genome is complemented to a double-stranded (ds) genome. The ITR serves as a primer with a free 3'-end for binding the polymerase and docking site for Rep78 and Rep68, termed Rep-binding elements (RBE). Since the AAV genome does not encode for a viral polymerase, AAVs rely on cellular polymerases for DNA replication (Fig. 1-5 a-b). After complete polymerization, the genome exists in a double-stranded DNA (dsDNA) intermediate with a covalently closed, hairpin structured end (Fig. 1-5 c). In this state, the helicase and endonuclease activities of Rep78 and Rep68 unwind the dsDNA, including the ITR, and induce a nick at the terminal resolution site (TRS), which is located opposite to the initial docking point for the DNA polymerase, creating a new free 3'-end (Fig. 1-5 d-e). The polymerase binds to this new starting site and replicates the now linearized ITR sequence, resulting in a full-length dsDNA construct. The presence of the palindromic sequences at the ends of both strands of the dsDNA leads to the spontaneous formation of the T-shaped secondary hairpin structures of the ITRs, creating a new primer and attachment site for the polymerase. Via elongation by the polymerase, the two strands are separated by single-strand displacement, leading to one AAV genome and one dsDNA intermediate that can re-enter the replication cycle as a template for more AAV genomes (Fig. 1-5 f). The roles of Rep52 and Rep40 are less characterized, but they are thought to play a role in separating and accumulating ssDNA viral genomes from dsDNA intermediates and packaging of ssDNA genomes into empty capsids [51, 65–67]. Although DNA replication and packaging and capsid assembly can theoretically happen in the absence of helper viruses, AAVs are dependent on the presence of distinct helper proteins from larger DNA viruses. For adenoviruses, these helper molecules have been narrowed down to the viral proteins early-region four open reading frame 6 (E4orf6) and early-region 2A (E2A) and a viral associated RNA (VA-RNA), while early-region 1A (E1A) and early-region 1B 55 kilodalton (E1b55K) also have beneficial effects on AAV infection. Overall, helper virus factors modify the host cellular environment to enhance AAV replication and facilitate AAV protein production [51, 68].

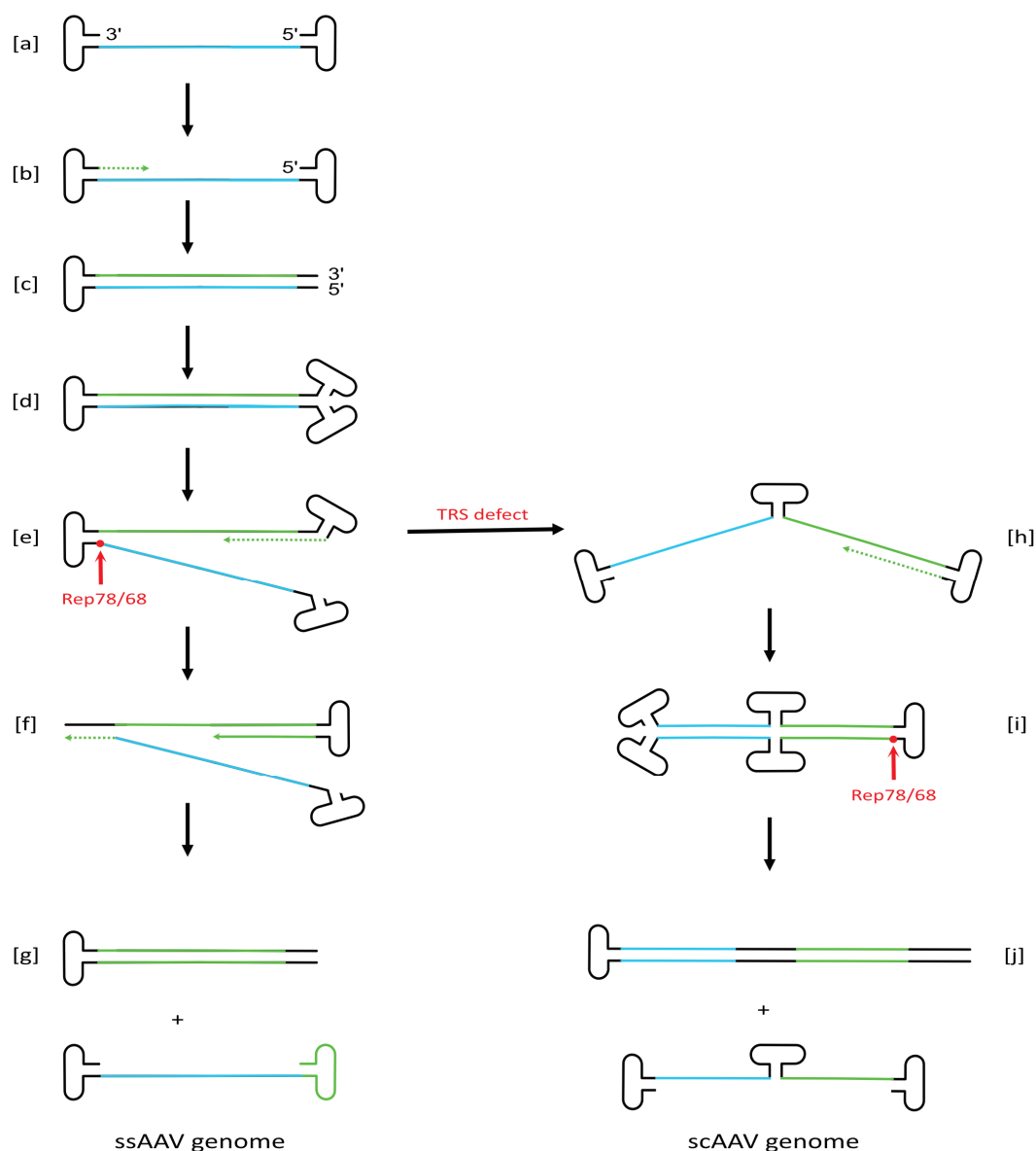


**Figure 1-5 Schematic representation of the AAV genome replication for WT AAVs or single-stranded (ssAAV) and self-complementary (scAAV) AAV vectors.** [a] After rescue from the host cell genome or the episomal state, the AAV genome is present in an open, ss form with flanking ITRs. The ss genome is complemented into a double strand by the host cell's polymerase, using the 3' end of the ITR as a starting point [b], which leads to a covalently closed, ds intermediate form of the AAV genome [c]. The free 3' and 5' end spontaneously form the characteristic hairpin structure of the ITR [d]. The host cell polymerase uses the newly generated 3' end as a primer for DNA polymerization, thereby displacing and unwinding the ds intermediate. During this process, Rep78 and Rep68 introduce a nick at the terminal resolution site (TRS) using their endonuclease activity [e], leading to two separate DNA strands. Both strands are complemented by the polymerase [f], which leads to the formation of one complete ssAAV genome ready for packaging and one covalently closed ds intermediate [g]. The intermediate can re-enter the replication process at stage [e]. In the production of recombinant scAAV vectors, the TRS of one ITR is mutated to prevent nicking and, therefore, separation of the single strands [h]. Because the strand displacement cannot take place, the whole genome is complemented, and a ds intermediate containing the same genetic information twice as palindromic sequence and a total of five ITR sequences is formed [i]. Now, nicking

at the functional TRS is initiated. This results in one ss scAAV genome and one complex intermediate that can re-enter the replication process at stage [h].

### 1.3.4 The cap proteins

As described above, the AAV genome is transcribed from three different promoters giving rise to at least eight different viral proteins. In the latent phase, low amounts of transcription from the p5 promoter take place to produce Rep78/68 proteins that seem to be required for repressing the other AAV promoters in the latent state, but also need to be readily available for genome excision as soon as helper virus co-infection takes place. After helper virus infection, transcription from the AAV genome is increased significantly, with a greater amount of *cap* transcripts being produced. The viral p40 promoter is the starting site for transcribing the *cap* gene, resulting in a single pre-mRNA transcript. After splicing the single intron of the *cap* pre-mRNA, the transcript is used to produce the biggest 87 kDa capsid protein VP1. A second transcript is generated from the *cap* mRNA using an alternate splice acceptor site. This shorter transcript contains two start codons from which the smaller VP2 (72 kDa) and VP3 (63 kDa) cap proteins are produced. Different promoter and splicing activity lead to the production of these proteins in a molar ratio of 1:1:10 and their assembly into a 60mer at the same stoichiometry. Fully assembled AAV capsids have a T=1 icosahedral symmetry [66, 69, 70]. During the formation of fully infectious virions, the assembly of full virus capsids occurs early and independently from DNA replication and export to the cytoplasm. Subsequently, ssDNA viral genomes are inserted into the virus capsids via capsid pore structures and the helicase activity of Rep52 [71]. Given the ratio of individual cap proteins in the fully assembled AAV capsid, it is evident that VP3 makes up most of the virus capsid and is even capable of forming virus-like particles on its own [72]. Due to its exposition on the capsid surface, VP3 is involved in primary steps of AAV infection, such as receptor binding. The unique N-terminus of VP1 was shown to contain an exclusive phospholipase A2 (PLA2) activity and a nuclear localization signal crucial for AAV infectivity, nuclear localization, and viral gene expression [73, 74]. So far, no essential role has been assigned to the VP2 protein, which seems to be dispensable for capsid formation [75]. To date, extensive investigation of the VP3 structure has been performed in several AAV serotypes. The VP3 protein possesses a characteristic secondary structure that is conserved across all further investigated serotypes and even in other members of the Parvoviridae. Depending on their phylogenetic relatedness, capsid proteins of different AAVs share between 53 and 99 % sequence homology, with the sequence differing greater in loop regions exposed on the surface of the assembled capsid. Direct sequence comparison revealed up to 12 variable regions in the VP3 protein that have been shown to be involved in the differential receptor binding across serotypes [76, 77].

### 1.3.5 Recombinant AAVs as viral vectors

#### 1.3.5.1 Characteristics

Given the favorable conditions that AAVs are not known to cause any disease in their host organisms and their low immunogenicity, AAVs were soon identified as suitable templates for novel viral vectors for gene therapy [78]. In the production process of recombinant AAV particles (rAAVs), almost all viral genetic elements can be removed from the genetic material packed inside the rAAV, leading to an increased packaging capacity of up to 4.7 kb (Fig. 1-6 A). The transgene must be flanked by the viral ITRs crucial for transgene replication and Rep-mediated transport to assembled capsids. On modern rAAV production plasmids, AAV2 ITRs are commonly used. The viral *rep* and *cap* genes can be supplied in *trans* on a separate plasmid. While the origin serotype of the *rep* gene has to match the origin serotype of the ITR, the *cap* gene can be derived from any other AAV serotype or variant and can even be genetically modified. A typical rAAV production system, therefore, consists of three plasmids: (1) a transfer plasmid coding for the transgene under the control of a suitable promoter and flanked by AAV2 ITRs, (2) a packaging plasmid carrying the AAV2 *rep* and any *cap* gene, and (3) a helper plasmid coding for the adenoviral molecules E2a, E4, and VA-RNA (Fig. 1-6 B). These three plasmids are transfected simultaneously into a production cell line, such as HEK293T, and rAAV particles carrying only the ITR flanked transgene are formed. Since rAAVs do not carry the genetic information to form viral proteins, the delivered transgene cannot replicate or integrate into the host cell genome but stays in an episomal form, potentially leading to the elimination of the transgene from the transduced cell based on its turnover rate [79–81]. Among rAAVs, two subtypes are distinguished based on the transgene organization, namely single-stranded (ssAAVs) and self-complementary (scAAV, Fig. 1-6 A). ssAAVs harbor an ssDNA molecule flanked by ITRs, analogous to WT AAV particles. As a disadvantage, the ssDNA has to be completed to a dsDNA molecule in the nucleus before transgene expression can occur, leading to a delayed and decreased onset of transgene expression due to DNA transport and instability of dsDNA intermediates. Therefore, high amounts of vector genome (vg) containing particles are needed to ensure sufficient transgene expression in the target cell [82, 83]. The usage of scAAVs circumvents these hurdles. Here, a mutation is inserted in the 3' ITR that destroys the TRS. As a result, the Rep proteins cannot introduce the nick at this ITR, which leads to the formation of an ssDNA molecule that contains three ITRs and two complementary copies of the transgene (Fig. 1-5 h). Nicking can only occur after complementation to a dsDNA intermediate, and DNA polymerase-mediated strand displacement will lead to the generation of one scAAV genome and a dsDNA intermediate that can re-enter the replication cycle (Fig. 1-5 i-j). Due to its inert complementarity, this rAAV genome spontaneously anneals to a dsDNA conformation either inside the AAV particle or right after entry and uncoating in the target cell and is readily available for transcription and transgene expression. To

ensure efficient packaging, the ssDNA molecule's length cannot exceed the size of 5 kb, including the three ITRs, resulting in a maximum transgene size of approximately 2.2 kb (Fig. 1-6 A) [83–85].

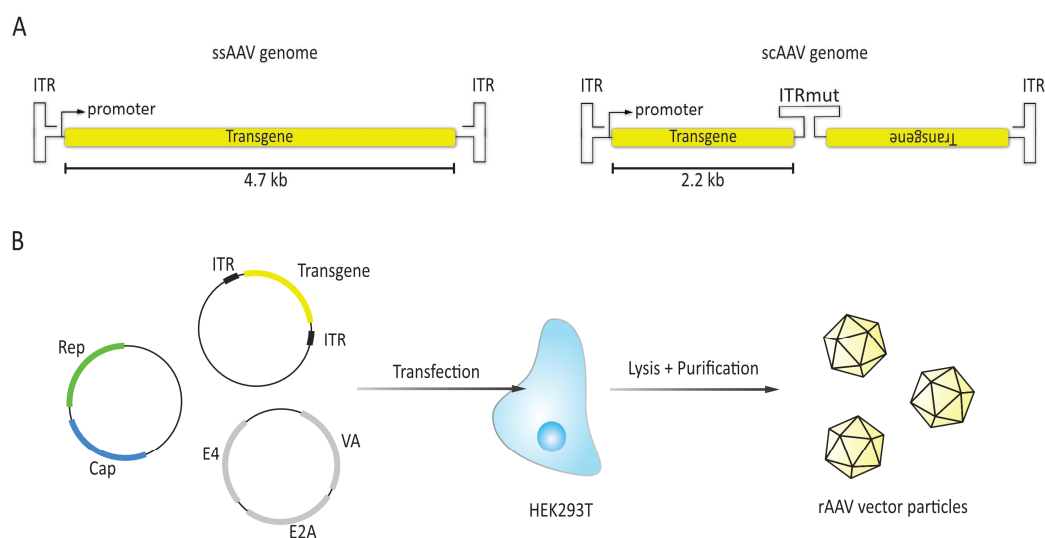


**Figure 1-6 rAAV as viral vectors.** (A) Modification of the AAV genome for use as a viral vector. For usage as an ssAAV vector, the *rep* and *cap* genes are replaced by the transgene under the control of a promoter. The only remaining viral elements are the ITRs flanking the transgene. The size of the transgene, including promoter elements, cannot exceed 5 kb. In scAAV genomes, a mutation in one of the ITRs leads to the formation of a genome containing two copies of the transgene separated by an additional ITR. This allows spontaneous assembly into a double strand after uncoating in the nucleus but also limits the maximum transgene size to 2.2 kb. (B) Schematic representation of the workflow for rAAV production. Three plasmids containing (a) the transgene flanked by ITRs, (b) the *rep* and the *cap* genes, and (c) the adenoviral elements E4, VA, and E2A are transfected simultaneously into HEK293T cells. After a 72 h incubation period, cells are harvested and lysed, and the rAAV particles are isolated and purified using a gradient.

### 1.3.5.2 Advantages of rAAVs as viral vectors

In comparison to other viral vectors such as LVs or adenoviruses, rAAVs show several characteristics that favor their usage for cell transduction *in vitro* and *in vivo* and their consideration in gene therapeutic approaches in humans. As the most important factor, WT AAV particles are unknown to cause any disease in any species investigated [86]. Besides, the removal of viral genes from the DNA within the viral particle leads to a decreased toxicity since no viral proteins can be produced from rAAV vectors. rAAV vectors were also shown to be poorly immunogenic in the host and only elicit a mild, mainly humoral immune response that is not aggravated by viral gene expression [57, 87]. In the absence of the Rep proteins, rAAV mediated transgenes do not integrate into the host cell genome like lentivirus-mediated transgenes, decreasing the risk of insertional mutagenesis. However, this leads to a sequential loss of transgene expression in frequently dividing cell populations [64, 88, 89]. rAAV vectors efficiently transduce non-dividing cells and promote a long-term transgene expression,

preferably in non-proliferating tissues [48, 89]. Among the currently known WT AAV serotypes and variants, a wide variety in cell and tissue tropism was observed. The last point broadens the possibilities for targeted cell transduction, as described in the next chapter.

### 1.3.5.3 rAAV vectors as research tools

As described before, rAAV vectors are suitable as viral vectors for various reasons related to their biological features that are unique among known virus species. These favorable characteristics can be used even better given that rAAV vectors are very susceptible to genetic modification of the viral genome and the *cap* genes. In combination with the modular nature of the rAAV vector production, this allows the tailoring of rAAV particles to modify their tissue selectivity, transduction efficiency, or even reduced interactivity with anti-AAV antibodies [90].

#### **rAAV pseudotyping**

Experiments using rAAV vectors and WT AAV particles in cell culture and animal models have revealed the broad variety of tissue tropisms among AAV serotypes. These cell transduction differences mainly depend on the binding of the serotype-specific capsid structure to surface molecules on the target cell. Post-entry events mainly influenced by the non-structural proteins and the VP1 capsid protein were shown to play a role in the onset timepoint and efficiency of transgene expression [91, 92]. Depending on the target cell, the adequate capsid gene can be chosen and used to cross-package the designed rAAV genome into the desired capsid structure. Comparison of pseudotyped rAAV vectors with identical genomes allows determination of the capsid that promotes the most efficient transduction on a given cell line [93]. Administration of the same transgene in several different capsids can help avoid the clearance of all rAAV vectors by pre-existing antibodies or antibodies induced by earlier rAAV injections [94].

#### **Family shuffling**

It is important to note that even though different capsids show preferences for certain cell types, it is impossible to limit the transduction of a naturally occurring serotype or variant to one single cell or tissue type. This originates in the fact that rAAV vectors usually do not bind to cell-specific receptors but ubiquitous cell surface molecules. These molecules include but are not limited to specific terminal glycan residues, such as sialic acid (SIA) or galactose (GAL), typical receptors for growth factors, extracellular matrix proteins, or even integrins (see Table 1 and references therein). The best investigated and mapped AAV primary receptor is membrane-associated heparan sulfate proteoglycan (HSPG), the central receptor of AAV2. The abundance of HSPG on all cell types explains the broad

tropism of AAV2 [95, 96]. However, differences in transduction efficiency are observed across cell types and are attributed to various co-receptors used by AAV2 that have been identified.

**Table 1-1 WT AAV serotypes with their respective tissue tropism in vivo and identified receptors.** Primary receptors are printed in bold. Coreceptors are printed in normal font. For detailed data on tissue tropism, see [57, 68, 97–99]. AAVR = AAV receptor, RPE = retinal pigment epithelium, FGFR1 = fibroblast growth factor receptor 1,  $\alpha v\beta 5$  = integrin alpha v beta 5,  $\alpha 5\beta 1$  = integrin alpha 5 beta 1, HGFR = hepatocyte growth factor receptor, LamR = 37/67 kDa laminin receptor, CD9 = cluster of differentiation 9, PDGFR = platelet derived growth factor, EGFR = epithelial growth factor receptor

AAV Serotype	Receptors	Tropism	References
1	<b>N-linked SIA</b> , AAVR	Skeletal muscle, CNS, RPE, heart	[100–102]
2	<b>HSPG</b> , FGFR1, $\alpha v\beta 5$ , $\alpha 5\beta 1$ , HGFR, LamR, CD9, AAVR	broad	[95, 102–109]
3	<b>HSPG</b> , FGFR1, HGFR, LamR, AAVR	Hematopoietic stem cells	[95, 102, 103, 108, 110, 111]
4	<b>O-linked SIA</b>	CNS, RPE, lung	[112–114]
5	<b>N-linked SIA</b> , PDGFR, AAVR	RPE, photoreceptor cells, CNS, lung	[102, 112–115]
6	<b>HSPG</b> , <b>N-linked SIA</b> , EGFR, AAVR	Skeletal muscle, lung	[100, 102, 116, 117]
8	LamR, AAVR	Heart, pancreas, skeletal muscle, RPE, CNS, liver	[102, 103]
9	<b>N-linked GAL</b> , LamR, AAVR	Liver, skeletal muscle, lung, CNS, heart	[102, 103, 118]

During receptor identification, it has become evident that specific regions of the capsids are responsible for the interaction with specific receptor molecules. In an approach called "domain swapping," receptor binding domains from different serotypes are combined in a new artificial rAAV vector to re-direct transduction and increase or decrease the transduction efficiency for the desired cell type. A more randomized, screen-like variant of this approach is "DNA family shuffling." In this method, capsids of different serotypes are not combined based on a previous body of knowledge but rather in a random fashion by enzymatic digestion and assembly of capsid proteins. Several rounds of *in vitro* or *in vivo* selection of the capsid libraries should eventually yield a combination of capsid residues that is most beneficial for the transduction of a given cell type [119, 120].

### Peptide display

Another approach for re-directing rAAV tropism is the insertion of small, randomized peptides in the viral capsid's surface-exposed regions. Here, the variable regions of different AAV serotypes come into

play since they are located on the virus capsid surface. The possibility for peptide insertion without interference with capsid assembly or viral infectivity was first described in AAV2. It was shown that the insertion of 7 amino acid (aa) peptides at the positions N587 or R588 is well tolerated and leads to atypical transduction patterns of rAAV2 after systemic injection. The underlying cause is the destruction of the HSPG binding site, which abolishes HSPG-driven transduction of hepatocytes and the retention of injected rAAV particles in the liver [121]. Since AAV2 is the most researched among all serotypes, it has been the backbone for peptide display studies for a long time. However, the high transduction efficiency promoted by HSPG-binding implies that the HSPG binding motif must be destroyed to observe efficient redirection of virus tropism. Peptides containing several basic aa are likely to mimic the HSPG binding motif, therefore, limiting the aa composition of inserted peptides [122, 123]. To circumvent this issue, peptide display approaches were applied to rAAVs that do not display a very high transduction efficiency to achieve a strong transduction bias to specific cell types. Successful examples include the insertion of arginine-glycine-aspartic acid (RGD)-peptides into AAV6 for efficient targeting of prostate, breast, and liver cancer cell lines and increased endothelial cell transduction by rAAV1 modified with RGD-peptides [124, 125]. Insertion of specific peptides has also been reported for AAV8 and AAV9 to improve breast and lung cancer tissue targeting *in vivo* [126]. Randomized peptide library approaches using AAV9 revealed new variants with better transduction of endothelial cells and reduced immunogenicity, while others displayed significantly increased transduction of CNS cells [127, 128]. Although rAAV vectors generated by peptide display show high transduction efficiencies, the clinical use of these variants is hindered by the problem that underlying molecular mechanisms for rAAV binding and cell selectivity are still elusive for most variants. Therefore, a close investigation of promising variants is needed to further advance their usage in research and clinic [120].

#### **1.4 Selective astrocyte targeting with rAAV**

As described above, AAV-derived vectors are considered the most promising candidates for experimental and clinical *in vivo* approaches due to their ability to transduce non-dividing cells and to mediate long-term transgene expression without integration into the host genome. Therefore, rAAVs are investigated as vector systems to target astrocytes in the CNS to develop novel treatment strategies for CNS-associated diseases. Unfortunately, rAAV vectors with the capsid of WT serotype AAV2 that performed well in cell culture experiments were found to transduce non-neuronal cell types only poorly *in vivo* [129, 130]. The serotypes AAV1, 5, 7, 8, and 9 show a broader tropism among CNS cells, and AAV4 was shown to preferentially target astrocytes after local injection [131–136]. While rAAV vector usage yields promising results for astrocytes targeting in cell culture and experimental

trials using different animal species, transferring these vectors to clinical use is very difficult. Most rAAVs show an astrocyte preference only after invasive, intra-cerebral, or even stereotactical injection with limited diffusion potential inside the brain tissue. One of the few AAV variants capable of crossing the BBB after intravenous injection is AAV9 and its derivatives, but a substantial virus load is required with only a few transduced cells in the CNS [137]. rAAV-PHP.B was generated from AAV9 by peptide display and efficiently transduced neurons and glial cells after systemic administration. In addition, rAAV-AS contains a polyalanine extension to the AAV9 VP2 protein, resulting in increased neuronal transduction [127, 138]. These approaches show the promising nature of AAV9 derived variants for crossing the blood-brain barrier and possible astrocyte transduction.

Since precise astrocyte selectivity cannot be achieved with serotype selection alone, restriction of transgene expression is limited to astrocytes by using astrocyte-specific promoters. The most prominent example is the use of the GFAP promoter. Due to the limited packaging capacity of rAAVs, two minimal promoters, *gfa2* (2.2 kb) and *gfaABC1D* (600 bp) were identified and used in combination with several serotypes [139, 140]. Expression of transgenes under GFAP promoter control has proven to be efficient and selective in many studies [141, 142]. However, the expression of GFAP is highly variable among astrocytes in the CNS and may be undetectable in non-reactive astrocytes. This approach leads to a bias of the vector for reactive astrocytes when only using GFAP dependent promoters. Unbiased, genome-wide studies on regulatory elements, alongside transcriptome studies, have been used to detect additional GFAP independent promoters highly active in astrocytes and upregulated proteins. Emerging candidates include the potential marker proteins sex-determining region Y box transcription factor 9 (*Sox9*) and hepatic and glial cell adhesion molecule (HEPACAM) and the promoters for solute carrier family 1 member 3 (*Slc1a3*), gap junction protein beta 6 (*Gjb6*), aldehyde dehydrogenase 1 family member L1 (*Aldh1l1*), glutamate transporter 1 (*GLT1*), and *GLAST* [143–145]. Caveats associated with these promoters are the spatial and temporal variability of promoter activity and the comparably large size of eukaryotic promoters that limit the space for transgene packaging in rAAVs and therefore need further optimization [146]. The most promising approaches so far are the tamoxifen-inducible *Aldh1l1*-cre recombination/estrogen receptor 2 (*Cre/ERT2*) transgenic mouse line as a vector free system and the rAAV2/5 virus capsid in combination with the *gfaABC1D* minimal promoter (see [142, 146] and references therein). Taken together, the dependency of astrocyte selectivity of rAAV vectors on transgenic mouse lines and astrocyte-specific promoters poses the problems of (1) cost and time-consuming breeding of transgenic mice, (2) spilling of transgene expression in other cell types due to lack of promoter specificity, (3) impossibility of pan-astrocyte targeting due to physiological heterogeneity of astrocytes, (4) reduced packaging capacity due to large mammalian promoter constructs, and (5) impossibility to use strong, ubiquitous promoters to ensure efficient transgene expression. Since no reliable astrocyte-specific cell surface

markers are identified to date, targeted modification of AAV capsid structures to increase astrocyte selectivity is impossible.

#### **1.4.1 rAAV9P1 – a vector for selective targeting of human astrocytes in cell culture**

To identify novel rAAV variants for selective targeting of human astrocytes, Kunze et al. performed a screening of five WT AAV serotypes (1, 2, 6, 8, and 9) modified with a library of six random peptides on a human neural stem cell line HNSC.100. They identified AAV9-derived vectors modified with a seven aa peptide (rAAV9P1) to transduce proliferating and differentiated HNSC.100, as well as primary astrocytes, significantly better than WT rAAV9 vector. In addition, rAAV9P1 was inefficient in transducing a neuronal cell line and primary neurons and even showed selective transgene expression in astrocytes in human induced pluripotent stem cell derived brain organoids under the control of a ubiquitous cytomegalovirus (CMV) promoter. Transduction ensured long-lasting and robust transgene expression in non-dividing astrocytes for a minimum of seven weeks, while rAAV transgene copy numbers got eliminated from proliferating cultures after approximately 25 d, indicating that there was no integration of the transgene. Combination of the rAAV9P1 with the minimal GfaABC1D promoter reduced transgene expression in HNSC.100 cells but strongly repressed transgene expression in potential off-target cell lines [147, 148]. A strong astrocyte selectivity that is only driven by modifications in the capsid amino acid composition is unprecedented until today and introduces rAAV9P1 as a promising candidate for possible *in vivo* research applications. Since systemic injection of rAAV9 leads to a low level and unspecific transduction of CNS cells, as well as heart, liver, and skeletal muscle cells, it is still up for investigation whether rAAV9P1 also shows this selectivity *in vivo* [149]. Further, the underlying molecular mechanisms of the rAAV9P1 astrocyte selectivity remain elusive.

#### **1.4.2 AAV9**

AAV9 was first identified in human isolates and belongs to the F clade, one of the smallest among all AAV clades containing only human and no primate isolates [53]. Its capsid sequence shows around 81 and 83 % identity with AAV2 and AAV8, respectively, but only 57 % identity with AAV4 [150]. In the last decade, an increasing number of studies were conducted to investigate this serotype's structural and functional properties due to its unique and interesting transduction pattern *in vivo*. rAAV9 targets tissues like cardiac and skeletal muscle, liver, and pancreas and cells in the eye more efficiently than other serotypes [145–151]. However, the most striking feature of rAAV9 is its capability to cross the BBB after systemic injection in mice and transduce CNS cells in the brain and spinal cord. This is of great importance since it offers the possibility to target the CNS without invasive injection directly into

the brain. It was observed that the rAAV9 transduction pattern in the brain is dependent on the developmental stage and species of the injected organism, indicating that rAAV9 is capable of transducing both neurons and glial cells and that its transduction is likely to be influenced by cell differentiation state and thus, receptor availability [137, 158]. Although the cell-binding behavior of AAV9 is far less investigated than the one of AAV2, several AAV9 receptor molecules and crucial capsid domains are in discussion. The primary receptor for AAV9 is the terminal galactose of N-linked glycans. The amino acid residues in the VP protein involved in galactose binding were mapped by site-directed mutagenesis studies to the positions N470, D271, N272, Y446, and W503. These amino acids form a galactose binding pocket on the capsid surface, which is likely to be necessary for discrimination of galactose from other sugars and physical binding of the capsid to the galactose moiety [118, 159]. Usage of glycans with terminal sialic acid has been shown for several other serotypes (see Table 1) but to date binding of galactose is a unique feature of AAV9.

Compared to its least related serotype, AAV4, the AAV9 VP protein shows nine highly variable regions (VR-I to VR-IX) that are likely to be involved in receptor binding. rAAV9 transduction efficiency significantly benefits from overexpression of LamR and is inhibited by small interfering RNA (siRNA) mediated knockdown of LamR, similar to rAAV8 transduction. The binding domains of AAV8 to LamR are mapped to aa 489 to 545 and aa 591 to 621 (laminin footprint), which are identical in AAV9 and therefore are likely to show the same interaction [103]. AAV9 also requires the transmembrane molecule Dyslexia associated protein KIAA0319 like (KIAA0319L, AAVR), which was recently identified in a genome-wide clustered regulatory interspersed small palindromic repeats (CRISPR)/CRISPR-associated 9 (Cas9) knockout screen, for efficient transduction. AAVR knockout in HeLa cells and transgenic mice completely abrogated transduction by rAAV9, but the underlying molecular interactions are not identified yet [102].

Although the receptor landscape needed for rAAV9 transduction is not fully understood, rAAV9 is a promising candidate as a gene therapy vector. An important factor is the reduced seroprevalence for neutralizing antibodies against AAV9 in comparison to AAV2. A study in a healthy cohort showed that IgG and neutralizing factors against rAAV9 are comparably low, reducing the risk of therapy failure due to vector elimination [160]. Between 2015 and 2019, more than 15 clinical trials were conducted using rAAV9 vectors. The targeted diseases were diverse (including spinal muscular atrophy, Batten disease, gangliosidosis, and Duchenne muscular dystrophy), which is in line with rAAV9s primary target organs, the CNS and skeletal muscle [61, 161].

## 1.5 Aim of the thesis

Selective targeting of astrocytes *in vitro* and *in vivo* is still one of the major obstacles to the development of efficient therapies for neuropathologies with proven or suspected astrocyte contribution. Further, studying the underlying involvement of astrocytes is hindered by the lack of selective non-invasive tools for targeting astrocytes in mixed human brain cell cultures or in animal models. While AAV variants generated by novel genetic engineering approaches show improved CNS penetrance after systemic injection, astrocyte-specific transgene expression is usually ensured by using supposedly astrocyte selective promoters, which introduces an inherent bias to the expression of the reporter or therapeutic agent. The AAV variant rAAV9P1 combines the BBB penetrance of its ancestor serotype AAV9 with an unprecedented astrocyte selectivity in co-culture with neuronal cells. However, the underlying molecules involved in this selective transduction remain elusive.

The aim of this work was to investigate target molecules on human astrocytes involved in cell-type selective transduction by rAAV9P1. This should be achieved by *in silico* modelling and structural analysis of the capsid protein as well as a hypothesis-driven approach to validate and identify receptors of rAAV9P1. In addition, a CRISPR/Cas9 knockout screen was used to identify intra-cellular pathways that might contribute to efficient and selective transduction of human astrocytes by rAAV9P1. The detailed receptor binding profile of rAAV9P1 elaborated in this thesis contributes to a better understanding of the extra- and intra-cellular parameters that drive astrocyte-selectivity in rAAV transduction and might classify rAAV9P1 as the backbone for new and optimized generation of astrocyte-selective vectors.

## 2 Material and methods

### 2.1 Material

#### 2.1.1 Consumables

Consumables	Manufacturer
8.9 ml Polyallomer OptiSeal® Centrifuge Tubes	Beckman Coulter, Brea, CA, USA
Aspiration pipet	Greiner Bio-One, Kremsmünster, AUT
Cell culture flasks (T25/75/175)	Sarstedt, Nümbrecht, GER
Cell scraper	TPP, Trasadingen, SUI
Cellstar® (6/12/24/48/96-well), flat-bottom, clear	Greiner Bio-One, Kremsmünster, AUT
Cellstar® (96-well), V-bottom, clear	Greiner Bio-One, Kremsmünster, AUT
Cellstar® dish (15 cm)	Greiner Bio-One, Kremsmünster, AUT
Cellstar® serological pipets (2/5/10/25/50 ml)	Greiner Bio-One, Kremsmünster, AUT
Combitips Plus (1/5/10 ml)	Eppendorf, Hamburg, GER
Corning® 96-well plate black, with clear bottom	Merck, Darmstadt, GER
Counting chamber - Fast-Read® 102	Immune Systems Ltd., Paignton, UK
EMD Millipore™ Steritop™ Sterile Vacuum Bottle-Top Filters 0.22µM	Thermo Fisher Scientific, Waltham, MA, USA
Falcon® 100 mm TC-treated Cell Culture dishes	Corning Inc., Corning, NY, USA
Falcon® 5 ml Polypropylene Round bottom tubes	VWR, Radnor, PA, USA
Glassware	Schoh DURAN, Wertheim, GER
Gloves – KIMTECH™ Science Purple Nitrile	Kimberly-Clark, Irving, TX, USA
Gloves – Nitril® NextGen®	Meditrade, Kiefersfelden, GER
Millex® HV 0.45 µm filter	Merck, Darmstadt, GER
Needle 23 G Sterican®	B. Braun SE, Melsungen, GER
Nitrocellulose Blotting Membrane Amersham™ Protran®	GE Healthcare, Chicago, IL, USA
Nunc™ CryoTubes™ cryogenic vials, 1.8 mL	Sigma-Aldrich, Darmstadt, GER
PCR Plate - FrameStar® (96-well)	40tude® Ltd., Wohon, UK
Parafilm®	Bemis Company Inc., Oshkosh, WI, USA
Pipet tips with and without filter – TipOne® (2.5 µl, 10 µl, 20 µl, 200 µl, 1,000 µl)	Starlab International GmbH, Hamburg, GER
Reaction tubes (15/50 ml)	Sarstedt, Nümbrecht, GER
Reaction tubes (0,5 ml) - amber/safe-lock	Eppendorf, Hamburg, GER
Reaction tubes (0,5/1,5/2 ml)	Eppendorf, Hamburg, GER
Reagent reservoir	Sorensen BioScience Inc., Salt Lake City, UT, USA
Syringes	Becton Dickinson, Franklin Lakes, NJ, USA

### 2.1.2 Chemicals and solutions

Chemical/solution	Manufacturer
1 kb Plus DNA ladder	New England Biolabs, Ipswich, MA, USA
30 % acrylamide mix	Bio-Rad, Munich, GER
$\alpha\beta$ 8-ligand 2a [c(GLRGDLp(NMe)K)]	[162]
Agar	Sigma-Aldrich, St. Louis, MO, USA
Agarose NEEO Ultra-Quality	Roth, Karlsruhe, GER
Ampicillin Gibco™	Thermo Fisher Scientific, Waltham, MA, USA
Antibiotic-Antimycotic (100x)	BioWest, Nuaille, FRA
Ammonium persulfate	Roth, Karlsruhe, GER
$\beta$ -Mercaptoethanol	Sigma-Aldrich, St. Louis, MO, USA
Benzonase® Nuclease	Merck Millipore, Burlington, MS, USA
Blasticidin	InvivoGen, Toulouse, FRA
BSA	Sigma-Aldrich, St. Louis, MO, USA
CaCl <sub>2</sub>	Roth, Karlsruhe, GER
Chloroform	Merck Millipore, Burlington, MS, USA
Cilengitide	Tocris Bioscience, Bristol, UK
Collagen	Serva Electrophoresis, Heidelberg, GER
Deoxycholate	Sigma-Aldrich, St. Louis, MO, USA
DMEM/F12 GlutaMAX™ Gibco™	Thermo Fisher Scientific, Waltham, MA, USA
DMEM with glutamine and 4,5 g/L Glucose Gibco™	Thermo Fisher Scientific, Waltham, MA, USA
DMSO, cell culture grade	PanReac AppliChem, Darmstadt, GER
DNase I	Qiagen, Hilden, GER
dNTPs	Thermo Fisher Scientific, Waltham, MA, USA
Dpnl (10 U/ $\mu$ l)	Thermo Fisher Scientific, Waltham, MA, USA
<i>Erythrina cristagalli</i> lectin-biotin	Vector Laboratories Inc., Burlingame, CA, USA
EDTA	Roth, Karlsruhe, GER
EGF	PeproTech Inc., Rocky Hill, NJ, USA
Ethanol	Roth, Karlsruhe, GER
Ethidium bromide	Sigma-Aldrich, St. Louis, MO, USA
FCS, heat-inactivated Gibco™	Thermo Fisher Scientific, Waltham, MA, USA
FGF-2	PeproTech Inc., Rocky Hill, NJ, USA
Gel Loading Dye, Purple (6x)	New England Biolabs, Ipswich, MA, USA
Glycerol	Roth, Karlsruhe, GER
Glycine	AppliChem GmbH, Darmstadt, GER
GoTaq® G2 DNA Polymerase	Promega, Madison, WI, USA
HCl	Roth, Karlsruhe, GER
Heparin sodium salt for cell culture	neoFroxx, Einhausen, GER

Hepes Gibco™	Thermo Fisher Scientific, Waltham, MA, USA
Iodixanol OptiPrep™ Gibco™	Thermo Fisher Scientific, Waltham, MA, USA
Isopropanol	Merck, Darmstadt, GER
KCl	Roth, Karlsruhe, GER
KH <sub>2</sub> PO <sub>4</sub>	Sigma-Aldrich, St. Louis, MO, USA
Light Cycler® 480 SYBR Green I Mastermix	Roche, Basel, Schweiz
Methanol	Roth, Karlsruhe, GER
MgCl <sub>2</sub>	Roth, Karlsruhe, GER
Milli-Q water (H <sub>2</sub> O)	Merck-Millipore, Burlington, MA, USA
N-2 supplement Gibco™ (100x)	Thermo Fisher Scientific, Waltham, MA, USA
Na <sub>2</sub> HPO <sub>4</sub> x 2 H <sub>2</sub> O	Roth, Karlsruhe, GER
NaCl	Sigma-Aldrich, St. Louis, MO, USA
NaOH	Roth, Karlsruhe, GER
NEB2 buffer	New England Biolabs, Ipswich, MA, USA
Neuraminidase	Merck-Millipore, Burlington, MA, USA
NP40	Sigma-Aldrich, St. Louis, MO, USA
NuPAGE™ sample buffer Invitrogen™ (4x)	Thermo Fisher Scientific, Waltham, MA, USA
Opti-MEM™ Gibco™	Thermo Fisher Scientific, Waltham, MA, USA
P11	Tocris Bioscience, Bristol, UK
PAGERuler™ Prestained Protein Standard	Thermo Fisher Scientific, Waltham, MA, USA
Penicillin/Streptomycin Gibco™	Thermo Fisher Scientific, Waltham, MA, USA
PfuUltra™ II Fusion High-fidelity DNA Polymerase	Agilent Technologies, Santa Clara, CA, USA
Phenol	Roth, Karlsruhe, GER
Phenol/Chloroform/Isoamylalcohol	Roth, Karlsruhe, GER
Phenol red	AppliChem GmbH, Darmstadt, GER
Phusion™ High-fidelity polymerase	Thermo Fisher Scientific, Waltham, MA, USA
Polybrene	Sigma-Aldrich, Darmstadt, GER
Polyethylenimine, Linear, MW25000	Polyscience Inc., Warrington, PA, USA
Poly-L-lysine	Sigma-Aldrich, Darmstadt, GER
Protease Inhibitor cOmplete®	Roche, Mannheim, GER
Proteinase K	VWR, Radnor, PA, USA
Puromycin	Sigma-Aldrich, Darmstadt, GER
RNase A	Thermo Fisher Scientific, Waltham, MA, USA
RNase-free DNase Set	Qiagen, Hilden, GER
SDS	Roth, Karlsruhe, GER
Skim milk powder	Roth, Karlsruhe, GER
Super optimal broth + 20 mM Glucose (S.O.C.) Medium	Thermo Fisher Scientific, Waltham, MA, USA
Sodium pyruvate Gibco™ (100x)	Thermo Fisher Scientific, Waltham, MA, USA

TEMED	Sigma-Aldrich, Darmstadt, GER
Tris-Acetate	Sigma-Aldrich, St. Louis, MO, USA
Tris-HCl	Sigma-Aldrich, St. Louis, MO, USA
Triton X-100	Roth, Karlsruhe, GER
Trypan blue (0.4 %)	Roth, Karlsruhe, GER
Trypsin (0,05 %)-EDTA ( 0,02 %) Gibco™ (1x)	Thermo Fisher Scientific, Waltham, MA, USA
Tryptone	Sigma-Aldrich, St. Louis, MO, USA
Tunicamycin	Tocris Bioscience, Bristol, UK
Tween 20	Sigma-Aldrich, St. Louis, MO, USA
Yeast extract	Sigma-Aldrich, Darmstadt, GER

### 2.1.3 Buffers and media

Buffer/medium	Composition
15 % Iodixanol solution	25 % (v/v) Iodixanol (60 % stock solution) 75 % (v/v) PBS-MK-NaCl
25 % Iodixanol solution	42 % (v/v) Iodixanol (60 % stock solution) 58 % (v/v) PBS-MK 2.5 µl/ml Phenol red stock solution
40 % Iodixanol solution	66 % (v/v) Iodixanol (60 % stock solution) 34 % (v/v) PBS-MK
60 % Iodixanol solution	100 % Iodixanol stock solution 2.5 µl/ml Phenol red stock solution
AAV lysis buffer	50 mM Tris-HCl 0.15 M NaCl pH 8.5 in H <sub>2</sub> O
Differentiation medium	DMEM/F12 GlutaMAX™ 1 % BSA 1x N-2 Supplement 5 mM Hepes 0.5 % FCS 1 % Penicillin/Streptomycin
Direct lysis buffer (2x)	10 mM Tris pH 7.5 3 mM MgCl <sub>2</sub> 1 mM EDTA 1 mM CaCl <sub>2</sub> 1 % (v/v) Triton X-100 In H <sub>2</sub> O 0.2 mg/ml Proteinase K
EDTA solution (2 mM)	1x PBS 2 mM EDTA

FACS buffer	1x PBS 1 % (v/v) FCS
Freezing medium	Respective culture medium 10 % DMSO
Full DMEM	DMEM (+ 4.5 g D-Glucose, + 25 mM Hepes, + L-Glutamine) 10 % FCS 1 % Antibiotic-Antimycotic 1 % Sodium pyruvate
LB-Agar	LB-Medium with 15 g/l Agar
LB-Medium	10 g/l Tryptone 5 g/l Yeast extract 10 g/l NaCl pH 7,5 in H <sub>2</sub> O
LB <sub>Amp</sub> selection medium	LB-medium 100 mg/ml Ampicillin
Phosphate buffered saline (PBS)	140 mM NaCl 5,9 mM KCl 9.7 mM Na <sub>2</sub> HPO <sub>4</sub> x 2 H <sub>2</sub> O 2 mM KH <sub>2</sub> PO <sub>4</sub> pH 7.4 in H <sub>2</sub> O
PBS-MK	1x PBS 1 mM MgCl <sub>2</sub> 2.5 mM KCl
PBS-MK-NaCl	1x PBS-MK 1 M NaCl
PBS-T	1x PBS 0.1 % (v/v) Tween 20
Phenol red stock solution	0.5 % (w/v) Phenol red in H <sub>2</sub> O
Proliferation medium	DMEM/F12 GlutaMAX™ 1 % BSA 1x N-2 Supplement 5 mM Hepes 0.5 % FCS 1 % Penicillin/Streptomycin 20 ng/ml FGF-2 20 ng/ml EGF
Tris-Acetate-EDTA (TAE) buffer (50x)	2 M Tris-Acetate 100 mM EDTA 10 mM Tris-HCl In H <sub>2</sub> O

Tris-EDTA (TE) buffer	10 mM Tris 1 mM EDTA pH 8.0 in H <sub>2</sub> O
TElysis buffer	10 mM Tris-HCl 1 mM EDTA 50 mM KCl 2 mM MgCl <sub>2</sub> pH 8.0 in H <sub>2</sub> O 200 µg/ml RNase A 25 ng/ml Proteinase K
Towbin buffer (2x)	50 mM Tris 400 mM Glycine 0.1 % (w/v) SDS 40 % (v/v) Methanol
Tris-Glycin-SDS (TGS) buffer	25 mM Tris 200 mM Glycine 0.1 % (w/v) SDS in H <sub>2</sub> O
Western blot lysis buffer	100 mM Tris-HCl pH 8.3 150 mM NaCl 1 % (v/v) Glycerol 1 % (v/v) NP40 0.5 % (w/v) Deoxycholate 0.1 % (w/v) SDS 0.1 % (v/v) Triton X-100 in H <sub>2</sub> O

#### 2.1.4 Kits and reagents

Kit/reagent	Manufacturer
CellTiter-Blue® Viability Assay	Promega, Madison, WI, USA
Lipofectamine™ Stem transfection reagent Invitrogen™	Thermo Fisher Scientific, Waltham, MA, USA
NucleoSpin® Gel and PCR Clean-up	Machery and Nagel, Düren, GER
NucleoBond® PC500/2000	Machery and Nagel, Düren, GER
NucleoSpin® Plasmid	Machery and Nagel, Düren, GER
Pierce™ BCA Protein Assay Kit	Thermo Fisher Scientific, Waltham, MA, USA
RNeasy® Mini Kit	QIAGEN, Hilden, GER
SuperScript™ II First-Strand Synthesis Kit Invitrogen™	Thermo Fisher Scientific, Waltham, MA, USA
SuperSignal™ West Femto Substrate Kit	Thermo Fisher Scientific, Waltham, MA, USA
QIAamp® DNA Mini Kit	QIAGEN, Hilden, GER
QIAshredder	QIAGEN, Hilden, GER

Qubit™ dsDNA BR assay kit Invitrogen™	Thermo Fisher Scientific, Waltham, MA, USA
X-tremeGene™ 9 DNA transfection reagent	Roche, Basel, SUI

### 2.1.5 Oligonucleotides

Single guide RNA (sgRNA) sequences in the oligonucleotides used for sgRNA cloning are indicated in bold. All oligonucleotides were ordered from Metabion International AG (Planegg, GER).

Name	Sequence	Usage
YFPnew forward	TTCTCGTTGGGGTCTTTGCT	qRT-PCR
YFPnew reverse	TGAACTCAAGATCCGCCACA	qRT-PCR
Cas9 forward	TCGGAAGCGACCACTTATCG	qRT-PCR
Cas9 reverse	TCCGGTCTGTACTTCGGTCT	qRT-PCR
RNAPolIII forward	GCACCACGTCCAATGACAT	qRT-PCR
RNAPolIII reverse	GTCGGCTGCTTCATAA	qRT-PCR
<i>ITGAV</i>	GGAAAGGACGAAACACCG <b>GGCAATAGAGATTATGCCA</b> GTTTTAGAGCTAGAAATAGCAAGTTAAAATAAGG	sgRNA cloning
<i>ITGB5</i>	GGAAAGGACGAAACACCG <b>TTTCTCTACACGGCACCGG</b> TTTTAGAGCTAGAAATAGCAAGTTAAAATAAGG	sgRNA cloning
<i>ITGB1</i>	GGAAAGGACGAAACACCG <b>TGGCGCGTGCAGGTAAGCT</b> GTTTTAGAGCTAGAAATAGCAAGTTAAAATAAGG	sgRNA cloning
<i>ITGB3</i>	GGAAAGGACGAAACACCG <b>GTGAGCTTTCGCATCTGGGG</b> TTTTAGAGCTAGAAATAGCAAGTTAAAATAAG	sgRNA cloning
<i>ITGB8</i>	GGAAAGGACGAAACACCG <b>TACCGCCATCTGTCCAGATG</b> TTTTAGAGCTAGAAATAGCAAGTTAAAATAAGG	sgRNA cloning
<i>AAVR</i>	GGAAAGGACGAAACACCG <b>TCGCAGAGAGCTGTAAGGT</b> GTTTTAGAGCTAGAAATAGCAAGTTAAAATAAGG	sgRNA cloning
<i>RPSA</i>	GGAAAGGACGAAACACCG <b>GGCCAGGTTTGTGGAACAG</b> GTTTTAGAGCTAGAAATAGCAAGTTAAAATAAGG	sgRNA cloning
Universal reverse strand oligo	AACGGACTAGCCTTATTTAACTTGCTATTTCTAGCTCTA AAAC	sgRNA cloning
<i>ITGAV</i> _Miseq forward	ACACTCTTCCCTACACGACGctcttccgatctCTATTTCTCAA CCTAGCTGGGGA	Miseq NGS
<i>ITGAV</i> _Miseq reverse	TGACTGGAGTTCAGACGTGTGctcttccgatctCTGTGTCTCC ACATAAACTGACT	Miseq NGS
<i>ITGB1</i> _Miseq forward	ACACTCTTCCCTACACGACGctcttccgatctAAGCGAAGGC ATCCCTGAAA	Miseq NGS
<i>ITGB1</i> _Miseq reverse	TGACTGGAGTTCAGACGTGTGctcttccgatctAACTGATC TTGTGGTGAGCAA	Miseq NGS
<i>ITGB3</i> _Miseq forward	ACACTCTTCCCTACACGACGctcttccgatctGCAGGTGGA GGATTACCCTG	Miseq NGS
<i>ITGB3</i> _Miseq reverse	TGACTGGAGTTCAGACGTGTGctcttccgatctGTCTGGAGG AGGGACTTACTCA	Miseq NGS

<i>ITGB5</i> _Miseq forward	ACACTCTTCCCTACACGACGctcttccgatctCTGTCCATGA AGGATGACTTGG	Miseq NGS
<i>ITGB5</i> _Miseq reverse	TGACTGGAGTTCAGACGTGTGctcttccgatctGCTAAATTT CCTGCTTCTCCA	Miseq NGS
<i>ITGB8</i> _Miseq forward	ACACTCTTCCCTACACGACGctcttccgatctGAAAGTACGC CAAACAACCTTAGT	Miseq NGS
<i>ITGB8</i> _Miseq reverse	TGACTGGAGTTCAGACGTGTGctcttccgatctAGCTTGACT CTGCTTTGTTGCTG	Miseq NGS
Miseq_AAVR forward	ACACTCTTCCCTACACGACGctcttccgatctTGAACCACAA GGCTGGAGCTTAC	Miseq NGS
Miseq_AAVR reverse	TGACTGGAGTTCAGACGTGTGctcttccgatctCCCAGTACC ATCTTAGGTCTTTG	Miseq NGS
Miseq_RPSA forward	ACACTCTTCCCTACACGACGctcttccgatctAAGTGCTGGG ATTACAGGCGTAG	Miseq NGS
Miseq_RPSA reverse	TGACTGGAGTTCAGACGTGTGctcttccgatctCTTCTGCCCT CACTTAGGCATCT	Miseq NGS
pLKO-1 seq	CGTGACGTAGAAAGTAATAATTTTC	Sanger sequencing
cap9_G263 seq	GGTGCTGTAGCCGAAGTAGG	Sanger sequencing
cap9 G263 forward	GCAAATCTCCAACGGCACATCTGGAGGATCTTCAAATGA CAACGCC	Quickchange PCR
cap9 G263 reverse	GGCGTTGTCAATTTGAAGATCCTCCAGATGTGCCGTTGGA GATTTGC	Quickchange PCR
NGS_short forward	TGAAAGTATTTTCGATTTCTTGGCT	CRISPR screen
NGS_short reverse	TGTCTCAAGATCTAGTTACGCCA	CRISPR screen
Forward NGS reverse	CCTCTCTATGGGCAGTCGGTGATTTGTCTCAAGATCTAGT TACGCCA	CRISPR screen
Forward NGS_BC1 forward	CCATCTCATCCCTGCGTGTCTCCGACTCAGCTAAGGTAAC GATTGAAAGTATTTTCGATTTCTTGGCT	CRISPR screen
Forward NGS_BC2 forward	CCATCTCATCCCTGCGTGTCTCCGACTCAGTAAGGAGAA CGATGAAAGTATTTTCGATTTCTTGGCT	CRISPR screen
Forward NGS_BC3 forward	CCATCTCATCCCTGCGTGTCTCCGACTCAGAAGAGGATTC GATTGAAAGTATTTTCGATTTCTTGGCT	CRISPR screen

### 2.1.6 Plasmids

**pHelper** encodes for the adenoviral proteins E2A and E4 and the long non-coding VA-RNA. This plasmid was used to produce rAAV particles and was a kind gift from Prof. Dirk Grimm (University of Heidelberg).

**pBSUF3-YFP** encodes for an enhanced yellow fluorescent protein (eYFP) reporter under the control of a CMV promoter, flanked by an AAV2 ITR and an AAV4 ITR. This Plasmid was used to produce recombinant scAAV particles and was a kind gift from Prof. Dirk Grimm (University of Heidelberg) [163].

**pTRrep2cap2** encodes for the AAV2 rep proteins (Rep78, Rep68, Rep52, and Rep40) and the AAV2 cap Proteins (VP1, VP2, and VP3). This plasmid was used to produce rAAV particles that carry an AAV2 derived capsid and was a kind gift from Prof. Dirk Grimm (University of Heidelberg).

**pTRrep2cap9** encodes for the AAV2 rep proteins (Rep78, Rep68, Rep52, and Rep40) and the AAV9 cap Proteins (VP1, VP2, and VP3). This plasmid was used to produce rAAV particles that carry an AAV9 derived capsid and was a kind gift from Prof. Dirk Grimm (University of Heidelberg).

**pTRrep2cap9P1** encodes for the AAV2 rep proteins (Rep78, Rep68, Rep52, and Rep40) and the AAV9 cap Proteins (VP1, VP2, and VP3), which were modified by the insertion of the seven amino acid artificial peptide P1. This plasmid was used to produce rAAV particles that carry the AAV9P1 capsid and was a kind gift from Prof. Dirk Grimm (University of Heidelberg).

**pTRrep2capS1P1** encodes for the AAV2 rep proteins (Rep78, Rep68, Rep52, and Rep40) and a capsid protein generated by family shuffling of the AAV1, 6, 8, and 9 capsid genes. In addition, the capsid protein is modified by the insertion of a seven amino acid artificial peptide P1. This plasmid was used to produce rAAV particles that carry the AAVS1P1 capsid and was a kind gift from Prof. Dirk Grimm (University of Heidelberg).

**pTRrep2capS10P1** encodes for the AAV2 rep proteins (Rep78, Rep68, Rep52, and Rep40) and a capsid protein generated by family shuffling of the AAV1, 6, 8, and 9 capsid genes. In addition, the capsid protein is modified by the insertion of a seven amino acid artificial peptide P1. This plasmid was used to produce rAAV particles that carry the AAVS10P1 capsid and was a kind gift from Prof. Dirk Grimm (University of Heidelberg).

**pTRrep2capH15P1** encodes for the AAV2 rep proteins (Rep78, Rep68, Rep52, and Rep40) and a capsid protein generated by family shuffling of the AAV1, 6, 8, and 9 capsid genes. In addition, the capsid protein is modified by the insertion of a seven amino acid artificial peptide P1. This plasmid was used to produce rAAV particles that carry the AAVH15P1 capsid and was a kind gift from Prof. Dirk Grimm (University of Heidelberg).

**pTRrep2capD20P1** encodes for the AAV2 rep proteins (Rep78, Rep68, Rep52, and Rep40) and a capsid protein generated by family shuffling of the AAV1, 6, 8, and 9 capsid genes. In addition, the capsid protein is modified by the insertion of a seven amino acid artificial peptide P1. This plasmid was used

to produce rAAV particles that carry the AAVD20P1 capsid and was a kind gift from Prof. Dirk Grimm (University of Heidelberg).

**pTRrep2cap9P1\_S263G** was generated from the pTRrep2cap9P1 plasmid by the amino acid exchange S263G in the VP1 protein sequence. This plasmid was used to produce rAAV particles that carry the AAV9P1<sub>S263</sub> capsid.

**pMD2.G** encodes for the envelope protein of the vesicular stomatitis virus VSV-G under the control of a CMV promoter. This plasmid was used as an envelope plasmid in the production of pseudotyped lentiviral particles. pMD2.G was a gift from Didier Trono (Addgene plasmid #12259).

**psPAX2** encodes for the lentiviral proteins Gag, Pol, Rev, and Tat. This plasmid was used as a packaging plasmid to produce pseudotyped lentiviral particles. psPAX2 was a gift from Didier Trono (Addgene plasmid #12260).

**lentiCas9-Blast** encodes for a codon-optimized Cas9 from *Staphylococcus pyogenes* and a blasticidin resistance. This plasmid was used as a transfer plasmid for the production of pseudotyped lentiviral particles and was a kind gift from Dr. Kamyar Hadian (Helmholtz Center Munich) [164].

**lentiGuide-Puro-(GeCKO v2 A)** encodes for the tracrRNA sequence for the Cas9 protein from *Staphylococcus pyogenes* under the control of a U6 promoter and contains the sgRNA sequences from the pooled human CRISPR knockout sub-library A (GeCKO v2 A)[164]. This plasmid was used as a transfer plasmid to produce lentiviral particles and was a kind gift from Dr. Kamyar Hadian (Helmholtz Center Munich).

**pMini\_U6\_sgRNA\_CMV\_Puro\_T2A\_Cas9** encodes for the tracrRNA sequence for the Cas9 protein from *Staphylococcus pyogenes* under the control of a U6 promoter and contains restriction sites for the insertion of sgRNA sequences. It also encodes for a Puromycin resistance gene under the control of a CMV promoter coupled to a codon-optimized Cas9 from *Staphylococcus pyogenes* via a T2A connection. This plasmid was used for the transient transfection of target cells and knockout generation and was a kind gift from Prof. Veit Hornung (LMU Munich).

### 2.1.7 Prokaryotic cells

**Invitrogen™ subcloning Efficiency™ DH5α** (Thermo Fisher Scientific, Waltham, MA, USA) are chemically competent *E. coli* cells used for subcloning of plasmids.

**XL10-Gold®** (Agilent Technologies, Santa Clara, CA, USA) are chemically ultracompetent *E. coli* cells used for *de novo* ligated plasmid cloning.

### 2.1.8 Eukaryotic cells

**H1299** (ATCC® CRL-5803™) are human lung cells derived from non-small cell lung cancer metastatic tissue.

**HEK293T** (ATCC® CRL-3216™) are human embryonic kidney cells. They are derived from 293 cells and contain the SV40 T-antigen.

**HeLa** (ATCC® CCL-2™) are human epithelial cells derived from cervix carcinoma tissue.

**HNSC.100** are human neural stem cells stably expressing the v-myc protein. These cells have a neural stem cell phenotype in their proliferating state and spontaneously differentiate into astrocyte-enriched cultures upon mitogen removal [147, 165–167].

**Huh7** are human hepatocytes derived from liver carcinoma tissue.

**U251MG** (ECACC 09063001) are human astrocytoma cells derived from a malignant glioblastoma tumor.

### 2.1.9 Antibodies and staining agents

Antibody	Host	Dilution/ concentration	Manufacturer
anti-hGAPDH	mouse	1:10,000	Merck Millipore, Burlington, MA, USA
anti-Cas9	mouse	1:10,000	Abcam, Cambridge, UK
anti-mouse Peroxidase	goat	1:5,000	Jackson ImmunoResearch Laboratories Inc., West Grove, PA, USA
anti- $\alpha\beta3$	mouse	5 $\mu\text{g}/10^6$ cells	R&D Systems, Minneapolis, MN, USA
anti- $\alpha\beta5$	mouse	2.5 $\mu\text{g}/10^6$ cells	R&D Systems, Minneapolis, MN, USA
anti-human integrin $\beta1$	mouse	0.25 $\mu\text{g}/10^6$ cells	R&D Systems, Minneapolis, MN, USA
anti-human integrin $\beta8$	mouse	0.5 $\mu\text{g}/10^6$ cells	R&D Systems, Minneapolis, MN, USA
anti-human $\alpha/CD51$ Alexa Fluor® 647	mouse	1 $\mu\text{g}/10^6$ cells	R&D Systems, Minneapolis, MN, USA
anti-mouse Alexa Fluor™ 488	goat	1:200	Thermo Fisher Scientific, Waltham, MA, USA
<i>Sambucus nigra</i> lectin (SNA)-Fluorescein		10 $\mu\text{g}/\text{ml}$	Vector Laboratories Inc., Burlingame, CA, USA

### 2.1.10 Software and online tools

Software	Manufacturer
Affinity Designer	Serif Ltd, Nottingham, UK
BLAST	NCBI, Bethesda, MD, USA
BLAT	UCSC Genome Bioinformatics, Santa Cruz, CA, USA
Diva	BD, Franklin Lakes, NJ, USA
FlowJo v10	FlowJo, LLC, Ashland, OR, USA
GeneRanker	Genomatix AG, Munich, GER
GraphPad Prism 9.0.2	GraphPad Software Inc., San Diego, CA, USA
i-control™ Software	Tecan Group, Männedorf, SUI
ImageJ	U.S. National Institutes of Health, Bethesda, MD, USA
In silico PCR	UCSC Genome Bioinformatics, Santa Cruz, CA, USA
LightCycler 480 Software (Version 1.5.0.39)	Roche, Basel, SUI
Mega7	[168]
Microsoft Office 2016	Microsoft Corp., Redmond, WA, USA
NanoDrop™ 2000c	Thermo Fisher Scientific, Waltham, MA, USA
Outknocker V 2.0	[169]
Phyre V 2.0	[170]
Quantity One Vers. 241 Build 008	Bio-Rad Laboratories Inc., Hercules, CA, USA
R/R Studio	The R Foundation
SerialCloner 2.6.1	Serial Basic
SnapGene Viewer 4.1.8	GSL Biotech LLC, Chicago, IL, USA
Swiss-model	[171, 172]
T-Coffee	[173]
Tm-Calculator version 1.13.0	New England Biolabs, Ipswich, MA, USA
UCSF ChimeraX 1.1	[174, 175]

## 2.2 Cell culture methods and rAAV-virology

All cell culture work was carried out in a sterile environment under a biological safety cabinet. Cells were cultured under standard conditions in a cell culture incubator (5 % CO<sub>2</sub>, 37 °C, 85 % humidity).

### 2.2.1 Thawing and freezing of cells

Frozen cells were rapidly thawed at room temperature (RT) by pipetting pre-warmed culture medium into the cryotube and resuspending the thawed cells in 10 ml pre-warmed culture medium. Cells were

centrifuged for 4.5 min at 200 g, the supernatant was discarded, and the cell pellet was resuspended in 10 ml fresh pre-warmed culture medium. The cell solution was transferred to a fresh (coated if necessary, see below for details) cell culture flask and incubated at 37 °C. For long-term storage, cells were counted, and  $1-5 \times 10^6$  cells were spun down for 4.5 min at 200 g, the pellet was resuspended in 1 ml freezing medium (culture medium supplemented with 10 % DMSO) and transferred to a 1.8 ml cryotube. Cells were frozen slowly in a freezing container at -80 °C for medium-term storage. For long-term storage, cells were transferred to a liquid nitrogen tank (-172 °C) after 24-48 h.

### **2.2.2 Cultivation and passaging of cells (except HNSC.100 cells)**

Cell lines were cultured in appropriate culture medium in sterile polystyrene flasks and passaged twice a week. Cell confluency was assessed under a light microscope, and cells were passaged when confluency was between 80 and 90 %. The medium was removed from the flasks and cells were washed once with PBS. The appropriate amount of Trypsin-EDTA solution was added (Table 2-1), the flask was tilted to cover the entire surface of the flask and incubated at 37°C for 3 min. Flasks were lightly tapped to loosen cells. Cells were harvested in full DMEM, and one tenth of the volume was transferred to a new culture flask, resulting in a splitting ratio of 1:10. The new cell culture flask was filled up to regular culture volume with full DMEM and incubated at 37 °C.

For cultivation of U251MG *ITGAV*<sup>-/-</sup>, U251MG *ITGB5*<sup>-/-</sup>, and U251MG *ITGB3/B5*<sup>-/-</sup> knockout cell lines flasks and other cell culture containers were coated with 1 % collagen in H<sub>2</sub>O for 10 min at RT, washed once with PBS, and used immediately for cell seeding.

### **2.2.3 Cultivation and passaging of HNSC.100 cells**

Proliferating, progenitor-like HNSC.100 cells (HNSC.100 prol) were cultured in proliferation medium in sterile polystyrene flasks coated with Poly-L-Lysine and passaged twice a week. For coating, polystyrene or glass culture vessels were incubated with enough Poly-L-Lysine solution to cover the entire culturing surface for 20 min at RT. Poly-L-Lysine was removed completely, culture vessels were washed twice with PBS, and air-dried for at least 1 h. Cell confluency of HNSC.100 cells was assessed under a light microscope, and cells were passaged when confluency was between 95 and 100 %. The medium was removed from the flasks, and cells were washed once with PBS. The appropriate amount of Trypsin-EDTA solution was added (Table 2-1), the flask was tilted to cover the entire culturing surface and incubated at 37 °C for 3 min. Flasks were lightly tapped to loosen cells, and cells were harvested in PBS + 10 % FCS and centrifuged for 4.5 min at 200 x g at RT to inactivate the trypsin. The supernatant was discarded, the pellet was resuspended in 5 ml proliferation medium, and one fifth

was added to a freshly coated, dry polystyrene flask. The new cell culture flask was filled up to regular culture volume with proliferation medium and incubated at 37 °C.

**Table 2-1 Cell culture numbers**

	Dish 10 cm Ø	Dish 15 cm Ø	T75	T175	6- well	12- well	24- well	48- well	96- well
<b>Culture medium [ml]</b>	10	20	10	20	2	1	0.5	0.25	0.1
<b>Trypsin-EDTA [ml]</b>	1	2	1	2	0.2	0.1	0.05	0.03	0.02

## 2.2.4 Seeding and harvesting of cells

To seed the cells, cells were harvested from their culture flasks as described above. After removing the appropriate volume of cells for maintenance, the remaining cells were counted using a cell counting chamber, and cells per ml were calculated according to the manufacturer's manual. In brief, 10-15 µl of cell suspension was pipetted in one of the ten compartments of the ready-to-use disposable counting slide, making sure that the cell suspension was distributed equally and bubble-free in the chamber space. For highly concentrated cell suspensions or cell lines that are difficult to count, cells were diluted 1:5 or 1:10 in 0.4 % Trypan blue solution before adding it to the counting chamber. Under a light microscope, cells in 16 of the smallest squares were counted, and cell number per ml was calculated with the following equation

$$\text{cells per ml} = \frac{\text{cell count} \times 10,000}{\text{squares counted}} \times \text{dilution factor}$$

From this concentration, the volume of cell suspension needed for the appropriate number of cells for seeding of the respective cell line (Table 2-2) was calculated using the following equation

$$\text{volume } [\mu\text{l}] = \frac{\text{cells needed}}{\text{cells per ml}} \times 1,000$$

To harvest cells, the culture medium was removed from the wells, and cells were washed once with PBS. The appropriate amount of Trypsin-EDTA solution was added to the wells, and cells were incubated at 37 °C for 2 to 4 min. Cell culture vessels were slightly tapped to loosen cells, and cells were harvested in PBS + 10 % FCS. Cells were transferred to an appropriate reaction tube and processed for downstream experiments as described in the respective sections.

**Table 2-2 Seeding density of different cell lines**

Cell line	Medium	Dish 10 cm Ø	Dish 15 cm Ø	6-well	12-well	24-well	48- well	96-well
HeLa, Huh7, H1299, HEK293T	DMEM full	2x10 <sup>6</sup>	11x10 <sup>6</sup>	2x10 <sup>5</sup>	1x10 <sup>5</sup>	5x10 <sup>4</sup>	3x10 <sup>4</sup>	1.5x10 <sup>4</sup>
U251MG	DMEM full	2x10 <sup>6</sup>		2x10 <sup>5</sup>	1x10 <sup>5</sup>	5x10 <sup>4</sup>	3x10 <sup>4</sup>	1.5x10 <sup>4</sup>
HNSC.100	Prol medium			4x10 <sup>5</sup>	2x10 <sup>5</sup>	1x10 <sup>5</sup>	6x10 <sup>4</sup>	3x10 <sup>4</sup>

## 2.2.5 Differentiation of HNSC.100

HNSC.100 cells were seeded in the appropriate format in proliferation medium and incubated at 37 °C. Once cells reached 100 % confluency, cells were washed once with PBS, and differentiation medium was added to cells. HNSC.100 cells were incubated at 37 °C for 14 days. During this time the medium was changed to fresh differentiation medium twice a week. The differentiation progress of cells was assessed by monitoring their change in morphology and cell proliferation arrest by light microscopy [147, 167]. After 14 days, successfully differentiated, astrocyte-enriched cultures (HNSC.100 diff) were used for follow-up experiments.

## 2.2.6 rAAV vector production by iodixanol gradient

HEK293T cells were seeded in 10 sterile polystyrene cell culture dishes (15 cm Ø) and incubated for 48 h to a confluency of 70-80 %. On the day of transfection, the transfection mix was prepared as described in Table 2-3, vortexed 5 times, and incubated for 10 min at RT. After incubation, the transfection mix was added dropwise to the plates, and cells were incubated for 72 h. Cells and supernatant were harvested using a sterile cell scraper and pooled into 50 ml reaction tube. The remaining cells in the plates were collected by flushing two plates with 10 ml PBS in total and adding it to the pooled cells. Dishes were stacked in a tilted manner, and the remaining liquid (collected at the lower rim of the plate) was transferred to the pooled cells.

Cells were centrifuged at 500 g for 15 min at RT, the supernatant was discarded, and cells were pooled into one 50 ml reaction tube with 20 ml PBS. Reaction tubes were flushed with 10 ml total to collect the remaining cells, and pooled cells were centrifuged again at 500 g for 15 min at RT. The supernatant was discarded the cell pellet was resuspended in 5 ml AAV lysis buffer and frozen at -80 °C. The lysate was subdued to 5 freeze-thaw cycles in liquid nitrogen and a 37 °C water bath. 50 U/ml of Benzonase<sup>®</sup> was added to the lysate, and it was incubated at 37 °C for 1 h while carefully inverting the falcon every

20 to 30 min. The cell lysate was centrifuged at 1500 g for 15 min at 4 °C, the supernatant was transferred to a new reaction tube and centrifuged again.

**Table 2-3 Transfection mix for transfection of one 20 cm Ø dish of HEK293T cells**

Reagent	Amount
pHelper plasmid	7.5 µg
pBSUF3-YFP plasmid	7.5 µg
Capsid plasmid	7.5 µg
Polyethyleneimine 1 mg/ml	67.5 µg
DMEM	up to 2 ml

Viral particles were purified from the supernatant by iodixanol density gradient centrifugation. The supernatant was transferred bubble-free to an 8.9 ml round bottom polypropylene centrifuge tube and under-layered with iodixanol solutions of different concentrations (15 %, 25 %, 40 %, 60 %) to create a gradient. Centrifuge tubes were topped up and leveled out to 0.01 g with AAV lysis buffer and centrifuged at 50,000 rpm for 2 h at 4 °C in a Optima LE-70 Preparative Ultracentrifuge with a fixed angle 70.1 TI rotor. The 40 % phase of the gradient, containing full rAAV particles, was extracted using a sterile 23 G syringe while being careful not to touch the white ring at the bottom of the 25 % phase, which contains the empty capsids. Purified virus stocks were divided into 50 µl aliquots and stored at -80 °C until further usage or at -20 °C until titration the next day.

### 2.2.7 Transduction with rAAV vectors

Target cells were seeded in different formats and incubated overnight. One well of every plate format used was washed once with PBS, detached with Trypsin-EDTA, and resuspended in 1 ml culture medium. Absolute cell number in one well was determined by cell counting, and the amount of virus stock needed for specific multiplicities of infection (MOI) was calculated as described in the equation below. Virus stock was diluted in culture medium, added to the cells, and incubated for the indicated time periods.

$$\text{virus stock per well } [\mu\text{l}] = \frac{(\text{cells per well}) \times \text{MOI } [\text{vg}]}{\text{virus titer } \left[ \frac{\text{vg}}{\text{ml}} \right]} \times 1,000$$

### 2.2.8 Cell treatment assays

Target cells were seeded in different formats and incubated overnight. After incubation, cells were treated and transduced at the following conditions.

For integrin inhibition, cells were overlaid with medium containing different concentrations of Cilengitide (CGT),  $\alpha\beta 8$ -ligand 2a, or P11 and co-incubated with rAAV9P1 or rAAV2 for 48 h at 37 °C.

For heparin competition, cells were co-incubated with different concentrations of soluble heparin and rAAV2 or rAAV9P1 for 4 h at 37 °C. After the incubation, the supernatant was removed, cells were washed once with pre-warmed PBS, overlaid with fresh, pre-warmed culture medium, and incubated for 48 h at 37 °C [128].

For modulation of surface glycans, cells were treated with 50 mU/ml Neuraminidase (Neu) from *Vibrio cholerae* diluted in full DMEM for 2 h at 37 °C to promote the removal of terminal sialic acid residues from cell surface glycans. Subsequently, cells were briefly washed with PBS, chilled on ice for 5 min, and co-incubated with 100  $\mu\text{g}/\text{ml}$  *Erythrina cristagalli* lectin (ECL) conjugated with biotin diluted in PBS and rAAV9P1 or rAAV2 for 1.5 h on ice. ECL masks N-terminal galactose residues and renders them unavailable for binding by rAAV capsids. Cells were washed three times with pre-chilled PBS and either incubated for 48 h at 37 °C or used immediately for an *in vitro* recombinant AAV-binding assay (rABA).

For tunicamycin (TUN) treatment, cells were treated with different concentrations of TUN diluted in full DMEM for 24 h at 37 °C. After this incubation period, the medium was changed, cells were pre-chilled on ice for 5 min and subsequently incubated with rAAV9P1 or rAAV2 for 1.5 h on ice. Subsequently, cells were washed three times with pre-chilled PBS and either incubated at 37 °C for 48 h or used immediately for an rABA.

In all experiments, untreated and/or untransduced cells served as controls. The transgene expression was determined 48 h after rAAV exposure by flow cytometry.

### 2.2.9 CellTiter-Blue® (CTB) viability assay

To assess metabolic activity and indirectly cell viability, a CellTiter-Blue® Cell Viability Assay was conducted. This test is based on the conversion of Resazurin to Resorufin via metabolic reduction, and the conversion rate can be calculated from the fluorescence intensities of the samples [176]. Cells were seeded in black 96-well plates with clear bottoms and incubated overnight at 37 °C. Cells were treated with the respective substance and incubated for varying time periods. After incubation, the culture medium was removed, and cells were supplemented with 65  $\mu\text{l}$  CTB reagent diluted 1:5 in culture medium. Dead cells, which were left without culture medium for the incubation time, and untreated

cells served as controls. Plates were incubated at 37 °C for 1-4 h depending on the metabolic activity of the respective cell line until the test reagent in wells with untreated control cells turned from blue to violet. Fluorescence activity of Resorufin was measured using an Infinite<sup>R</sup> M200 microplate reader (Excitation wavelength 550 nm, Emission wavelength 600 nm). Viability was determined relative to untreated controls, with untreated controls being considered 100 %.

#### **2.2.10 *In vitro* rAAV-binding assay (rABA)**

Cells were seeded in 48-well plate and incubated overnight at 37 °C. One well was harvested and counted for absolute cell number determination. Cells in plates were pre-chilled for 5 min on ice and subsequently exposed with different rAAV vectors for 30 min on ice to allow surface binding of virus vectors without effective cell transduction. Untransduced cells served as negative controls. Samples from glycan modulation assays were treated and transduced as described in above. Cells were washed twice with ice-cold PBS to remove unbound virus particles and lysed directly in the well with 50 µl 1x direct lysis buffer supplemented with 40 µg/ml Proteinase K. Lysates were collected by flushing the bottom of the well repeatedly with the lysis buffer in the well and transferred to a 0.2 ml PCR tube. Lysis was conducted for 1 h at 56 °C, and Proteinase K was inactivated for 15 min at 95 °C. Lysates were cooled back to RT and stored subsequently at -20 °C until further analysis by quantitative real-time PCR (qRT-PCR) [177].

#### **2.2.11 Fluorescence-activated cell sorting (FACS)**

Cells were harvested as described before and transferred to a 96-well V-bottom plate. After harvesting, all steps were performed on ice. Cells were centrifuged, accumulation of cells in the bottom of the wells was checked visually, and the supernatant was discarded by rapidly emptying the plate into the sink and shortly blotting the plate against a stack of paper towels to remove all liquid from the wells. Cells were resuspended in FACS buffer and washed once again using the same technique as described before and resuspended in 200 µl FACS buffer. Samples were transferred to 5 ml polystyrene tubes and analyzed on a three-laser BD FACSCanto II device. Data was processed using the FlowJo v10 software. In the first step, live cells were manually gated in the forward scatter (FSC)-side scatter (SSC) plot where events with small size and low granularity were excluded as dead cells or debris. Proceeding with live gated cells, cells negative for the fluorescence marker were gated using a sample of untransduced and/or unstained cells that were cultured in the same format for the same time as the treated cells. Experimental cells were analyzed for the expression of the respective fluorescence marker by the percentage of positive cells and the median fluorescence intensity (MFI).

To assess expression of target proteins on the cell surface, cells were harvested by incubation in 2 mM EDTA in PBS for 10 min at 37 °C, transferred to a V-bottom 96-well plate, and washed as described above. Cells were stained in 50 µl primary antibody diluted in FACS buffer for 30 min on ice, supplemented with 100 µl FACS buffer, and washed one additional time. If required, samples were stained in 50 µl anti-mouse Alexa Fluor™ 488 for 30 min on ice. Cells were washed again and analyzed by flow cytometry as indicated above.

## **2.3 Molecular biology methods**

### **2.3.1 gDNA isolation**

Cells were harvested using Trypsin-EDTA solution, washed once with PBS, and pelleted for 5 min at 500 g in a tabletop centrifuge. The supernatant was discarded, and gDNA was isolated using the QIAamp® DNA Mini Kit, according to the manufacturer's manual. The gDNA was eluted from the column in 30 µl dH<sub>2</sub>O and concentration was determined by NanoDrop™ analysis. Samples were stored at -20 °C until further analysis.

### **2.3.2 PCR**

PCRs were performed using the GoTaq® G2 DNA Polymerase according to the manufacturer's manual. For amplification of segments of gDNA or plasmid DNA, 50-100 ng total DNA were used for each 50 µl reaction. The optimal annealing temperature for each primer pair was assessed beforehand by using the T<sub>m</sub>-calculator tool from New England Biolabs web site. Amplicons were subsequently purified using the NucleoSpin™ Gel and PCR clean-up kit according to the manufacturer's manual or analyzed by agarose gel electrophoresis.

### **2.3.3 Quickchange PCR**

Quickchange PCR was performed for site-directed mutagenesis of the pTRrep2cap9P1 plasmid. The cap9 G263 forward primer was designed to contain the desired G→A nucleotide substitution in its middle, flanked by 10-30 nucleotides to ensure efficient binding of the primer despite the mismatch. The cap9 G263 reverse primer represents the reverse complement sequence of the cap9 G263 forward primer. The reaction mix was prepared, and the PCR was conducted according to the protocols in Table 2-4.

After the PCR, 10 µl of the reaction mix were mixed with 2 µl Gel Loading Dye and analyzed for correct size and circularity of the plasmid on a 0.8 % agarose gel. The remaining 40 µl were supplemented with

1  $\mu$ l DpnI to digest any unmethylated template plasmid DNA and incubated for 1 h at 37 °C. Subsequently, the reaction was transformed into chemically competent bacteria.

**Table 2-4 Reaction mix and thermo cycler protocol for a standard quickchange PCR**

Reagent	Volume	Step	Temp [°C]	Time	Cycles
10x PfuUltra™ II reaction buffer	5 $\mu$ l	Denaturation	98	2 min	1
dNTPs (10 mM)	2 $\mu$ l	Denaturation	95	60 s	17
cap9 G263 forward (125 ng/ $\mu$ l)	1 $\mu$ l	Annealing	50	40 s	
cap9 G263 reverse (125 ng/ $\mu$ l)	1 $\mu$ l	Elongation	68	10 min	
PfuUltra™ II Fusion High-fidelity	1 $\mu$ l	Elongation	68	10 min	1
pTRrep2cap9P1 (25 ng/ $\mu$ l)	1.0 $\mu$ l	Storage	4	$\infty$	1
H <sub>2</sub> O	39 $\mu$ l				

### 2.3.4 Agarose gel electrophoresis

To obtain 0.8-2 % agarose gels for gel electrophoresis, 0.8-2 g of ultra-quality agarose powder were weighed into an Erlenmeyer flask and heated in 100 ml 1x TAE buffer in a microwave until the agarose was completely dissolved. The flask with the dissolved agarose was cooled under running water with constant swirling and was subsequently supplemented with 200 ng/ml ethidium bromide. The agarose solution was transferred to a gel casting system with an inserted comb and cooled until complete polymerization. The gel was placed in a gel electrophoresis chamber and submerged in 1x TAE buffer. 10-50  $\mu$ l of the sample were loaded depending on gel pocket size, and 5  $\mu$ l 1 kb Plus DNA ladder was used as a standard. Gel electrophoresis was conducted for 0.5-1.5 h at 100-130 V. Separated DNA pieces were visually analyzed using a GelDoc Gel Imaging System or cut from the gel using a clean scalpel. Gel pieces were transferred to a fresh 2 ml reaction tube, and DNA was isolated using the NucleoSpin™ Gel and PCR CleanUp Kit, according to the manufacturer's manual.

### 2.3.5 Ligation independent cloning (LIC) for sgRNA expression plasmids

For CRISPR/Cas9 mediated knockout generation, sgRNAs sequences were taken from the "Brunello" sgRNA library [178]. The sgRNA sequences were incorporated in cloning oligonucleotides and cloned into the pMini\_U6\_gRNA\_CMV\_Puro\_T2A\_Cas9 vector using LIC. To prepare the vector for cloning, it needs to be cut and "chewed" to generate single-stranded DNA overhangs as described in Schmid-Burgk et al. [179].

To integrate the sgRNA into the recipient vector, the prepared vector was diluted with reaction buffer, H<sub>2</sub>O, and the short universal reverse strand oligo. Gene-specific sgRNA oligonucleotides were diluted to a final concentration of 0.25  $\mu$ M, and 2.5  $\mu$ l diluted oligonucleotide were mixed with 2.5  $\mu$ l of diluted vector and ligated in a PCR cycler following the protocol in Table 2-5. The 5  $\mu$ l of LIC reaction mix were transformed in chemically ultra-competent XL10-Gold<sup>®</sup> bacteria, and the plasmid was propagated in chemically competent bacteria and isolated. Integration and the correct sequence of the target sgRNA were verified by Sanger sequencing.

**Table 2-5 Reaction mix and thermo cycler protocol for the LIC of an sgRNA oligonucleotide with recipient vector**

Reagent	Volume	Step	Temp [°C]	Time [s]	Cycles
10x NEB2 buffer	2 $\mu$ l	Denaturation	70	60 s	1
“Chewed” vector	10 $\mu$ l	Annealing	65	60 s	1
Short universal reverse strand oligo (100 $\mu$ M)	0.5 $\mu$ l	Annealing	60	30 min	1
H <sub>2</sub> O	69.5 $\mu$ l	Annealing	55-25	- 1 °C/cycle	29
		Storage	12	$\infty$	1

### 2.3.6 Transformation of competent bacteria

For propagation of plasmids, heat shock transformation of chemically competent bacteria was performed. 30  $\mu$ l of competent bacteria were slowly thawed on ice, plasmid DNA was added, and the mixture was incubated on ice for 25 min. Bacteria supplemented with water instead of plasmid DNA were used as a negative control. Bacteria were heat-shocked for 40 s in a 42 °C water bath and instantly put back on ice for another 3 min. 500  $\mu$ l S.O.C. medium were added, and bacteria were incubated at 37 °C for 30-60 min with constant shaking. Bacteria were spun down for 10 min at 3,000 g, and the supernatant was discarded down to 50-100  $\mu$ l. The pellet was resuspended, plated on LB<sub>Amp</sub> plates, and plates were incubated overnight at 37 °C. When the control plate did not show growth of any colonies, grown colonies were picked from the other plates and transferred to 5 ml (Miniprep), 300 ml (Maxiprep), or 400 ml (Megaprep) of liquid LB<sub>Amp</sub> medium. Liquid cultures were incubated overnight at 37 °C with constant shaking.

### **2.3.7 Plasmid isolation**

Liquid cultures were spun for 20 min at 4,500 g at 8 °C, and the supernatant was discarded. Plasmids were isolated from the pellet using the NucleoSpin™ Plasmid Mini Kit (Minipreps), NucleoBond™ PC 500 Kit (Maxiprep), or the NucleoBond™ PC 2000 Kit (Megaprep) according to the manufacturer's manual. Plasmids were eluted in 30 µl, 100 µl, or 200 µl dH<sub>2</sub>O, respectively, and concentration was measured in a NanoDrop™ spectrophotometer. Plasmid preparations were stored at -20 °C.

### **2.3.8 Sanger sequencing**

Plasmid and PCR amplicon sequences were verified by Sanger sequencing. The sequencing mix was prepared by mixing 15 µl DNA solution (50-100 ng/µl Plasmid DNA or 1-20 ng/µl PCR amplicon) with 2 µl gene-specific sequencing primer and sent to Eurofins Genomics (Ebersberg, GER) for Sanger sequencing.

### **2.3.9 rAAV lysis**

For alkaline lysis of virus particles, 10 µl of virus stock were mixed with 10 µl sterile TE buffer and lysed by addition of 20 µl 2 M NaOH and incubated at 56 °C for 30 min. As a negative control, 10 µl dH<sub>2</sub>O were used instead of virus stock. The mixture was neutralized by the addition of 38 µl 1 M HCl and diluted to 1:1,000 ml with dH<sub>2</sub>O. Diluted lysates were vortexed and stored on ice until titration by qRT-PCR.

### **2.3.10 RNA isolation and complementary DNA (cDNA) synthesis**

Cells were harvested using Trypsin-EDTA solution, washed once with PBS, and pelleted for 5 min at 300 g in a tabletop centrifuge. The supernatant was discarded, and RNA was isolated using the RNeasy® Mini Kit and the QIAshredder kit according to the manufacturer's manual. As indicated in the RNeasy® Mini handbook, an on-column DNase digestion was performed using the RNase-Free DNase Set according to the manufacturer's manual. The RNA was eluted from the column in 20 µl nuclease-free dH<sub>2</sub>O and the concentration was determined by NanoDrop™ analysis. Samples were stored at -80 °C until further analysis. 150 ng to 1 µg total RNA per sample were used for cDNA synthesis using the SuperScript™ II First-Strand Synthesis System according to the manufacturer's manual. Isolated cDNA was stored at -20 °C until use in qRT-PCR.

### 2.3.11 qRT-PCR

#### 2.3.11.1 qRT-PCR from DNA

qRT-PCR was conducted for titration of rAAV vector stocks and analysis of the rABA. For the standard curve, a serial dilution was prepared using the pBSUF3-YFP plasmids at starting concentrations of 30-15 ng/ $\mu$ l, followed by 1:5 dilutions with dH<sub>2</sub>O in 10 steps. The reaction mix was prepared as described in Table 2-6, and 2  $\mu$ l of either diluted virus lysate, standard, or test lysate was added. Reactions were performed in technical duplicates.

**Table 2-6 Reaction mix and light cycler protocol for a standard qRT-PCR**

Reagent	Volume	Step	Temp [°C]	Time	Cycles
2x LightCycler® 480 SYBR Green Master Mix	5 $\mu$ l	Denaturation	95	3 min	1
Gene-specific forward primer (10 $\mu$ M)	1 $\mu$ l	Denaturation	95	10 s	45
Gene-specific reverse primer (10 $\mu$ M)	1 $\mu$ l	Annealing	60	10 s	
rAAV lysate/rABA lysate/cDNA	2 $\mu$ l	Elongation	72	10 s	
dH <sub>2</sub> O	1 $\mu$ l	Melting curve	65-97	+ 2.2 °C/s	1

The qRT-PCR was performed according to the protocol in Table 2-6 in a Light Cycler 480 Instrument II from Roche. An absolute number of molecule copies in the standard curve was calculated as described in the equation below and plotted against cycle threshold (Ct) values to generate a standard curve. Ct values from test samples were interpolated to obtain absolute viral genome copies per ml in the virus stock or absolute viral genome copies per reaction in rABA test samples.

$$\frac{DNA\ copy\ number}{\mu l} = \frac{plasmid\ concentration\ \left[\frac{g}{\mu l}\right]}{molecular\ weight\ of\ plasmid\ \left[\frac{g}{mol}\right]} * Avogadro\ constant\ \left[\frac{1}{mol}\right]$$

#### 2.3.11.2 qRT-PCR from cDNA

qRT-PCR was conducted from cDNA template for gene expression analysis. The reaction mix was prepared as described in Table 2-6, and 2  $\mu$ l of cDNA was added to each reaction. For every sample, two primer pairs were used. The first primer pair was specific for the gene of interest (GOI), while the second one was specific for the housekeeping gene RNA polymerase II (RP11). Reactions were performed in technical duplicates. The qRT-PCR was performed according to the protocol in Table 2-6

in a Light Cycler 480 Instrument II from Roche. Ct values from all samples were extracted and the expression of the GOI relative to housekeeping gene expression was calculated using the  $\Delta$ Ct method according to the following equation

$$\text{Relative expression(GOI)} = 2^{-[\text{Ct value (GOI)} - \text{Ct value(RPII)}]}$$

### 2.3.12 Bicistronic acid (BCA) protein assay

A BCA assay was performed to determine the protein concentration in protein lysates for subsequent SDS polyacrylamide gel electrophoresis (SDS-PAGE) and immunoblot analysis. Cells were harvested using Trypsin-EDTA solution and centrifuged for 5 min at 300 g. The supernatant was discarded, and cells were washed once in PBS with the same centrifugation conditions. The pellet was resuspended in the appropriate amount of western blot lysis buffer supplemented with 1x cOmplete™ EDTA-free protease inhibitor (prepared according to the manufacturer's manual) and incubated for 20 min at 4 °C with constant agitation. Lysates were spun for 10 min at 16,000 g to pellet nucleic acids and cell debris, and the supernatant was carefully transferred to a fresh reaction tube and stored at -20 °C until further analysis. For determination of the protein concentration in the cell lysate, a BCA protein assay was performed using the Pierce™ BCA Protein Assay Kit according to the manufacturer's manual. 25 µl of either test sample or a previously prepared BSA standard (concentrations from 2,000-0 µg/ml) were pipetted into a transparent 96-well plate. The test reagent was prepared by mixing provided buffers A and B in a 50:1 ratio, and 200 µl test reagent was pipetted into each well. The plate was swirled shortly, wrapped in tin foil for light protection, and incubated at 37 °C for 30 min. Absorption of samples was measured in a Infinite<sup>R</sup> M200 microplate reader at 562 nm, and a standard curve was generated by plotting absorption of the standards against their protein concentrations. Test sample concentrations were determined by interpolating their absorption values using the standard curve.

### 2.3.13 SDS-PAGE and immunoblot analysis

Polyacrylamide gels for SDS-PAGE were cast using the Protean<sup>®</sup> Gel casting system. For the preparation of the gels, mixtures for the separation and stacking gel were prepared separately, as described in Table 2-7. TEMED and 10 % APS were only added right before casting of the gel to prevent premature polymerization in the reaction tube. First, the separation gel mixture was filled between the glass plates and overlaid with 1 ml isopropanol to smooth the top edge and prevent air bubble formation. When the gel was polymerized entirely, isopropanol was discarded, and the stacking gel was cast on top of the separation gel, and a comb was inserted to generate pockets. After complete polymerization, the comb was removed, and gels were used for SDS-PAGE.

**Table 2-7 Mastermix for preparation of a 12 % separation gel and stacking gel for acrylamide gel electrophoresis**

Reagent	12 % Separation gel [ml]	Stacking gel [ml]
dH <sub>2</sub> O	1.6	1.4
30 % Acrylamid Mix	2	0.33
1.5 M Tris (pH 8.8)	1.3	-
1 M Tris	-	0.25
10 % SDS	0.05	0.020
10 % APS	0.05	0.020
TEMED	0.002	0.002

For SDS-PAGE sample preparation, 10 µg total protein were mixed with 4x NuPAGE™ sample buffer and dH<sub>2</sub>O to a total volume of 12-18 µl depending on gel pocket size and incubated at 95 °C for 10 min for protein denaturation. Samples were loaded onto the gel in a Mini-Protean® Tetra cell gel electrophoresis chamber next to 4 µl of PageRuler™ pre-stained protein standard. Gel electrophoresis was conducted in TGS Buffer for 1.5 h at 20 mA per gel.

Proteins were blotted onto a 0.45 µm nitrocellulose membrane by wet transfer using the Tetra Blotting Module for the Mini-Protean® Tetra Cell. For every gel, two sponges and Whatman-paper were soaked in 1x Towbin buffer, and the blotting setup was assembled in the following manner: anode, sponge, Whatman-paper, acrylamide gel, nitrocellulose membrane, Whatman-paper, sponge, cathode. Protein transfer was conducted at 0.33 A for 1-1.3 h at RT with a cooling pack to prevent overheating.

After protein transfer, membranes were blocked in 5 % milk in PBS-T for 1 h at RT and incubated in primary antibody diluted in 5 % milk in PBS-T overnight at 4 °C. The next day, the membranes were washed 3x 10 min in PBS-T and incubated with secondary antibody diluted in 5 % milk in PBS-T for 1.5 h at RT. The membrane was rewashed 3x 10 min in PBS-T. Before image acquisition, the membrane was overlaid with SuperSignal™ West Femto Substrate Kit, incubated for 1 min in the dark, and the signal was acquired using a Fusion FX chemiluminescence detector.

## 2.3.14 CRISPR/Cas9 mediated gene targeting

### 2.3.14.1 sgRNA transfection

One day prior to the experiment, U251MG cells were seeded in a 24-well plate and incubated overnight. Cells were transfected with pMini\_U6\_gRNA\_CMV\_Puro\_T2A\_Cas9 containing the respective sgRNA sequence using the Lipofectamine™ Stem Transfection reagent according to the manufacturer's manual. In detail, 500 ng of plasmid DNA were mixed with 2 µl transfection reagent in 50 µl Opti-MEM™, vortexed briefly, and incubated for 30 min at RT. The transfection mix was added dropwise to the well, swirled, and incubated for 24 h at 37 °C. Cells were detached using Trypsin-EDTA and re-seeded in a fresh 12-well plate in selection medium containing 0.8 µg/ml puromycin. Untransfected cells served as negative controls. Transfected cells were selected for 1-3 days or until the control cells died completely. If necessary, the puromycin selection medium was refreshed after 24 h. After complete selection, the medium was changed to regular full DMEM, and cells were allowed to recover and expand.

### 2.3.14.2 Limiting dilution and clonal expansion

Selected cells were harvested using Trypsin-EDTA solution, counted, and seeded in 96-well plates at densities of 1 to 3 cells per well in full DMEM and 5 plates per cell line. Since a reduced surface attachment was expected when knocking out crucial attachment receptors such as  $\alpha$ v or  $\beta$ 5 integrins, 96-well plates were coated with 1 % collagen in dH<sub>2</sub>O for 10 min at RT prior to plating. Plated cells were incubated at 37 °C for 3-4 weeks until clones had expanded in the wells. Grown colonies were identified by visual inspection, pooled on a 96-well plate, and incubated at 37 °C until cells having reached confluency. Plates were duplicated and used for either cell lysis and genotyping or further cell maintenance.

### 2.3.14.3 Genotyping – Miseq

25 µl of cell suspension were transferred to a 96-well PCR plate, and 25 µl of 2x direct lysis buffer supplemented with 200 µg/ml Proteinase K were added to each well. Lysates were mixed by slow resuspension with a multichannel pipet, and lysis was conducted at 65 °C for 10 min, and Proteinase K was inactivated for 15 min at 95 °C.

Lysates were used to analyze genomic target regions for mutations by Illumina sequencing. For this, gRNA target sites were amplified from the lysates using target site-specific primer pairs containing adaptor sequences for binding of barcode primers in a first PCR (Table 2-8). Annealing temperatures for different primer pairs were determined with the T<sub>m</sub>-calculator tool from New England Biolabs.

**Table 2-8 Reaction mix and thermo cycler protocol for the first PCR for MiSeq sample preparation**

First PCR		First PCR			
Reagent	Volume	Step	Temp [°C]	Time	Cycles
5x HF polymerase buffer	1.2 µl	Denaturation	95	3 min	1
dNTPs (10 mM)	0.12 µl	Denaturation	95	30 s	18
Gene-specific primer forward (50 µM)	0.06 µl	Annealing	62	30 s	
Gene-specific primer reverse (50 µM)	0.06 µl	Elongation	72	30 s	
Phusion® polymerase	0.06 µl	Elongation	72	3 min	1
Lysate	1.0 µl	Storage	12	∞	1
H <sub>2</sub> O	3.5 µl				

In the second PCR, target gene-specific amplicons were tagged with barcodes to enable pooling of multiple samples in one sequencing run. Using barcodes, sequencing results can be tracked back to their position on the PCR plate from the first PCR, and hence, their knockout identity can be determined. For the second PCR (Table 2-9), barcoded primers containing Illumina sequencing adaptors that bind to the adaptor sequences introduced in the first PCR were used.

PCR products from the second PCR containing unique barcodes were pooled, and amplicon size was validated by separating 5 µl each of the first and the second PCR in agarose electrophoresis. A part of the remaining pooled sample was also run in an agarose gel electrophoresis, and the region of the gel with the amplicon of the correct size was cut and purified from the gel. PCR products were applied to further purification and Illumina sequencing (performed by the group of Prof. Veit Hornung).

**Table 2-9 Reaction mix and thermo cycler protocol for the second PCR for MiSeq sample preparation**

Second PCR		Second PCR			
Reagent	Volume	Step	Temp [°C]	Time	Cycles
5x HF polymerase buffer	1.2 µl	Denaturation	95	3 min	1
dNTPs (10 mM)	0.12 µl	Denaturation	95	30 s	18
Barcode primer	1.5 µl	Annealing	62	30 s	
Phusion® polymerase	0.06 µl	Elongation	72	30 s	
PCR 1 product	1.0 µl	Elongation	72	7 min	1
H <sub>2</sub> O	2.42 µl	Storage	12	∞	1

The obtained sequencing files were analyzed for frameshift mutations using the OutKnocker.org software [169]. The FastQ files were aligned to the reference WT amplicons, including the used target sequence, and the number of reads was counted. The software output is a read number of a certain sequence at their barcoded position in reference to the WT sequence. Clones with insertions/deletions leading to out-of-frame mutations are colored in red/orange, while clones with in-frame mutations are colored in dark and light blue. All found WT sequences are colored in grey. All clones with exclusively out-of-frame mutation reads, especially those with two different out-of-frame mutations (one for each of both alleles), were considered as knockouts.

Knockout clones with identified frameshift mutations were picked from the 96-well plate, expanded, and used for follow-up experiments.

### 2.3.15 CRISPR/Cas9 knockout screen

#### 2.3.15.1 Lentivirus production

HEK293T cells were seeded in 10 cm dishes to grow to a confluency of 60-70 % overnight. Cell culture medium was aspirated and exchanged for 7 ml fresh full DMEM medium. For transfection, a transfection mix was prepared as described in Table 2-10 and incubated at RT for 30 min. “Transfer plasmid” accounts for a 3<sup>rd</sup> generation lentiviral transfer plasmid that encodes the transgene transmitted by the lentiviral particles. The transfection mix was added dropwise to the dishes, swirled, and incubated at 37 °C for 72 h. Lentiviral particles produced by HEK293T cells were released into the cell culture supernatant.

*Table 2-10 Transfection mix for the production of lentiviral particles*

Reagent	Cas9-Blast Lentivirus Production	GeCKO V2 A-Puro Lentivirus production
pMD2.G plasmid	1 µg	2.5 µg
psPAX2 plasmid	1.5 µg	3.75 µg
“Transfer plasmid”	1 µg	5 µg
X-tremeGene™ 9 DNA transfection Reagent	8 µl	33.75 µl
Opti-MEM™	up to 250 µl	Up to 800 µl

#### 2.3.15.2 Generation of U251MG-Cas9 stable cell line

U251MG cells were seeded in 6-well plates and incubated overnight. Supernatant from one 10 cm dish of virus-producing HEK293T cells was collected, filtered through a 0.45 µm filter, and polybrene was added at a concentration of 8 µg/ml. Cas9-Blast lentivirus was diluted 1:2 in full DMEM. The medium from U251MG cells was removed, diluted Cas9-Blast lentivirus was added and incubated at 37 °C for 24 h. The remaining virus stock was stored at -80 °C for later use. After incubation, cells were harvested and re-seeded in medium containing 20 µg/ml blasticidin. As controls, one well of untransduced cells was cultured in selection medium. U251MG-Cas9 cells were selected for three days or until all untransduced cells died under selection pressure, and transduced cells were further cultured and propagated in full DMEM for further experiments. Successful integration and expression of the transgene were evaluated by PCR, qRT-PCR, or immunoblot.

#### 2.3.15.3 Lentivirus sgRNA library titration

For the generation of the stable U251MG-Cas9-GeCKO cell pool, the produced sgRNA library lentivirus was titrated to determine an MOI of 0.4 for the target cell transduction. U251MG-Cas9 cells were seeded in 6-well plates and incubated overnight. The next day, cells were supplemented with varying dilutions of sgRNA library lentivirus stock ranging from 1/10 to 1/40 in 2 ml total medium supplied with 8 µg/ml polybrene. The cells were transduced for 24 h at 37 °C. Subsequently, the medium was removed, cells were washed, detached from the plate using Trypsin-EDTA, and re-plated in a new 6-well plate in selection medium containing 0.8 µg/ml puromycin. Untransduced U251MG-Cas9 cells served as a negative control. Cells were incubated in selection medium for three days and until all control cells have died due to puromycin selection. Subsequently, cells in all wells were harvested, and surviving cells were counted with a counting chamber. The amount of virus stock that yielded 40 % surviving cells after the selection was chosen for the following experiments.

#### 2.3.15.4 Generation of U251MG-Cas9-GeCKO cell pool

U251MG-Cas9 cells were seeded in 6-well plates and incubated overnight. To ensure that every sgRNA is represented at least 400x in the cell pool, 90 wells were seeded to obtain a minimum of  $6.1 \times 10^7$  cells on the day of transduction. The next day, cells were transduced with GeCKO v2 A lentivirus library diluted 1:50 in full DMEM and supplemented with 8 µg/ml polybrene and cells incubated for 24 h at 37 °C. Three wells remained untransduced as controls. After lentivirus transduction, all wells were harvested, pooled, and homogenously re-seeded in selection medium containing 0.8 µg/ml puromycin. Untransduced control cells were not pooled but also re-seeded in selection medium. Cells were selected for three days. After successful selection, surviving U251MG-Cas9-GeCKO cells were

harvested, pooled, and equally distributed in T175 flasks for further maintenance. Ten vials with  $6 \times 10^6$  cells each (100x library coverage) were pelleted and frozen for gDNA isolation. These samples served as a quality control (QC) to analyze the distribution of sgRNAs within the population.

#### 2.3.15.5 CRISPR/Cas9 screen

U251MG-Cas9-GeCKO cells were seeded in 18x 10 cm dishes one day prior to the experiment for the actual screen. The next day, nine dishes were exposed to rAAV9P1 at MOI 100,000 and incubated for 48 h at 37 °C. The second set of nine dishes was not exposed to rAAV9P1 as a control. After incubation, cells were harvested, pooled, and centrifuged for 5 min at 300 g. The supernatant was discarded, and the pellet of untransduced cells (C) was stored at -20°C until further analysis. Transduced cells were resuspended in PBS supplemented with 2 mM EDTA and 2 % (w/v) BSA and sorted on a BD FACSAria III for eYFP negative cells (Neg). Gates were assigned with untransduced cells as reference. The sorted cells were collected, centrifuged for 5 min at 300 g, and the pellet was stored at -20 °C until further analysis.

The gDNA was isolated from all frozen pellets (QC, C, Neg) by Phenol-Chloroform extraction. Cell pellets were resuspended in 300-500  $\mu$ l TELysis buffer supplemented with 200  $\mu$ g/ml RNase A and 625 ng/ml Proteinase K and lysed overnight at 60 °C. Proteinase K was inactivated by incubation at 95 °C for 2 min. Subsequently, one volume of phenol was added, and the tube was inverted 5-8 times. The samples were centrifuged for 5 min at 10,000 g and 4 °C until the aqueous phase has separated from the organic phase. The aqueous phase was carefully transferred to a fresh tube and supplemented with one volume of phenol/chloroform/isoamyl alcohol, followed by inverting 5-8 times and another centrifugation step. The aqueous phase was again transferred to a fresh tube, one volume of chloroform was added, inverted, and centrifuged. In the next step, the upper aqueous phase was mixed with 2.5 volumes of 100 % ethanol, the tube was inverted, and incubated at -20 °C overnight to precipitate the DNA. The DNA was pelleted by centrifugation for 5 min at 10,000 g and 4 °C, the supernatant was discarded, and the DNA was resuspended in 30-50  $\mu$ l sterile, HPLC grade H<sub>2</sub>O. The gDNA was dissolved for 30 min at 55 °C and subsequently stored at -20 °C. The concentration of gDNA was determined by NanoDrop™ analysis.

The amplicon library for amplicon sequencing was generated by performing two subsequent PCRs. In the first PCR, the region in the host cell genome with integrated sgRNA was amplified with universal primers in the U6 promoter and the sgRNA scaffold region. These regions are integrated into the host cell genome regardless of the sgRNA sequence. Each reaction contained 5  $\mu$ g gDNA, and 32 separate reactions were prepared per population (QC, C, Neg) to ensure representation of at least 400x the sgRNA library (Table 2-11). The PCR products were purified using the NucleoSpin™ Gel and PCR Clean-

up Kit according to the manufacturer's manual, eluted, and pooled. In a second PCR, barcodes for the IonTorrent NGS were attached to the amplicons from the first PCR with at least 7 independent reactions per population (QC, C, Neg; Table 2-12). PCR products were again purified, eluted, and pooled. The amplicon concentration was determined with the Qubit™ dsDNA BR Assay Kit according to the manufacturer's manual in a Qubit™ Fluorometer and sent for NGS by PrimBio (Exton, PA, USA).

**Table 2-11 Reaction mix and thermo cycler protocol for amplification of sgRNA integration sites from gDNA**

First PCR		First PCR			
Reagent	Amount	Step	Temp [°C]	Time	Cycles
5x HF polymerase buffer	10 µl	Denaturation	95	3 min	1
dNTPs (10 mM)	1 µl	Denaturation	95	30 s	18
Primer NGS short forward (10 µM)	1 µl	Annealing	60	30 s	
Primer NGS short reverse (10 µM)	1 µl	Elongation	72	30 s	
Phusion® Polymerase	0.5 µl	Elongation	72	3 min	1
gDNA	5 µg	Storage	12	∞	1
H <sub>2</sub> O	up to 50 µl				

**Table 2-12 Reaction mix and thermo cycler protocol for indexing and barcoding of amplicon library**

Second PCR		Second PCR			
Reagent	Volume	Step	Temp [°C]	Time	Cycles
5x HF polymerase buffer	10 µl	Denaturation	95	3 min	1
dNTPs (10 mM)	1 µl	Denaturation	95	30 s	18
NGS barcode primer forward (10 µM)	1 µl	Annealing	60	30 s	
Universal NGS primer reverse (10 µM)	1 µl	Elongation	72	30 s	
Phusion® Polymerase	0.5 µl	Elongation	72	3 min	1
PCR 1 product	10 µl	Storage	12	∞	1
H <sub>2</sub> O	40 µl				

Analysis of the sequencing data was performed by Dr. Joel Schick (Helmholtz Center Munich) and Dr. Thomas Werner (Scientific & Business Consulting). From the sequencing data, detected sgRNA sequences in the different populations were matched to their respective protein-coding genes. Based on the design of the sgRNA library each protein-coding gene is targeted by three individual sgRNAs but usually only one of the three sgRNAs was efficient in knockout induction. To compensate for these

differences between genes, downstream analyses were performed with the one best-performing sgRNA per gene as determined by most reads detected in the sequencing. The enrichment of sgRNAs in the eYFP-negative sorted population in comparison to the unsorted control population was calculated as fold increase of sgRNA reads. To increase the biological significance of the obtained results the minimum number of reads for an sgRNA to be considered in the comparison was set to 100 and the lower threshold of fold increase was set to 2fold. The obtained list of enriched sgRNAs in the YFP-negative sorted population was subjected to pathway, tissue, gene ontology (GO-) and medical subject headings (MeSH-) Term analysis using the GeneRanker tool (Genomatix AG, Munich).

## **2.4 *In silico* modelling and alignments**

Alignment of the VP3<sub>AAV9</sub> and VP3<sub>AAV9P1</sub> amino acid sequences was performed with the T-coffee online tool [173]. The coordinates of the VP3<sub>AAV9P1</sub> model were generated using wild-type AAV9 protein data bank (PDB) coordinates (PDB model ID: 3UX1) as template in the Phyre2 online tool [170]. Multimer assembly of AAV9P1 was generated using the SWISS-MODEL online tool [171, 172]. Cartoon representation of the VP3-monomers and 60-mer, structural alignments, and depth-cue surface representations were generated using the UCSF-ChimeraX software [174, 175].

## **2.5 Transmission electron microscopy**

Sample preparation and image acquisition were performed by the group of Prof. Andreas Klingl. For the analysis via transmission electron microscopy, samples were applied to carbon-coated copper grids and negatively stained with 2% uranyl acetate as described previously [180]. After air drying, the samples were investigated at 80 kV with a Zeiss EM 912, equipped with an integrated OMEGA filter in the zero-loss mode. Images were acquired using a 2k x 2k CCD camera (TRS Tröndle Restlichtverstärkersysteme, Moorenweis, Germany) with the respective software package. Images of particles were analyzed using the ImageJ image processing software.

## **2.6 Statistical analysis**

The GraphPad Prism 9.0.2 software was used for all statistical analyses. Individual values from all experimental replicates were entered into the software and statistical significance of differences was assessed by using a one-way or two-way ANOVA. In the case of the influence of multiple factors, Sidak's correction for multiple comparisons was employed. Data is represented as mean plus standard error of the mean (SEM) of two to three independent experiments.; \*  $p \leq 0.05$ ; \*\*  $p \leq 0.01$ ; \*\*\*  $p \leq 0.001$ ; Not significant (ns)  $p > 0.05$ .

### 3 Results

#### 3.1 rAAV9P1 transduces human astrocytic cell lines more efficiently than rAAV9 and more selectively than rAAV2

The rAAV vector rAAV9P1 was generated from the naturally occurring serotype AAV9 by peptide display. This novel variant was identified in a crude lysate screen and was shown to efficiently and selectively transduce astrocytes even in co-culture with neurons [147]. Vectors from various AAV serotypes have been shown to efficiently transduce different cell lines *in vitro*. Here, the efficiency and selectivity profile of rAAV9P1 vectors was compared with those of rAAV9 and rAAV2 vectors in side-by-side transduction experiments on four human cell lines. In all experiments, rAAV vectors containing sc genomes were used. Optimal comparability of the different vectors and high transgene expression was ensured with an eYFP transgene under the control of a ubiquitous CMV promoter. Figure 3-1 A shows the analysis of transduced cells for eYFP expression by flow cytometry 48 h after exposure to rAAV vectors. In the initial experiment, the neural stem cell line HNSC.100 and the glioblastoma cell line U251MG were chosen as representatives for astrocytic cell lines, as well as the two frequently used cell lines HEK293T and HeLa. As expected, rAAV9P1 vectors transduced proliferating HNSC.100 as well as U251MG cells with high efficiencies. In contrast, the non-astrocytic cell lines HEK293T or HeLa cells were not efficiently transduced by rAAV9P1 vectors with transduction efficiencies below 25 % in both cell lines. rAAV9 vectors failed to transduce any of the investigated cell lines efficiently. rAAV2 vectors showed a strong and unselective transduction pattern on all cell lines irrespective of their origin tissue, with mean transduction of over 80 %. Taken together, rAAV9P1 vectors transduce human astrocytic cells much more efficiently than rAAV9 vectors and display a higher selectivity for astrocytic cells in comparison to rAAV2 vectors.

In this experimental setup, the transduction efficiencies were analyzed by monitoring the expression of the eYFP transgene delivered to the target cell by rAAV vectors. To ensure that the observed differences in transduction efficiency are evoked by changes of cell surface attachment rather than by alterations of post-entry processes such as intracellular trafficking, uncoating, or gene expression, a cell surface rABA was performed. This assay allows the binding of rAAV vector particles to the cell surface at 4 °C without effective transduction of the cells. Cells with attached virus particles were harvested, lysed, and the number of rAAV vector genomes was measured by qRT-PCR. To compare the binding efficiencies, U251MG cells were analyzed in the rABA for their binding of rAAV9P1, rAAV9, and rAAV2 virus particles (Fig. 3-1 B). The rABA showed that the number of bound virus particles differs between the three rAAV vectors, with rAAV2 being the most efficient in cell binding. rAAV9P1 particles bound to the cell surface at significantly higher numbers than rAAV9 particles.

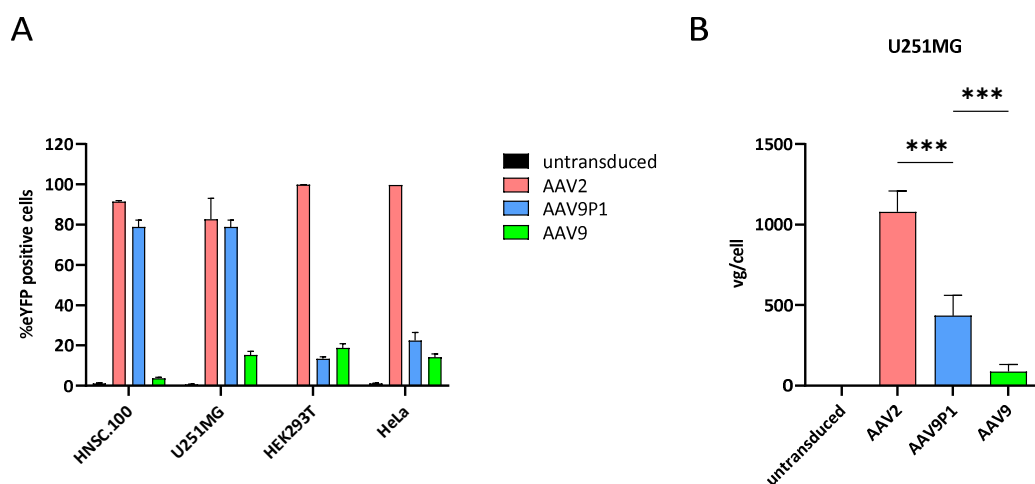


**Figure 3-1 Transduction profile of rAAV2, rAAV9P1, and rAAV9 on different cell lines.** (A) Indicated cell lines were transduced with rAAVs at MOI 10,000, and eYFP expression was determined 48 h post-transduction by flow cytometry. (B) U251MG cells were incubated with rAAVs at MOI 10,000 for 30 min on ice for virus particles to attach to the cell surface without productive transduction. Cells were washed, lysed, and the number of bound virus particles was analyzed by detecting vector genomes (vg) per cell by qRT-PCR. Data depicts mean + SEM of three independent experiments. Statistical significance was determined by One-way ANOVA. \*\*\*  $p \leq 0.001$ , \*\*  $p \leq 0.01$ , \*  $p \leq 0.05$ , ns  $p > 0.05$

### 3.2 The P1 peptide is located on an exposed position in the capsid

While rAAV9P1 and rAAV9 vectors are very closely related they show significant differences in effective transduction of and cell surface binding to astrocytic cells. The efficiency of rAAV particles to bind to cells is dependent on the interaction of the AAV capsid with a specific subset of receptor molecules on the target cell. To detect parts of the rAAV9P1 capsid that have a high potential to be involved in binding astrocyte selective receptor molecules, the sequence and structure of the capsid proteins VP1, VP2, and VP3 of AAV9P1 were compared with AAV9. Figure 3-2 shows the sequence alignment of the VP1 protein of AAV9P1 (VP1<sub>AAV9P1</sub>), AAV9 (VP1<sub>AAV9</sub>), and the prototypical AAV2 (VP1<sub>AAV2</sub>). Due to the structure and ORF organization of the AAV *cap* gene (see Figure 1-3), the sequences of the VP2<sub>AAV9</sub> (starting at VP1<sub>156</sub>) and VP3<sub>AAV9</sub> (starting at VP1<sub>219</sub>) proteins are contained within the VP1<sub>AAV9</sub> protein. In the sequence alignment, identical regions are indicated in grey, while mismatches are displayed on a white background. The VP1<sub>AAV9P1</sub> differs from the VP1<sub>AAV9</sub> sequence in only 14 amino acid residues between Q<sub>585</sub> and A<sub>600</sub>. The seven amino acids RGDGLGS (dark blue background) represent the inserted P1 peptide, while the flanking amino acids are altered due to the cloning process. The insertion site of the peptide is located in the VP3 region, rendering it present in all members of the cap proteins. In addition, the P1 peptide is inserted in VR-VIII, which is associated with high inter-serotype sequence variability [150].

```

AAV9P1 1 MAADGYLPDWLEDNLSEGIREWALKPGAPQPKANQQHQDNARGLVLPGYKYLGPGNGLDKGEPVNAADAAALEHDKAYDQQLKAGDNPY
AAV9 1 MAADGYLPDWLEDNLSEGIREWALKPGAPQPKANQQHQDNARGLVLPGYKYLGPGNGLDKGEPVNAADAAALEHDKAYDQQLKAGDNPY
AAV2 1 MAADGYLPDWLEDLTLSEGI RQWWKLPKPGPPFPKPAERHKDDSRGLVLPGYKYLGPFNGLDKGEPVNEADAAALEHDKAYDRQLDSDGNPY

AAV9P1 91 LKYNHADAEFQERLKEDTSFGGNLGRAVFOAKKRLLLEPLGLVEEAAKTAPGKKRPVEQSPQEPDSSAGIGKSGAQPAKKRLNFGQTDTE
AAV9 91 LKYNHADAEFQERLKEDTSFGGNLGRAVFOAKKRLLLEPLGLVEEAAKTAPGKKRPVEQSPQEPDSSAGIGKSGAQPAKKRLNFGQTDTE
AAV2 91 LKYNHADAEFQERLKEDTSFGGNLGRAVFOAKKRVLLEPLGLVEEVPKTA PGKKRPVEHSEVEPDSSSGTGKAGQQPAKKRLNFGQTDGAD

AAV9P1 181 SVPDFQPIGEPAAAPSGVGLTMSAGGGAPVADNNEGADGVGSSSGNWHCDSQWLGDRVITTTSTRTWALPTYNNHLYKQISNSTSGGSSN
AAV9 181 SVPDFQPIGEPAAAPSGVGLTMSAGGGAPVADNNEGADGVGSSSGNWHCDSQWLGDRVITTTSTRTWALPTYNNHLYKQISNSTSGGSSN
AAV2 181 SVPDFQPLGQPPAAPSGGLGTNTMATGSGAPMADNNEGADGVGSSSGNWHCDSTWMGDRVITTTSTRTWALPTYNNHLYKQISSQ--SGASN

AAV9P1 271 DNAYFGYSTPWGYPDFNRFHCHFSPRDWQRLINNNWGRPKRLNFKLFNIQVKEVTDNNGVKTIANNLSTVQVFTDSDYQLPYVLGSAH
AAV9 271 DNAYFGYSTPWGYPDFNRFHCHFSPRDWQRLINNNWGRPKRLNFKLFNIQVKEVTDNNGVKTIANNLSTVQVFTDSDYQLPYVLGSAH
AAV2 271 DNAYFGYSTPWGYPDFNRFHCHFSPRDWQRLINNNWGRPKRLNFKLFNIQVKEVTDNDGTTTIANNLSTVQVFTDSEYQLPYVLGSAH

AAV9P1 361 EGCLPPFPADVFMI PQYGYLTLNDGSAVGRSSFFCYLEYFQSMLRTGNNFQFSYEFENVFFHSSYAHSQSLDRMLNPLIDQYLYL LSKT
AAV9 361 EGCLPPFPADVFMI PQYGYLTLNDGSAVGRSSFFCYLEYFQSMLRTGNNFQFSYEFENVFFHSSYAHSQSLDRMLNPLIDQYLYL LSKT
AAV2 361 QGCLPPFPADVFMI PQYGYLTLNNGSQAVGRSSFFCYLEYFQSMLRTGNNFQFSYEFENVFFHSSYAHSQSLDRMLNPLIDQYLYL LSRIT

AAV9P1 451 INSGGQNNQ--TLKFSVAGPSNMAVQGRNYIPGPSYRQQRVSTTVTQNNNSEFAWPGASSWALNGRNSLMNPGPAMASHKEGEDRFFPLSG
AAV9 451 INSGGQNNQ--TLKFSVAGPSNMAVQGRNYIPGPSYRQQRVSTTVTQNNNSEFAWPGASSWALNGRNSLMNPGPAMASHKEGEDRFFPLSG
AAV2 449 NTPSGTTTQSR LQFSQAGASDI DQSRNWLPGPCYRQQRVSKTSADNNNSEYSGATKYHLNGRDSL VNNPGPAMASHKDEEKFPPQSG

AAV9P1 540 SLIFGKQGTGRDNVDADKVMITNEEEIKTTNPVATESYGVQVATNHQGSQAQAQTGWVQNGI LPGMVWQDRD VYLQGP IWA
AAV9 540 SLIFGKQGTGRDNVDADKVMITNEEEIKTTNPVATESYGVQVATNHQSAQ-----AQAGTGWVQNGI LPGMVWQDRD VYLQGP IWA
AAV2 539 VLIFGKQGTGRDNVDIEKVMITDEEEIRTTNPVATEQYGSVSTNLQRGN-----RQAATADVNTQGV LPGMVWQDRD VYLQGP IWA

AAV9P1 630 KIPHTDGNFHPSPMLGGFGMKHPPPQILIKNTPVPADPPTAFNKDKLNSFITQYSTGQVSV EIEWELQKENS KRWNPEIQYTSNYKSN N
AAV9 621 KIPHTDGNFHPSPMLGGFGMKHPPPQILIKNTPVPADPPTAFNKDKLNSFITQYSTGQVSV EIEWELQKENS KRWNPEIQYTSNYKSN N
AAV2 620 KIPHTDGHFHPSPMLGGFGLKHPPPQILIKNTPVPANPSTTF SAAKFASFITQYSTGQVSV EIEWELQKENS KRWNPEIQYTSNYN KSVN

AAV9P1 720 VEFVNTTEGVYSEPRPIGTRYLTRNL
AAV9 711 VEFVNTTEGVYSEPRPIGTRYLTRNL
AAV2 710 VDFVDTTEGVYSEPRPIGTRYLTRNL

```

**Figure 3-2 Sequence alignment of the AAV9P1, AAV9, and AAV2 capsid proteins.** Sequences of the AAV VP1 (aa 1-745), VP2 (aa 157-745), and VP3 (aa 220-745) proteins are aligned. Identical sequence regions are indicated with grey background, while mismatches are indicated with white background. The inserted P1 peptide is colored with a dark blue background. Published binding sites in the AAV9 sequence for galactose and LamR are highlighted in yellow and teal, respectively. Amino acid numbering refers to standard VP1 numbering. In the AAV2 sequence, HSPG binding residues (light blue) and predicted AAVR binding sites according to Meyer et al. (magenta) are indicated [181]. Roman numbers and arrows show variable regions VR-I to VR-IX in the VP1<sub>AAV9</sub> sequence.

The fully assembled AAV capsid is formed by the interaction of the cap proteins VP1, VP2, and VP3 in a stoichiometry of 1:1:10, and it has been shown that capsid assembly can be achieved with VP3 alone in the absence of the other two cap forms [72]. This indicates that the structural integrity of the VP3 protein is crucial for capsid formation and functioning.

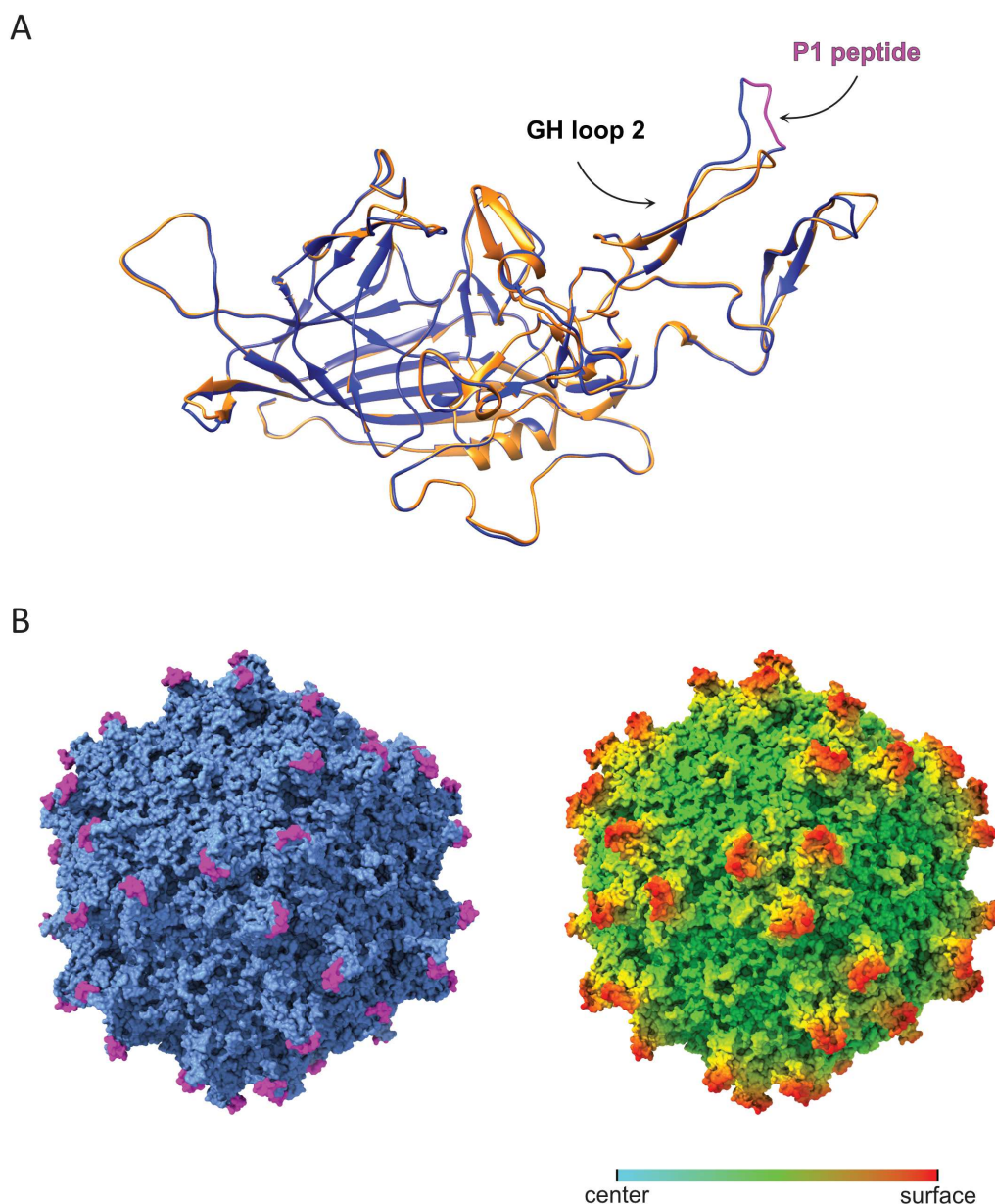


**Figure 3-3 Structural analysis of VP3<sub>AAV9P1</sub>.** (A) Alignment of the predicted VP3<sub>AAV9P1</sub> structure (blue) with the published crystal structure of VP3<sub>AAV9</sub> (PDB ID 3UX1, orange). The insertion site of the P1 peptide, which is located on the GH loop 2, is indicated in magenta. (B) Predicted assembly of the VP3<sub>AAV9P1</sub> 60mer. Left: AAV9P1 virion with P1 peptide highlighted in magenta. Right: AAV9P1 virion with radial coloring corresponding to radial depth cueing. The color transition from blue to red indicates amino acid localization from surface to center.

To assess whether the introduction of the P1 peptide may influence VP3<sub>AAV9P1</sub> folding and polymerization, modeling of the VP3<sub>AAV9P1</sub> protein monomer and 60mer was performed with Phyre2 and subsequently aligned with the published structure of the VP3<sub>AAV9</sub> protein. The structural alignment showed that the P1 peptide did not influence the folding of the VP3<sub>AAV9P1</sub> monomer and that the secondary and tertiary structure shows high identity with VP3<sub>AAV9</sub> (Fig. 3-3 A). In addition, the modeling showed that the modified VP3<sub>AAV9P1</sub> is still capable of assembling into the whole capsid (Fig. 3-3 B).

It has been shown for several AAV serotypes that they can interact with surface receptor molecules via specific domains of the VP3 protein. Therefore, we assessed whether the P1 peptide has a high probability of engaging in receptor binding of rAAV9P1. In Figure 3-3 A, the P1 peptide is depicted in magenta and is shown to induce the formation of a bulge in the so-called GH loop 2. This loop contributes to the protrusions from the capsid surface around the 3-fold axis of symmetry by interacting with the GH loops from two additional VP3 subunits. The comparison of the localization of the P1 peptide on the fully assembled capsid with the coloring of the capsid according to surface depth cueing revealed that the P1 peptide co-localizes with the reddest, and therefore most surface exposed, regions of the assembled capsid (Fig. 3-3 B). The sequence of the P1 peptide, including its flanking amino acid residues, contains several relatively small amino acids like glycine that increase the flexibility of this loop and decrease the rigidity of the pocket formed at the 3-fold axis. Taken together, the P1 peptide is located in an exposed position on the capsid surface and displays favorable characteristics for interaction with receptor molecules.

This *in silico* finding was further corroborated by the conduction of transmission electron microscopy analysis of rAAV vector stocks purified by iodixanol gradient. rAAV9P1 particles displayed the typical hexagonal shape and did not differ in their morphology from analyzed virus particles from rAAV2 or rAAV9 vector stocks (Fig. 3-4 A). From each rAAV variant, 100 particles were analyzed for their diameter, which revealed no significant difference between rAAV9P1 (26.16 nm) and rAAV9 (25.73 nm) or rAAV2 (26.68 nm) (Fig. 3-4 B).

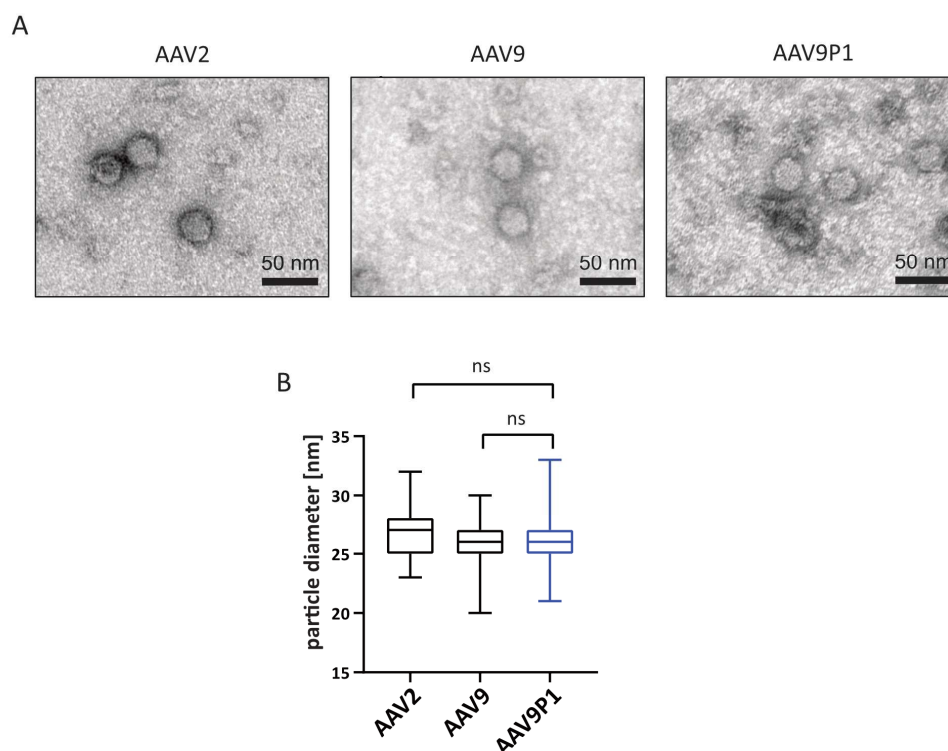


**Figure 3-4 Analysis of rAAV9P1 particle morphology and size in comparison to rAAV2 and rAAV9.** Samples from rAAV vector stocks purified by iodixanol gradient were analyzed by transmission electron microscopy. (A) Samples pictures of rAAV2, rAAV9P1, and rAAV9 vector particles. Scale bar indicates 50 nm. (B) Per rAAV vector production, the diameter of 100 particles was analyzed. Data depicts mean  $\pm$  SEM. Statistical significance was determined by One-way ANOVA. \*\*\*  $p \leq 0.001$ , \*\*  $p \leq 0.01$ , \*  $p \leq 0.05$ , ns  $p > 0.05$

### 3.3 Subunits of RGD-binding integrins are differentially expressed on astrocytes and neurons

The P1 peptide originates from a random peptide library used to perform genetic modification of the capsid genes from different AAV serotypes by peptide display to redirect the tropism of rAAV vectors to different cell types. So far, this peptide has been used in the capsid of an AAV2 derived vector to increase transduction of breast cancer cells by Michelfelder et al, but its potential proteinaceous interaction partner is unknown [122]. To identify possible interaction partners of this peptide, we focused on the harbored RGD amino acid motif in the N-terminal end of the P1 peptide. The amino acid sequence arginine (R), glycine (G), and aspartic acid (D) is a common part of extracellular matrix (ECM) proteins and serves as a minimal recognition motif for a subset of integrins [182]. Integrins are transmembrane proteins that are expressed rather ubiquitously on the animal cell surface. Integrins always consist of an  $\alpha$ - and a  $\beta$ -subunit, forming a functionally active heterodimer (Fig. 4-1 A). The specific integrin combinations that have been described to interact with the RGD-motif are  $\alpha\beta1$ ,  $\alpha\beta3$ ,  $\alpha\beta5$ ,  $\alpha\beta6$ ,  $\alpha\beta8$ ,  $\alpha11\beta1$ ,  $\alpha5\beta1$ , and  $\alpha8\beta1$  (Fig. 4-1 B) [183, 184].

Although the integrin landscape differs between cell types, no single astrocyte-specific integrin has been identified so far. Since rAAV9P1 vectors were shown to efficiently discriminate between astrocytic and neuronal cells in terms of transduction [147], the differential expression of integrin subunits involved in RGD-binding on astrocytes and neurons was analyzed using a published RNA sequencing dataset. This dataset was generated by the laboratory of Dr. Ben Barres using antibody-assisted cell separation and subsequent RNA isolation and next-generation sequencing [185].

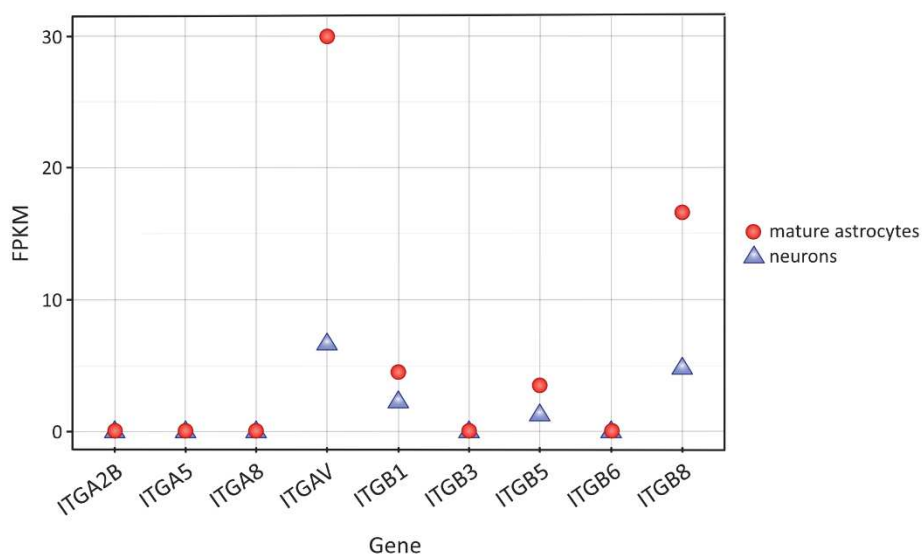


**Figure 3-5 Expression levels of genes for integrin subunits in mature astrocytes and neurons.** Analysis of the differential expression of integrin subunits that are known to form RGD-binding heterodimers in mature astrocytes and neurons. This graph was generated by re-analysis of a published RNA sequencing dataset from antibody-assisted cell sorting of human CNS cells published by Zhang et al. in 2016 [185]. Mature astrocytes and neurons were sorted using anti-HepaCAM and anti-Thy1 antibodies, respectively. FPKM (fragments per kilobase per million mapped reads) depicts the relation between detected reads that are mapped to the respective gene and the total number of mapped reads in the library while also considering the gene length for normalization.

In this analysis, the data obtained from mature astrocytes was compared with neurons (Fig. 3-5). The analysis revealed that among the investigated  $\alpha$ -subunits, only  $\alpha_v$  was expressed at detectable levels in both neurons and astrocytes and was expressed in astrocytes at more than 4-fold higher levels than in neurons. Among the  $\beta$ -subunits,  $\beta_8$  shows the most striking difference between astrocytes and neurons, with more than 3-fold higher expression levels in astrocytes. Expression levels of Integrin subunit  $\beta_1$  and  $\beta_5$  are about twice as high in astrocytes than in neurons, while  $\beta_3$  and  $\beta_6$  are not expressed at detectable levels in either cell type. These results demonstrate that specific integrin subunits are expressed at higher levels in astrocytes than in neurons.

### **3.4 rAAV9P1 transduction is prevented by pharmacological inhibition of $\alpha\beta3$ and $\alpha\beta5$ or $\alpha\beta8$**

To investigate the involvement of integrin heterodimers formed by these subunits in rAAV9P1 transduction, the effects of selected integrin ligands on the transduction behavior of rAAV9P1 in human astrocytes were analyzed. The subclass of RGD-binding integrins shares the characteristic that they use the RGD sequence as a minimal recognition motif for protein binding. However, integrin heterodimers can discriminate between different RGD-containing ligands. This discrimination is promoted by the amino acids flanking the RGD motif but also by the conformation of the motif within the protein structure [186]. Research is ongoing to develop peptides with stable conformations to selectively bind to a specific integrin heterodimer for efficient and selective inhibition.

One selective inhibitor is the cyclic pentapeptide cilengitide (CGT) that is described to bind to  $\alpha\beta3$  and  $\alpha\beta5$  integrins in the nanomolar range and occupies their RGD binding site [187]. To investigate the effect of blocking  $\alpha\beta3$  and  $\alpha\beta5$  on the transduction efficiency of rAAV9P1 HNSC.100 and U251MG cells were treated with different concentrations of CGT and simultaneously exposed to rAAV9P1 or rAAV2 vectors. Transduction efficiency was measured 48 h after vector addition by flow cytometry analysis of eYFP positive cells. Before the experiment, a range of non-toxic CGT concentrations for treatment of cells was determined by cell CTB assay. The CTB assay showed no effect on the viability of proliferating HNSC.100 cells up to concentrations of 25  $\mu\text{M}$  (Fig. 3-6 B). Viability of U251MG cells was not affected at CGT concentrations  $\leq 2 \mu\text{M}$  and was decreased to  $\leq 50 \%$  at concentrations exceeding 5  $\mu\text{M}$  (Fig. 3-6 F). Therefore, HNSC.100 prol cells were treated with 10, 5, and 0.5  $\mu\text{M}$  and U251MG cells with 2, 1, and 0.5  $\mu\text{M}$  of CGT. The treatment of both cell lines with CGT showed a dose-dependent decrease in transduction efficiency of rAAV9P1.

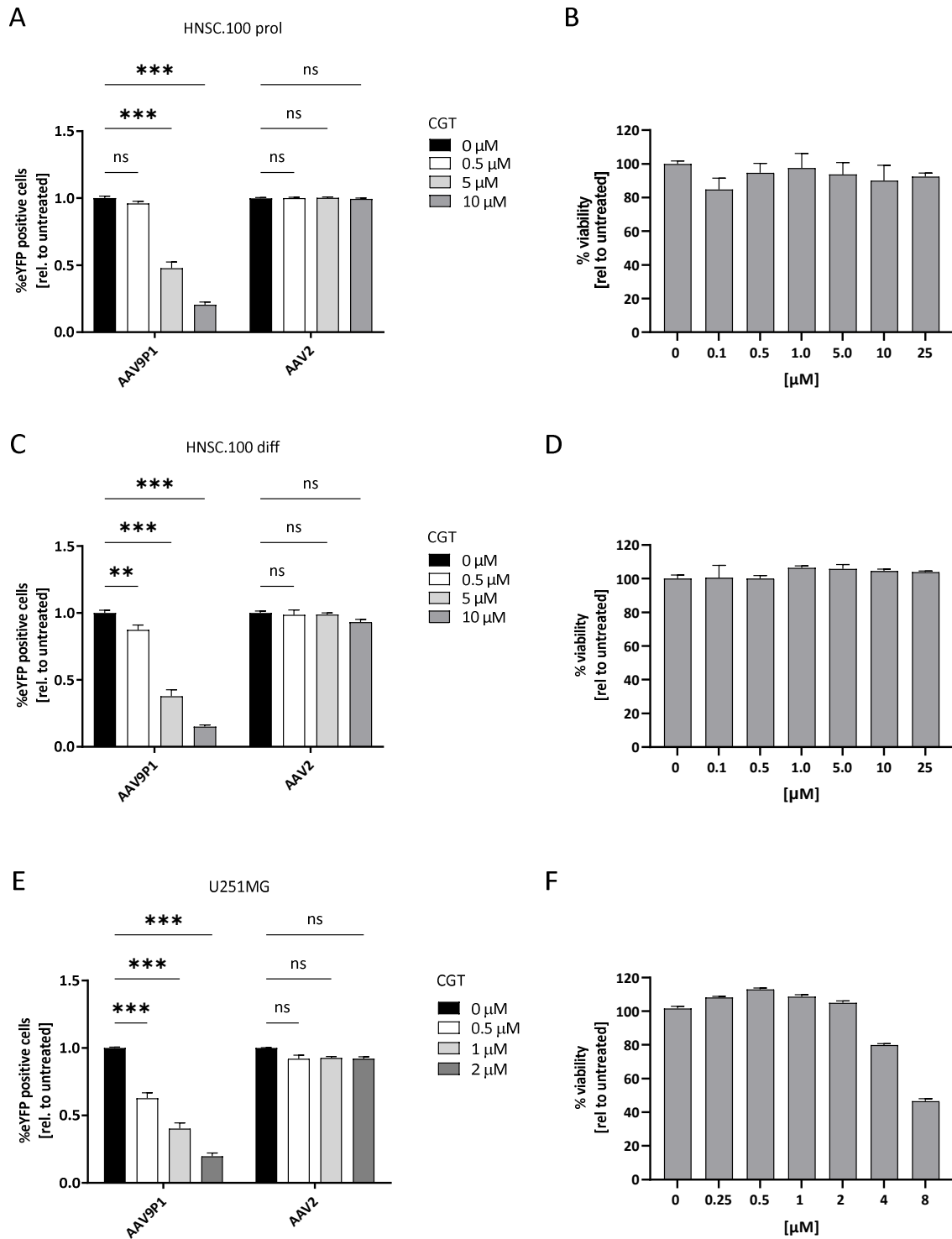


**Figure 3-6 Effects of pharmacological inhibition of  $\alpha v\beta 3$  and  $\alpha v\beta 5$  integrins by Cilengitide (CGT) on rAAV9P1 and rAAV2 transduction efficiency.** HNSC.100 prol (A), HNSC.100 diff (C), or U251MG (E) were treated with non-toxic concentrations of CGT (viability  $\geq 80\%$ ), and co-incubated with rAAV vectors at MOI 10,000 for 48 h, and eYFP expression was determined 48 h post-transduction by flow cytometry. Data depicts mean + SEM of three independent experiments. Statistical significance was determined by two-way ANOVA. \*\*\*  $p \leq 0.001$ , \*\*  $p \leq 0.01$ , \*  $p \leq 0.05$ , ns  $p > 0.05$ . Non-toxic CGT concentrations on HNSC.100 prol (B), HNSC.100 diff (D), or U251MG (F) were determined beforehand by treatment of cells with different concentrations of CGT for 48 h, followed by assessment of cell viability by CTB. Data depicts mean + SEM of two independent experiments.

Treatment of proliferating HNSC.100 with 5 and 10  $\mu\text{M}$  lead to a significant decline of rAAV9P1 transduction by 52.2 % and 79.4 %, respectively (Fig. 3-6 A). All three concentrations used on U251MG cells reduced the transduction efficiency of rAAV9P1 by 37.3 %, 59.8 %, and 80.4 %, respectively, in a dose-dependent fashion (Fig. 3-6 E). In contrast, transduction by rAAV2 was not affected by any concentration of CGT on either cell line. To investigate whether this effect was limited to proliferating cells, the experimental procedure was repeated with differentiated HNSC.100 cells, which represent post-mitotic, astrocyte-enriched cultures. The dose-dependent reduction of rAAV9P1 transduction efficiency was similar to the effect found in proliferating HNSC.100 cells, while rAAV2 transduction was not affected (Fig. 3-6 C+D).

As shown in the analysis of the RNA sequencing dataset, expression of  $\alpha\text{v}$  and  $\beta\text{8}$  is increased on mature astrocytes in comparison to neurons. To investigate the contribution of the  $\alpha\text{v}\beta\text{8}$  heterodimer on rAAV9P1 transduction we blocked this integrin subtype by incubation of the target cells with the cyclic pentapeptide c(GLRGDLp(NMe)K) ( $\alpha\text{v}\beta\text{8}$ -ligand 2a) which was described to bind to  $\alpha\text{v}\beta\text{8}$  with high selectivity and only low or no cross-interaction with  $\alpha\text{v}\beta\text{3}$  or  $\alpha\text{v}\beta\text{5}$  [162]. HNSC.100 or U251MG cells were incubated with different concentrations of  $\alpha\text{v}\beta\text{8}$ -ligand 2a and simultaneously exposed to rAAV9P1 or rAAV2 vectors. None of the concentrations used resulted in impaired cell viability of any cell line as analyzed by CTB assay (Fig. 3-7 B+F). Treatment of proliferating HNSC.100 and U251MG cells with  $\alpha\text{v}\beta\text{8}$ -ligand 2a resulted in a strong and dose-dependent reduction of the transduction efficiency of rAAV9P1 with a reduction of over 85 % even at the lowest concentration of 0.5  $\mu\text{M}$  (Fig. 3-7 A+E). This dose-dependent reduction could be replicated in non-dividing, differentiated HNSC.100 cells, although the inhibitory effect was slightly reduced with a decrease of 56.8 % and 83.5 % at 0.5  $\mu\text{M}$  and 10  $\mu\text{M}$ , respectively (Fig. 3-7 C). Transduction by rAAV2 was not affected by treatment with  $\alpha\text{v}\beta\text{8}$ -ligand 2a in any of the investigated cell lines.

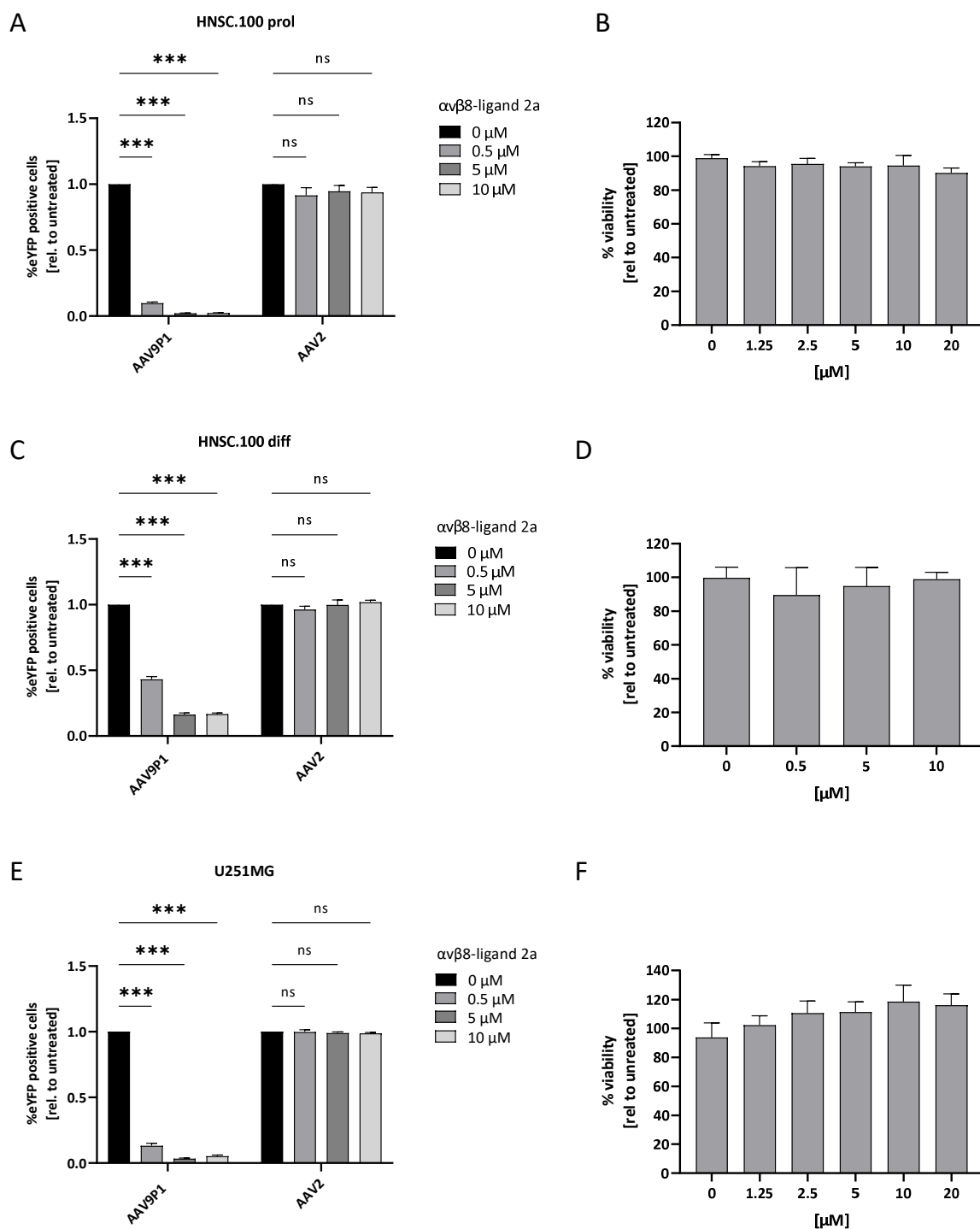


**Figure 3-7 Effects of pharmacological inhibition of integrin  $\alpha\text{v}\beta\text{8}$  by  $\alpha\text{v}\beta\text{8}$ -ligand 2a on rAAV9P1 and rAAV2 transduction efficiency.** HNSC.100 prol (A), HNSC.100 diff (C), or U251MG (E) were treated with different concentrations of  $\alpha\text{v}\beta\text{8}$ -ligand 2a, and co-incubated with rAAVs at MOI 10,000 for 48 h, and eYFP expression was determined 48 h post-transduction by flow cytometry. Data depicts mean + SEM of three independent experiments. Statistical significance was determined by two-way ANOVA. \*\*\*  $p \leq 0.001$ , \*\*  $p \leq 0.01$ , \*  $p \leq 0.05$ , ns  $p > 0.05$ . Concentrations of  $\alpha\text{v}\beta\text{8}$ -ligand 2a tolerated by HNSC.100 prol (B), HNSC.100 diff (D), or U251MG (F) cells were determined beforehand by treatment of cells with different concentrations of anti- $\alpha\text{v}\beta\text{8}$  for 48 h, followed by assessment of cell viability by CTB. Data depicts mean + SEM of two independent experiments.

The combinatorial inhibition of  $\alpha\beta 3$  and  $\alpha\beta 5$  with CGT significantly inhibited the transduction of astrocytic cells by rAAV9P1. To further dissect whether the inhibition of a single subtype of integrin heterodimers is sufficient for reducing rAAV9P1 transduction, we performed integrin inhibition experiments using P11, a commercially available, selective peptide inhibitor for  $\alpha\beta 3$ .

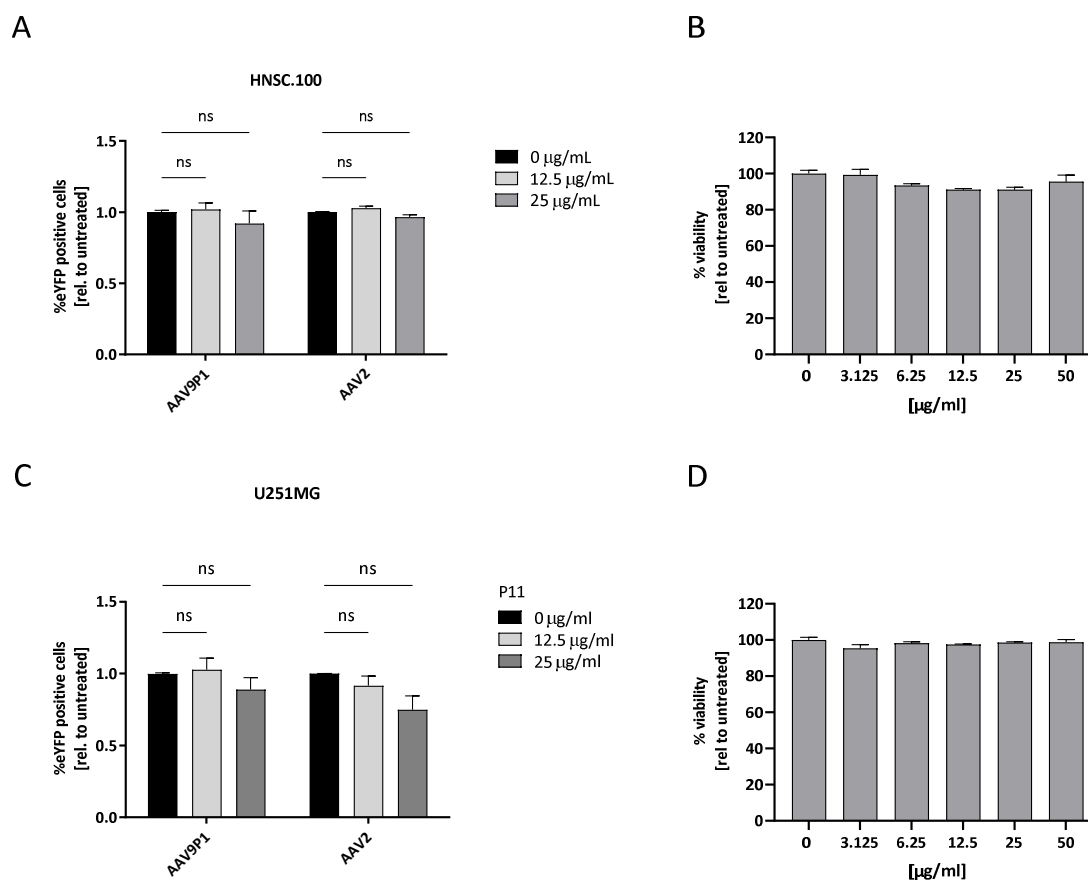


**Figure 3-8 Effects of pharmacological inhibition of integrin  $\alpha\beta 3$  by P11 on rAAV9P1 and rAAV2 transduction efficiency.** Proliferating HNSC.100 (A) or U251MG (C) were treated with different concentrations of P11, and co-cubated with rAAVs at MOI 10,000 for 48 h, and eYFP expression was determined 48 h post-transduction by flow cytometry. Data depict mean  $\pm$  SD of three independent experiments. Statistical significance was determined by Two-way ANOVA. \*\*\*  $p \leq 0.001$ , \*\*  $p \leq 0.01$ , \*  $p \leq 0.05$ , ns  $p > 0.05$ . Effects on cell viability on HNSC.100 prol (B) or U251MG (D) were assessed by treating cells with different concentrations of P11 for 48 h and conduction of CTB. Data depicts mean + SEM of two independent experiments.

P11 does not contain an RGD motif but was predicted to occupy the RGD binding site of  $\alpha\beta 3$  [188]. In the CTB assay, neither proliferating HNSC.100 nor U251MG cells were significantly affected in their viability by P11 concentrations of up to 50  $\mu\text{g/ml}$  (Fig. 3-8 B+D). Figures 3-8 A+C show the analysis of eYFP positive cells by flow cytometry after 48 h of simultaneous exposure of HNSC.100 and U251MG cells to rAAV9P1 or rAAV2 vectors and P11. Treatment with P11 concentrations as high as 25  $\mu\text{g/ml}$  did not significantly influence the transduction efficiency of rAAV9P1 or rAAV2 (Fig. 3-8 A+C). Taken

together, pharmacological inhibition of both  $\alpha\beta3$  and  $\alpha\beta5$  or  $\alpha\beta8$  alone has a strong negative influence on the transduction of astrocytic cells by rAAV9P1.

### **3.5 Genetic ablation of integrin subunits $\alpha$ , $\beta8$ , or $\beta3/\beta5$ decreases the transduction efficiency of rAAV9P1**

Analysis of RNA sequencing data revealed increased expression of the  $\alpha$ -subunit ( $\alpha$ ) and several  $\beta$ -subunits ( $\beta1$ ,  $\beta5$ , and  $\beta8$ ) on astrocytes compared to neurons (Fig. 3-5). Furthermore, pharmacological inhibition of  $\alpha\beta5$  and  $\alpha\beta3$  or  $\alpha\beta8$  significantly influenced transduction of astrocytic cell lines by rAAV9P1. To further investigate the possible contribution of RGD-binding integrins to rAAV9P1 transduction, frameshift mutations were introduced into the genes of *ITGAV*, *ITGB1*, *ITGB3*, *ITGB5*, and *ITGB8* of U251MG cells using CRISPR/Cas9 mediated gene targeting. U251MG cells were transfected with a plasmid directing expression of Cas9, an sgRNA directed against an early exon of the respective gene, and a puromycin resistance gene. Transfected cells were selected for antibiotic resistance and clones were generated by limiting dilution and clonal expansion. Clones with frameshift mutations in both alleles of the target genes were identified by Illumina MiSeq sequencing. Clones with frameshift mutations in both alleles were considered as knockouts and chosen for further analysis and testing. *ITGAV*<sup>-/-</sup>, *ITGB5*<sup>-/-</sup>, and *ITGB3/B5*<sup>-/-</sup> cells displayed severely reduced attachment to standard cell culture plasticware. This phenotype could be reversed by coating cell culture ware with 1 % collagen in H<sub>2</sub>O for 10 min before seeding the cells. In addition to sequence analysis, knockouts were also validated by surface staining of U251MG knockout cell lines with antibodies against assembled integrin heterodimers ( $\alpha\beta3$  and  $\alpha\beta5$ ) or the individual integrin subunits  $\alpha$ ,  $\beta1$ , or  $\beta8$  and subsequent analysis by flow cytometry (Fig. 3-9 A). In all knockout cell lines (U251MG *ITGB1*<sup>-/-</sup>, *ITGB3*<sup>-/-</sup>, *ITGB5*<sup>-/-</sup>, *ITGB8*<sup>-/-</sup>, *ITGB3/B5*<sup>-/-</sup>) fluorescence intensity for the staining with the antibody against the respective  $\beta$ -subunit or assembled integrin heterodimer was reduced to background fluorescence levels confirming absence of subunit expression. In the  $\alpha$ -subunit knockout cell line (U251MG *ITGAV*<sup>-/-</sup>) fluorescence intensity of the  $\alpha$  staining was reduced to background level, as expected. Furthermore,  $\alpha$  knockout also lead to abrogated expression of assembled  $\alpha\beta3$  and  $\alpha\beta5$  integrin heterodimers as well as  $\beta8$  subunit expression (Fig. 3-9 A).

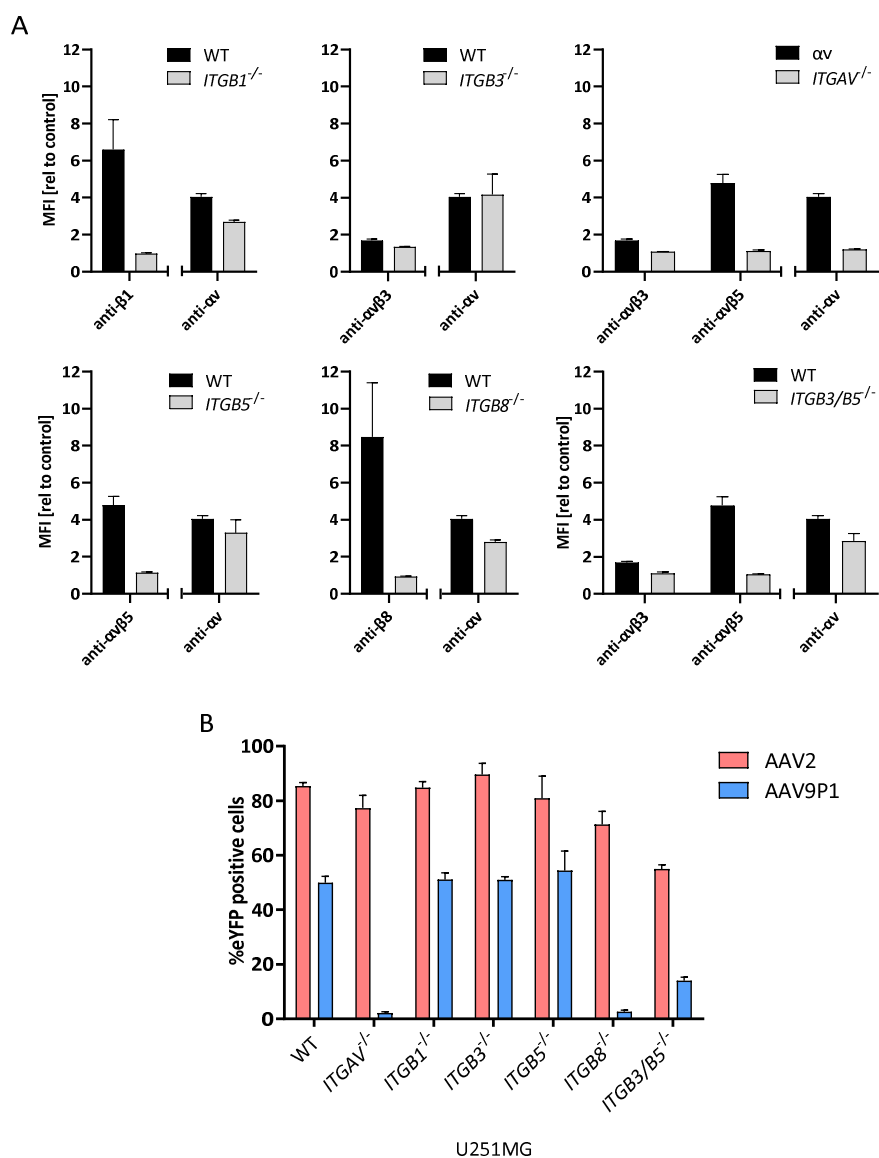


**Figure 3-9 Effects of genetic ablation of subunits of RGD-binding integrins on transduction by rAAV9P1 and rAAV2.** CRISPR/Cas9 gene editing was used to target the indicated integrin subunit genes in U251MG cells. All clones carry out-of-frame mutations of both alleles as identified by Illumina MiSeq sequencing. (A) Surface staining of knockout cell lines with antibodies against assembled  $\alpha\beta3$  or  $\alpha\beta5$  heterodimers, or the subunits  $\beta1$ ,  $\beta8$  or  $\alpha v$ . Data depict FITC-MFI relative to samples stained with anti-m $\alpha$  Alexa Fluor<sup>®</sup> 488 only (for anti- $\alpha\beta3$ , anti- $\alpha\beta5$ , anti- $\beta1$ , and anti- $\beta8$ ) and APC-MFI relative to unstained samples (for anti- $\alpha v$  Alexa Fluor<sup>®</sup> 647). (B) Knockout cell lines were exposed to rAAV vectors at MOI 10,000, and eYFP expression was determined 48 h post-transduction by flow cytometry. Data depicts mean + SEM of three independent experiments.

Figure 3-9 B shows the proportion of eYFP expressing cells detected by flow cytometry 48 h after transduction of U251MG WT and integrin knockout cell lines with rAAV9P1 and rAAV2 vectors. Compared to WT cells, knockout of the *ITGAV* genes, and therefore ablation of all integrin

heterodimers containing the  $\alpha$ v subunit, resulted in a drastic reduction of rAAV9P1 transduction of U251MG cells to almost undetectable levels.

Among the  $\beta$ -subunits, cell clones with knockouts of either the *ITGB1*, *ITGB3*, or *ITGB5* genes did not show in a decrease of rAAV9P1 transduction compared to the WT cells. Strikingly, knockout of the  $\beta$ 8 integrin subunit had a very strong impact on rAAV9P1 transduction, similar to that of an  $\alpha$ v knockout, with a decrease of rAAV9P1 transduction by 97.37 % compared to the WT cells. The transduction efficiency of rAAV2 did not change between the U251MG WT and single integrin subunit knockout cell lines.

As shown above, blocking of  $\alpha$ v $\beta$ 3 and  $\alpha$ v $\beta$ 5 by treatment with CGT significantly reduced the transduction of U251MG and HNSC.100 cells with rAAV9P1. To mimic the effect of CGT on a genetic level, U251MG *ITGB3/B5*<sup>-/-</sup> double knockouts were generated by transfecting established U251MG *ITGB5*<sup>-/-</sup> knockout cells with an sgRNA against the *ITGB3* gene and subsequent selection, clonal expansion, and sequencing. U251MG *ITGB3/B5*<sup>-/-</sup> double knockout cells were transduced by rAAV9P1 at significantly lower levels than WT cells with a reduction of 85.96 % (Fig. 3-9 B). The double knockout cells also affected rAAV2 transduction efficiency with a reduction of 44.99 %. Taken together, transduction of U251MG cells is dependent on the presence of  $\alpha$ v $\beta$ 8 and to a lesser extent on the combination of  $\alpha$ v $\beta$ 3 and  $\alpha$ v $\beta$ 5.

### 3.6 The P1 peptide is not sufficient for efficient astrocyte transduction

All known AAV serotypes are described to attach to cells via interaction with several cell surface molecules rather than a single primary receptor (Table 1-1). Therefore, it can be hypothesized that the high transduction efficiency of rAAV9P1 on astrocytes is promoted by engagement with other co-receptors next to RGD-binding integrins. The *in silico* analysis of AAV9P1 revealed a high probability for the P1 peptide to participate in receptor binding. To investigate whether the presence of the P1 peptide is sufficient to promote efficient transduction of astrocytes, we analyzed four different rAAV vector variants rAAVS1P1, rAAVS10P1, rAAVH15P1, and rAAVD20P1. These rAAV variants were created by family shuffling of the *cap* genes of the AAV serotypes 1, 6, 8, and 9 and selected *in vivo* to efficiently transduce different tissues (Grimm D., unpublished data). All variants contain the P1 peptide at the same position as the AAV9P1 capsid. The rAAV variants were produced with the same protocol as the rAAV9P1 stocks, and all carry an eYFP transgene under the control of a CMV promoter. HNSC.100 cells were transduced with the rAAV variants, and the transduction efficiency was determined 48 h post-transduction by eYFP detection via flow cytometry. As seen in Figure 3-10 A, none of the investigated P1 variants reached the levels of rAAV9P1 transduction efficiency on astrocytic cells. While rAAVH15P1

displayed the highest transduction efficiency of 51.24 %, the other variants were weaker in transduction with 13.15 %, 35.56 %, and below 2 % for rAAVS1P1, rAAVS10P1, and rAAVD20P1, respectively. The rABA also revealed lower levels of surface binding for all P1 variants compared to rAAV9P1 (Fig. 3-10 B). However, cell surface binding of the P1 variants did not completely reflect the transduction effectiveness on HNSC.100 cells. These results indicate that cell surface molecules other than RGD-binding integrins are involved in efficient rAAV9P1 binding to astrocytes.

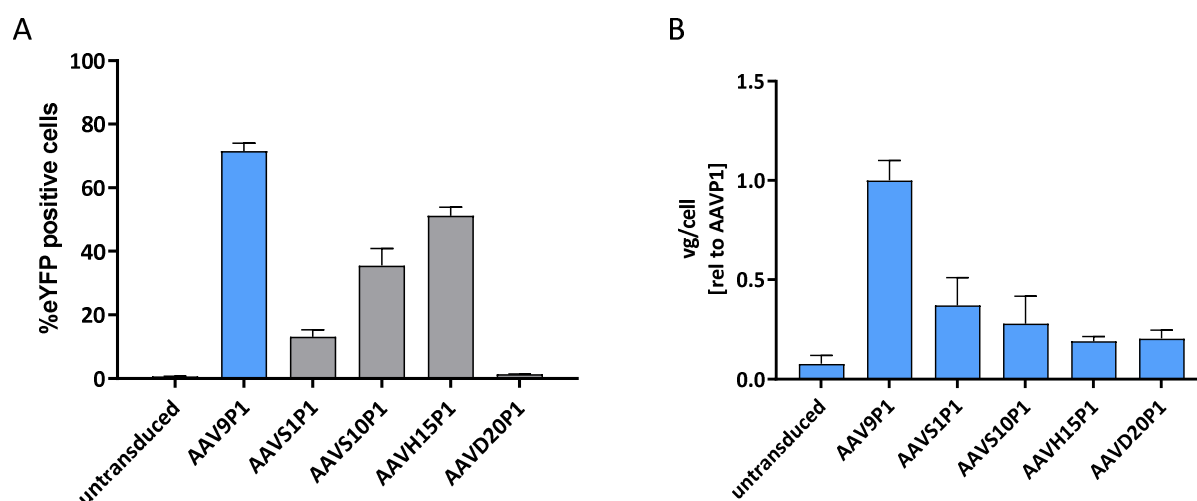


**Figure 3-10 Transduction and binding efficiency of P1 variants on HNSC.100 cells.** Proliferating HNSC.100 were transduced with rAAV9P1, or four rAAV vector variants that contain the P1 peptide at the same position as AAV9P1. (A) Cells were transduced with rAAVs at MOI 10,000, and eYFP expression was determined 48 h post-transduction by flow cytometry. Data depict mean + SEM of three independent experiments. (B) rABA of rAAV9P1 and P1 variants on HNSC.100 prol cells. Data depicts mean + SEM of two independent experiments.

### 3.7 S263 is an essential amino acid residue for rAAV9P1 transduction

In the previous experiment, two rAAV variants rAAVS1P1 and rAAVD20P1 were identified, that carry the RGD-containing P1 peptide at the same position as rAAV9P1 but displayed the lowest transduction efficiencies on HNSC.100 cells. To identify possible regions of the VP1<sub>AAV9P1</sub> that are crucial for efficient transduction of astrocytes, a comparison of the sequences of the VP proteins from all tested P1 variants was performed and analyzed for amino acid substitutions that are unique to VP1<sub>AAVS1P1</sub> and VP1<sub>AAVD20P1</sub>. Here, a particular focus was put on the sequence of the VP3 protein and the variable regions therein because they have a higher potential to engage in receptor interactions. The VP3 sequence alignment revealed that the only change unique to these two variants is an S263G substitution in VR-I. In addition, the sequences of both variants contain the substitution S268A and S269T, but these substitutions can also be detected in the rAAVS10P1 variant, which showed increased transduction efficiencies compared to rAAVS1P1 and rAAVS10P1. To analyze the importance of the

S263G substitution for astrocyte transduction, the variant rAAV9P1<sub>S263G</sub> was generated by introducing the S263G mutation into the pBSUF3-YFP plasmid by quickchange PCR and subsequent rAAV production by iodixanol gradient. rAAV9P1<sub>S263G</sub> failed to transduce HNSC.100 cells and displayed equally low transduction efficiencies as rAAVD20P1, even at an MOI of 10,000. This effect turned out to be not astrocyte-specific since neither rAAVD20P1 nor rAAV9P1<sub>S263G</sub> was able to transduce the investigated cell lines Huh7 and H1299 (Fig. 3-11). Taken together, S<sub>263</sub> seems to play an essential role in transduction by rAAV9P1 that does not contribute to astrocyte selectivity but rather overall infectivity of the vector.

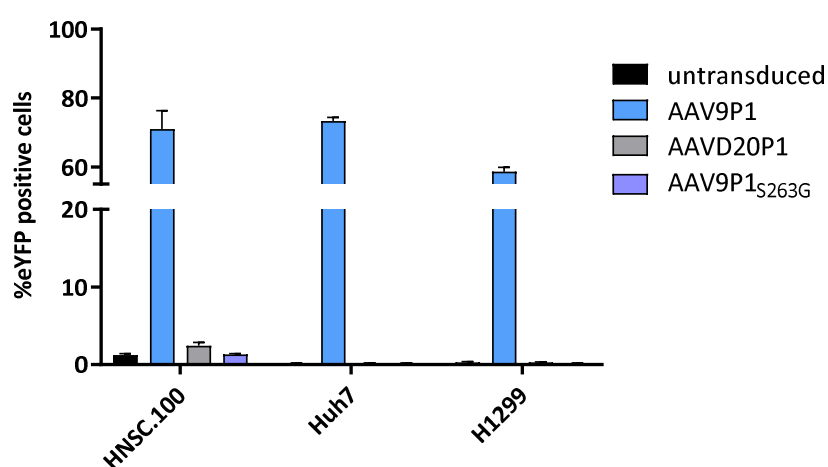


**Figure 3-11 Transduction of different cell lines by rAAV9P1<sub>S263G</sub>.** Proliferating HNSC.100, a human hepatocellular carcinoma cell line Huh7, and human non-small cell lung carcinoma cell line H1299 were transduced with rAAV9P1, rAAVD20P1, or rAAV9P1<sub>G163S</sub> at MOI 10,000, and eYFP expression was determined 48 h post-transduction by flow cytometry. Data depicts mean + SEM of three independent experiments.

### 3.8 rAAV9P1 does not require HSPG, but N-linked glycans with terminal GAL for efficient astrocyte transduction

The first receptor to be identified for an AAV serotype was HSPG and its interaction with AAV2 [95]. It is known that AAV2 binds to HSPG via a binding pocket that is created by four basic amino acids and that is located on the GH loop 2 [189]. Membrane HSPGs are proteins in the cellular membrane, that are modified by the covalent attachment of one or more heparin sulfate chains [190]. The WT AAV9 serotype lacks these basic amino acids and, therefore, cannot bind to HSPG [118]. The P1 peptide of AAV9P1 contains several basic amino acids that might potentially mimic the HSPG binding pocket of AAV2 and mediate rAAV9P1 binding to HSPG. To identify possible dependencies of rAAV9P1 transduction on interaction with HSPG, a heparin competition assay was performed. Since heparin is a

highly sulfated form of heparan sulfate, it binds to the HSPG-interaction motif of the virus capsid and therefore inhibits cell binding and transduction. Here, U251MG cells were simultaneously treated with different concentrations of soluble heparin and rAAV2 or rAAV9P1 for 4 h at 37 °C and subsequently incubated for 48 h until analysis of eYFP positive cells by flow cytometry (Fig. 3-12).

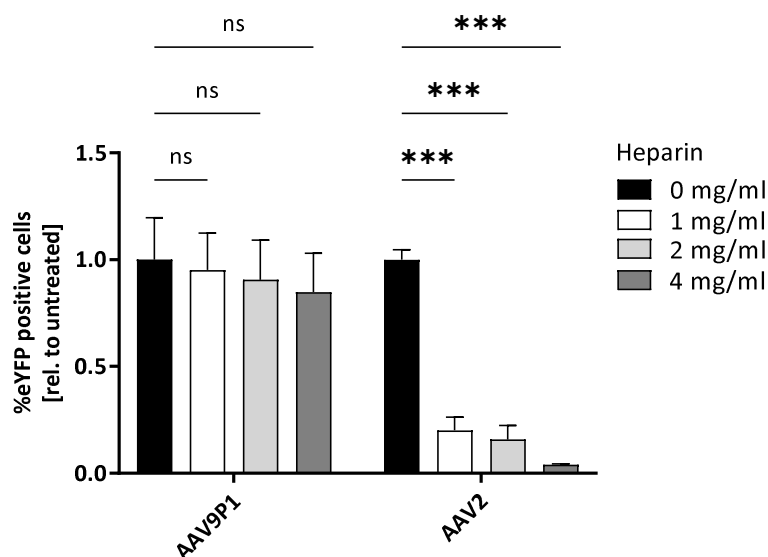


**Figure 3-12 Effects of heparin competition on transduction by rAAV9P1 or rAAV2.** U251MG WT cells were treated with 0, 1, 2, or 4 mg/ml soluble heparin and simultaneously incubated with rAAV9P1 or rAAV2 at MOI 10,000 for 4 h at 37 °C. Cells were washed, and YFP expression was measured 48 h post-transduction by flow cytometry. Data depicts mean + SEM of three independent experiments. Statistical significance was determined by Two-way ANOVA. \*\*\*  $p \leq 0.001$ , \*\*  $p \leq 0.01$ , \*  $p \leq 0.05$ , ns  $p > 0.05$

Treatment of U251MG cells with heparin resulted in a strong and dose-dependent reduction of rAAV2 transduction efficiency with a decrease by 79.9 % even at the lowest tested concentration of 1 mg/ml. In contrast, transduction by rAAV9P1 was not significantly affected even at high heparin concentrations of 4 mg/ml. This indicates that transduction of astrocytes by rAAV9P1 is not dependent on the interaction of the capsid with HSPG.

Like other AAV serotypes, AAV9 utilizes glycans that are attached to the extracellular region of membrane proteins as primary attachment partners. As a unique feature, AAV9 binds to terminal galactose via a binding pocket in the capsid that consists of five distinct amino acid residues in the VP3 protein [118, 159]. Since these amino acids are still present in the AAV9P1 VP3 protein, it was analyzed whether the binding to surface glycans and specifically terminal GAL promotes efficient astrocyte transduction by rAAV9P1. In a first experiment, we exploited the effect of diminished N-linked glycosylation in the whole cell by treatment with tunicamycin (TUN). TUN prevents the first step of the

formation of N-linked glycans in the endoplasmic reticulum (ER) by inhibiting the UDP-N-acetylglucosamine-dolichyl-phosphate N-acetyl-glucosamine-phosphotransferase (DPAGT1) [191]. U251MG cells were treated with varying concentrations of TUN for 24 h, and the effect on surface glycosylation was analyzed by surface staining of the cells with the *Sambucus nigra* lectin (SNA) coupled to fluorescein (FITC) and subsequent flow cytometry analysis. SNA belongs to the family of lectins and selectively stains sialylated glycans on the cell surface and is a tool to estimate total surface glycosylation. We found that treatment of cells with 100 ng/ml TUN reduced the surface glycosylation of U251MG cells by approximately 50 % (Fig. 3-13 A). Higher concentrations did not result in stronger deglycosylation but impaired morphology of the cells with fewer astrocyte-like processes and a rounded shape (data not shown). Since TUN is known to cause ER stress and reduce proliferation, the proliferation of treated U251MG cells was monitored over three days. U251MG cells stopped proliferating when treated with 100 ng/ml TUN while untreated cells proliferated as expected (Fig. 3-13 B). To compensate for this discrepancy in cell number at the day of transduction, treated and untreated cells were counted separately for MOI determination. U251MG cells were treated with 100 ng/ml TUN for 24 h and subsequently exposed to rAAV9P1 or rAAV2 as a control. Transduction efficiency was analyzed 48 h post transduction by detection of eYFP positive cells by flow cytometry. Figure 3-13 C shows the results of the TUN treatment assay. rAAV9P1 transduced TUN-treated cells with 42.5 % lower efficiency than untreated cells, while transduction by rAAV2 was only mildly affected by TUN treatment (Fig. 3-13 C). To confirm that this effect is not caused by the reduced viability of the cells, we performed an rABA and found, that rAAV9P1 binding to TUN-treated cells was reduced at a similar extent as in the effective transduction analyzed by flow cytometry when compared to untreated cells (Fig. 3-13 D). Noticeably, rAAV2 binding to the cells was mildly, yet not significantly, reduced in the rABA.

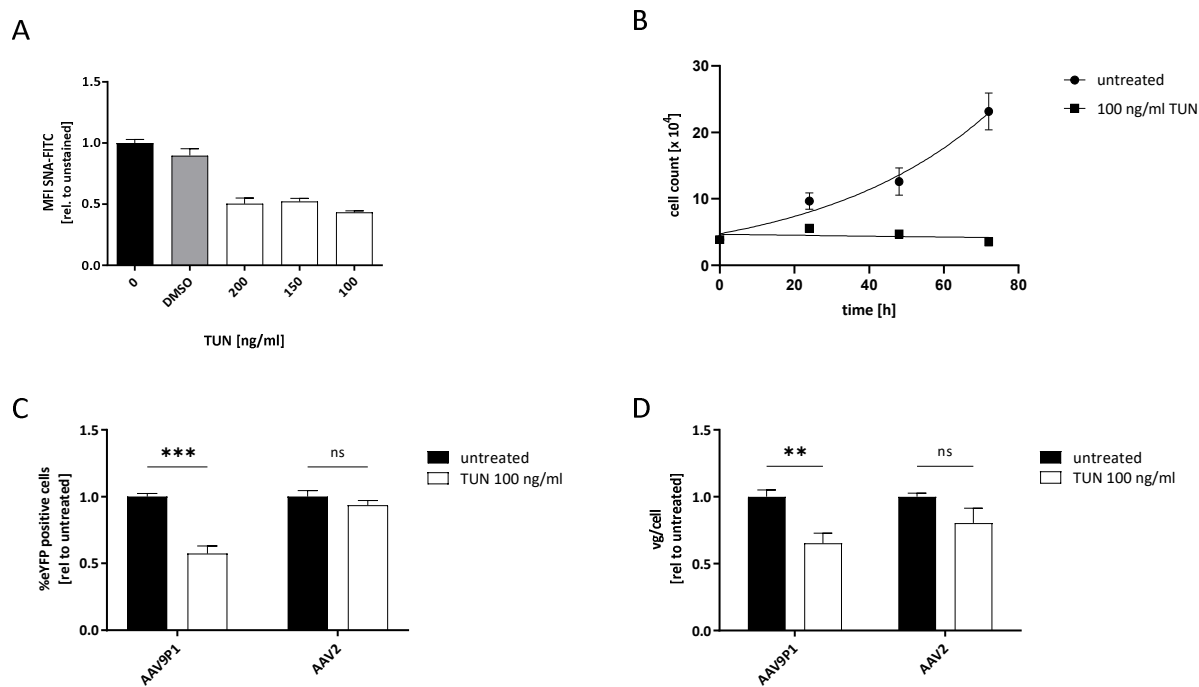


**Figure 3-13 Effects of inhibition of N-linked glycosylation on U251MG cells on transduction with rAAV9P1 and rAAV2.** (A) U251MG cells were treated with different concentrations of Tunicamycin (TUN) for 24 h, and whole surface glycosylation was assessed by surface staining with 10  $\mu$ g/ml SNA-FITC and flow cytometry analysis. (B) U251MG cells were treated with 100 ng/ml TUN for 24, 48, or 72 h, and viable cell number was assessed by cell counting with trypan blue. (C + D) U251MG cells were treated with 100 ng/ml TUN for 24 h. (C) Cells were washed and subsequently transduced with rAAV9P1 or rAAV2 at MOI 10,000. eYFP expression was measured 48 h post-transduction by flow cytometry. (D) Cells were washed and subsequently incubated with rAAVs at MOI 10,000 for 30 min on ice for virus particles to attach to the cell. The graph shows the results of the rABA of rAAV9P1 and rAAV2 on treated U251MG cells. Data depicts mean + SEM of three independent experiments. Statistical significance was determined by Two-way ANOVA. \*\*\*  $p \leq 0.001$ , \*\*  $p \leq 0.01$ , \*  $p \leq 0.05$ , ns  $p > 0.0$

Reduction of overall surface glycosylation inhibited transduction of astrocytic cells by rAAV9P1. To identify the distinct terminal sugar moieties that take part in rAAV9P1 transduction, U251MG cells were treated with Neuraminidase (Neu) and *Erythrina cristagalli* lectin (ECL). Neu removes terminal SIA residues from N-linked glycans and therefore exposes underlying sugars, increasing the availability of non-SIA sugars on cell surface glycans. ECL is a lectin that selectively captures terminal GAL on N-linked glycans, thereby masking their accessibility. U251MG cells were treated with 50 mU/ml Neu for 2 h at 37  $^{\circ}$ C and subsequently incubated with 100  $\mu$ g/ml ECL and rAAV9P1 or rAAV2 for 1.5 h on ice. Transduction efficiency was analyzed 48 h after cells were returned to the incubator by flow cytometry. Removal of SIA by Neu treatment significantly increased the transduction efficiency of rAAV9P1 by 3.6-fold. In contrast, treatment with ECL alone or in combination with Neu resulted in almost complete inhibition of transduction by rAAV9P1 (Fig. 3-14 A). This behavior could be replicated in the performed rABA (Fig. 3-14 B). Modulation of the glycan landscape by Neu and/or ECL did result in a reduction of

transduction efficiency of rAAV2 by 22 % in flow cytometry analysis and by 45.5 % in the rABA analysis. Notably, removing SIA resulted in slightly decreased transduction by rAAV2, in contrast to rAAV9P1 (Fig. 3-14 A+B). Taken together, rAAV9P1 transduction is dependent on N-linked surface glycans that do not carry SIA, but GAL as their terminal sugar moiety.

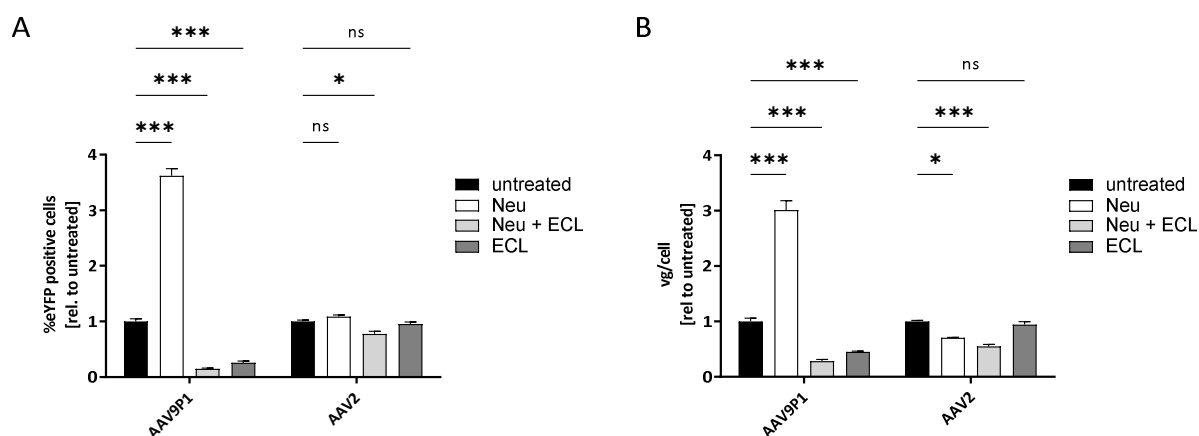


**Figure 3-14 Effects of desialylation and glycan masking on U251MG cells on transduction with rAAV9P1 and rAAV2.** (A + B) U251MG cells were treated with 50 mU/ml Neuraminidase (Neu) for 2 h at 37 °C. Subsequently, cells were washed and supplemented with 100 µg/ml Erythrina cristagalli lectin (ECL) and co-incubated with rAAV9P1 or rAAV2 at MOI 10,000 for 1.5 h on ice. (A) Cells were washed, returned to the incubator, and eYFP expression was measured 48 h post-transduction by flow cytometry. (B) rABA of rAAV9P1 and rAAV2 on treated U251MG cells. Data depicts mean + SEM of three independent experiments. Statistical significance was determined by Two-way ANOVA. \*\*\*  $p \leq 0.001$ , \*\*  $p \leq 0.01$ , \*  $p \leq 0.05$ , ns  $p > 0.05$

### 3.9 LamR and AAVR are involved in rAAV9P1 transduction

Besides terminal galactose, two additional receptor molecules have been associated with efficient transduction of target cells by rAAV9. siRNA-mediated knockdown of LamR in NIH 3T3 cells promoted a decreased transduction efficiency of rAAV9, and knockout of AAVR in HeLa completely blocked transduction by rAAV9 [103, 192]. To investigate whether these molecules contribute to efficient transduction of astrocytic cells by rAAV9P1, U251MG knockout cell lines of the LamR (*RPSA* gene) and AAVR (*KIAA0319L* gene) were generated using the CRISPR/Cas9 gene targeting system. Knockout of LamR resulted in a reduction of transduction efficiency by rAAV9P1 of 79.9 % compared to WT, while transduction with rAAV2 was unchanged. U251MG AAVR<sup>-/-</sup> cells were completely resistant to transduction by rAAV9P1 and rAAV2 (Fig. 3-15). In summary, we could show a dependence of rAAV9P1 transduction on AAVR and LamR, while rAAV2 transduction is only affected by the knockout of AAVR.

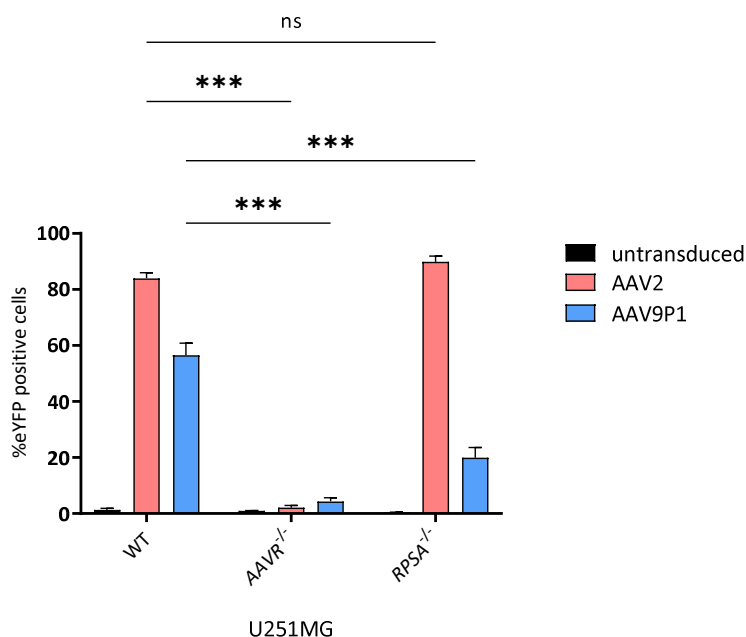


**Figure 3-15 Effects of AAVR and LamR knockout in U251MG on transduction by rAAV9P1 and rAAV2.** U251MG AAVR<sup>-/-</sup> or U251MG RPSA<sup>-/-</sup> cells were transduced with rAAV9P1 or rAAV2 at MOI 10,000, and eYFP expression was analyzed 48 h post-transduction by flow cytometry. Data depicts mean + SD of three independent experiments. Statistical significance was determined by Two-way ANOVA. \*\*\*  $p \leq 0.001$ , \*\*  $p \leq 0.01$ , \*  $p \leq 0.05$ , ns  $p > 0.05$

### 3.10 Identification of post-entry pathways in astrocytes relevant for rAAV9P1 transduction by genome-wide CRISPR/Cas9 knockout screening

Besides interaction with cellular surface receptors, the transduction efficiency of AAVs is also dependent on various intra-cellular parameters and pathways that enable post-entry processing and trafficking of the virus particle through the cytosol and into the nucleus. In addition, AAV genome expression is entirely dependent on the cellular transcription and translation machinery [193]. To investigate intra-cellular molecules and pathways that influence the transduction of astrocytes by rAAV9P1, an unbiased, genome-wide CRISPR/Cas9 knockout screen in U251MG cells was conducted. A U251MG cell line stably expressing Cas9 was generated by lentiviral transduction and selection with blasticidin. To minimize any effects derived from mixed populations of sub-optimally transduced cells, a limiting dilution of the U251MG-Cas9 cell line was performed to obtain monoclonal cell lines.

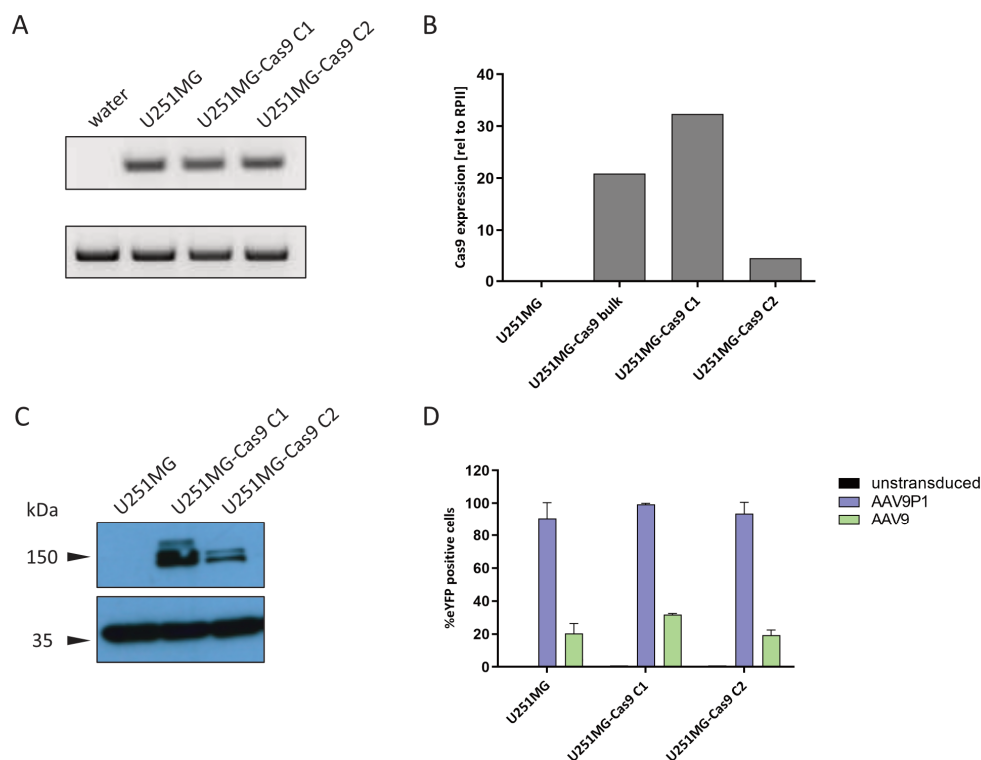


**Figure 3-16 Establishment of the U251MG-Cas9 cell line.** U251MG cells were lentivirally transduced with Cas9-Blast, selected, and clonally expanded. Results show U251MG WT cells (U251MG), transduced cells before (U251MG-Cas9 bulk) and after limiting dilution (U251MG-Cas9 C1 and C2). (A) Agarose gel electrophoresis of PCR amplicons after amplification of Cas9 and RNA Polymerase II (RPII). (B) qRT-PCR analysis of Cas9 expression levels normalized to RPII expression. (C) Immunoblot analysis of Cas9 and GAPDH expression in protein lysates. (D) Indicated cell lines were transduced with rAAV9P1 or rAAV9 at MOI 100,000, and eYFP expression was analyzed 48 h post-transduction by flow cytometry.

Two clones (U251MG-Cas9 C1 and U251MG-Cas9 C2) were analyzed for the integration of the Cas9 transgene and expression of the transgene by qRT-PCR and immunoblot. From the two selected clones, U251MG-Cas9 C1 (termed U251MG-Cas9 in the following) proved to have the highest Cas9 expression on RNA as well as protein level and was therefore selected for subsequent experiments (Fig. 3-16 A-C). U251MG-Cas9 C1 proved to be transduced at high efficiencies by rAAV9P1 (Fig. 3-16 D).

Using the U251MG-Cas9 cell line we performed a pooled genome-wide screen (Fig. 3-17 A) with the GeCKO v2 sub-library A that contains 65,383 individual sgRNAs targeting 19,050 protein-coding genes and 1,000 non-targeting control sgRNAs. U251MG-Cas9 cells were transduced with the lentivirus library at MOI 0.4 and selected with puromycin. The selected single-knockout cell pool was transduced with rAAV9P1-eYFP at MOI 100,000, incubated for 48 h, and sorted for eYFP-negative cells. A batch of untransduced, unsorted cells served as control population. Both cell populations were subjected to gDNA isolation, PCR amplification, and NGS and the detected sgRNAs were matched to their respective protein-coding genes. The results of the screen are depicted schematically in Figure 3-17 B. From each

protein-coding gene, the one sgRNA showing the highest fold-change was selected for further analysis resulting in a gene list of 2715 individual candidate knockout genes (GL-2715), i.e. genes enriched in the eYFP-negative population, compared to the unsorted control population. This initial candidate list was restricted to genes with a minimum of 100 reads per sgRNA and a minimum increase of 2.0-fold in the eYFP-negative sorted population to increase the biological significance of the results. The filtered gene list consisted of 1326 genes (FGL-1326) with an average increase of 10.23 (ranging from 2.0 to 148) and was subjected to further analyses using the GeneRanker Tool.

In the first step, a MeSH-term and tissue association analysis was performed to verify that the genes found show the expected tissue or disease association. It could be detected that brain tissue as well as brain diseases ranked very high in the list of associated terms and included more than 50 % of all genes in both lists. Next, FGL-1326 was subjected to GO-term (biological process) and pathway enrichment analysis. For biological processes we only considered the top 30 % of matches as relevant (sorted by p-value) to increase biological significance. Pathways detected by the GeneRanker Tool can include canonical pathways taken from different databases and associated pathways derived from literature analysis. This analysis resulted in four canonical and five associated pathways of which we found two pathways each to show a strong relevance in astrocytes as determined by literature review (see Discussion). These canonical pathways are sonic hedgehog (Shh) and inositol-phosphate metabolism, while the associated pathways are granulocyte colony stimulating factor (G-CSF) and EGFR. The GO-term analysis resulted in 85 enriched biological processes that contained the single biological process somatostatin (SST) signaling as an astrocyte-associated process within the top 30 %. In an independent approach, it was analyzed whether these nine enriched pathways have been described in association with rAAV transduction. The literature review showed that one associated (EGFR pathway) and one canonical pathway (inositol-phosphate metabolism) have been proposed to be involved in rAAV binding or intra-cellular processing. For a more detailed discussion of these pathways, see section 4.6.

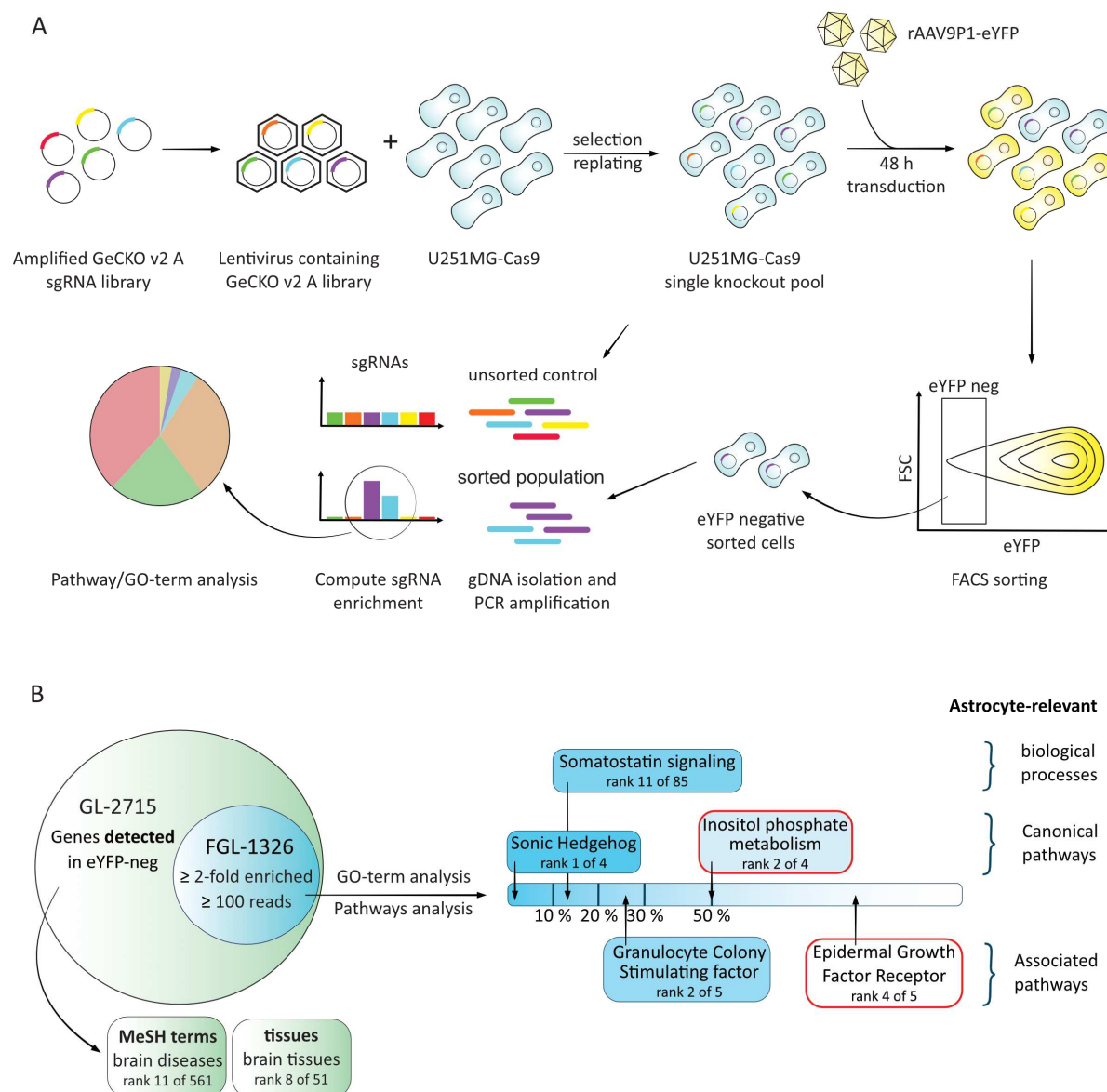


**Figure 3-17 Genome-wide CRISPR/Cas9-knockout screen in U251MG-Cas9.** (A) Workflow of the CRISPR/Cas9 knockout screen. The GeCKO v2 sub-library A was packaged in VSV-G pseudotyped lentivirus particles and used for transduction of the stable U251MG-Cas9 cell line at MOI 0.4. After selection with puromycin and replating, the single-knockout U251MG cell pool was transduced with rAAV9P1 at MOI 100,000 for 48 h and cells lacking eYFP-expression isolated by FACS sorting. An untransduced, unsorted population served as control. gDNA was isolated from eYFP-negative and control cells and integrated sgRNAs were amplified by PCR and sequenced by NGS. The distribution of sgRNAs in both populations was analyzed and the enrichment of all sgRNAs in the sorted population in relation to the unsorted control was calculated. The sgRNAs showing the highest fold change per gene were selected, filtered ( $\geq 100$  reads,  $\geq 2$ -fold enrichment), and analyzed for enriched pathways. (B) Enrichment of astrocyte-relevant and rAAV-associated pathways in the eYFP-negative sorted population. Genes detected in the whole eYFP-negative sorted population (GL-2715, green) are prominently brain tissue and brain disease associated. This also applies to a sub-population (FGL-1326, blue) that was filtered to increase biological significance. The filtered sub-population was subjected to GO-term and enriched pathways analysis. The Figure shows the astrocyte-relevant pathways/processes and placement on the scale (blue to white) indicates their rank relative to the total number of respective pathways/processes (sorted by p-value). Pathways with red outline are the two candidates in all pathways that show a relation to rAAV transduction based on literature review.

Percentages indicate rank of respective pathways relative to number of all enriched pathways of a certain category.

## 4 Discussion

rAAV vectors are considered the gold standard for *in vivo* transduction of cells because of their favorable characteristics. These include absent pathogenicity in humans and mice, long-term transgene expression even in post-mitotic cells, and lack of transgene integration into the host cell genome [66]. Further, rAAVs are highly susceptible to genetic engineering processes and efficient recombinant production [194]. For these reasons, rAAV vectors are widely used in basic research and have been the subject of many (pre-) clinical trials [76, 161]. AAV-based products have a proven safety and efficacy record that even resulted in the approval of three gene therapy drugs for clinical use [195–197]. However, the use of rAAVs in more specific research and clinical settings, such as targeting selected cell populations in the CNS, is still limited by the lack of selectivity of currently available rAAV vectors. The technique of genetically engineering rAAV capsids by peptide display has great potential to increase the transduction efficiency of rAAV variants on selected cell types. However, the lack of information about the underlying target molecules hinders the advance of these vectors into clinical settings [120, 198]. Here, we performed an in-depth analysis of the profile of cellular target molecules required for efficient transduction of human astrocytes by the novel rAAV vector rAAV9P1 and investigated the contribution of the inserted P1 peptide to efficient and selective astrocyte targeting.

### 4.1 rAAV9P1 shows a unique transduction behavior for human astrocytes

rAAV9P1 was described before to efficiently transduce primary astrocytes, the human neural stem cell line HNSC.100 in the proliferating and differentiated state, and the human glioblastoma cell lines U251MG and U87MG [147]. To further characterize the unique transduction pattern of rAAV9P1, this variant was tested in side-by-side experiments with vectors carrying capsid proteins from the two naturally occurring serotypes AAV9 and AAV2. AAV9 is the parental serotype of rAAV9P1 and, therefore, the most closely related AAV serotype. AAV2 belongs to Clade B and was the first AAV serotype to be established as an infectious, recombinant virus [53, 54]. Therefore, AAV2 is profoundly investigated and acknowledged for its high transduction efficiency on various cell lines and also primary cells [98]. The transduction of different cell lines from several tissues revealed that the transduction efficiency of rAAV9P1 was increased significantly on astrocytic cell lines and glioblastoma cell lines compared to rAAV9. In contrast, the two non-astrocytic cell lines HEK293T and HeLa cells were inefficiently transduced by rAAV9P1 with no drastic difference to rAAV9. In these experiments, rAAV2 also transduced the investigated astrocytic cell lines with very high efficiency, which usually slightly exceeded rAAV9P1. However, rAAV2 did not discriminate between the different cell lines and promoted transduction of over 80 % in all investigated cell lines. The high and ubiquitous transduction efficiency of rAAV2 originates in the primary interaction of the VP3<sub>AAV2</sub> protein with HSPG, which is an

integral component of the surface of many different cell types [95, 199, 200]. Heparin-competition experiments with rAAV2 and rAAV9P1 on U251MG cells revealed that rAAV2 transduction could be abrogated by co-incubation with soluble heparin, while rAAV9P1 transduction was completely unaffected. This indicated that the efficient transduction of astrocytes by rAAV9P1 involves cellular target molecules that are independent from HSPG and, thus, uses a profoundly different mode-of-transduction than rAAV2.

While peptide insertions can influence the binding of rAAV variants to the cell surface and, thus, increase or decrease the transduction efficiency of a given vector, it has to be considered that the AAV VP proteins are also involved in post-entry mechanisms such as intracellular trafficking, uncoating, and nuclear localization. Rossi et al. showed that a peptide insertion into rAAV2 led to decreased capsid stability and, therefore, accelerated genome release and efficient transduction of dendritic cells and other immune system cells without changing its target receptors [201]. Here, the rABA is an essential virological tool to discriminate between effects on cell binding and attachment by the virus and effects on productive transduction and transgene expression. We found that significantly more particles of rAAV9P1 bound to the surface of U251MG cells than those of rAAV9, indicating that the increased transduction of astrocytes is indeed promoted by increased binding to the cell surface. The binding of rAAV2 particles proved to be more efficient than the binding of rAAV9P1 to U251MG cells after 30 min of incubation on ice. This corroborates our hypothesis that rAAV9P1 and rAAV2 use different receptor combinations for cell surface binding.

While rAAV9P1 shows selectivity in the transduction of astrocytes over neurons and does not efficiently transduce some non-astrocytic cell lines, it is important to mention that rAAV9P1 did transduce cell lines derived from liver (Huh7) and lung carcinomas (H1299) with good efficiencies. This indicates that rAAV9P1 might not be an astrocyte-specific vector which needs to be considered for the systemic usage of rAAV9P1 derived vectors.

#### **4.2 The P1 peptide is likely to be involved in capsid-receptor interactions**

Over the last decades, various techniques have been applied to identify novel receptor molecules for different AAV serotypes. These techniques include CRISPR/Cas9 knockout and yeast two-hybrid screens, modulation of surface glycosylation, competition experiments, and detailed analysis of potential interaction motifs within the AAV capsid (see Table 1-1 and references therein). To identify target molecules of rAAV9P1, its close phylogenetic relationship to rAAV9 was used to determine capsid regions that might be involved in efficient astrocyte transduction. rAAV9P1 differs from rAAV9 only by the insertion of a seven amino acid peptide at position Q588 and subsequent modification of

the seven flanking amino acid residues. *In silico* modeling revealed that this peptide insertion does not influence the secondary or tertiary structure of the cap monomer, nor the assembly of the 60mer capsid. These findings are in line with other publications that have used a similar insertion site for peptide display approaches in different serotypes [202]. In addition, several screens for new rAAV variants *in vitro* and *in vivo* have been conducted with peptide libraries inserted in this region [128, 202–205]. The reasoning behind this is the favorable localization of this region within the VP3 monomer, and therefore also in the assembled virion. Even though the sequence identity between capsid protein from different serotypes can be as low as 55 %, the structure of the VP3 capsid protein is highly conserved across serotypes and consists of a core eight-stranded  $\beta$ -barrel ( $\beta$ B- $\beta$ I), one additional  $\beta$ -strand ( $\beta$ A), and a conserved  $\alpha$ -helix ( $\alpha$ A). Amino acid stretches between the  $\beta$ -strands contribute to the formation of loops, which promote interaction of capsid monomers for 60mer assembly and define the surface features of the virion [206, 207]. Within the tertiary structure of the VP3 protein, the insertion site of the P1 peptide is located on subloop 2 of the GH loop (between  $\beta$ G and  $\beta$ H). This part of the GH loop of three VP3 monomers contributes to the formation of prominent protrusions around the threefold symmetry axis, which is a unique feature for AAVs and is lacking in closely related parvoviruses or densoviruses [208]. These protrusions are the most exposed structures of the AAV capsid, as shown in the depth-cued map of the rAAV9P1 assembled capsid in Figure 3-3 B. Peptides inserted at this position have a high probability of interacting with cellular receptor molecules for cell attachment. This probability is further increased if the nature of the peptide increases the flexibility of the GH loop, as does the glycine-rich P1 peptide.

#### **4.3 RGD-binding integrin heterodimers $\alpha$ v $\beta$ 8 and $\alpha$ v $\beta$ 3/ $\alpha$ v $\beta$ 5 are required for astrocyte transduction by rAAV9P1**

Taken together, the localization of the P1 peptide within the capsid monomer and 60mer renders this peptide highly probable to engage in capsid-receptor interactions. In many cases, interaction partners of peptides can be determined by the presence of minimal recognition motifs in the amino acid sequence [209]. In the case of rAAV9P1, the P1 peptide harbors the amino acid sequence RGD at the N-terminal site of the inserted sequence. This RGD-motif has first been discovered in the extra-cellular matrix (ECM) protein fibronectin and has later been found to be present in several cell-adhesive ECM proteins as the minimal binding motif for a subset of integrins [182]. Integrins are ECM adhesion receptors that bind to ECM proteins for cell attachment and promote reactions and physiological changes of the cell to environmental cues. These reactions include changes in cell migration, proliferation, and angiogenesis, but also induction of survival or apoptosis [186, 210]. By combining members of the 18  $\alpha$ - and eight  $\beta$ -subunits in a specific manner, the human cell is able to generate 24

combinations of functional integrin heterodimers, eight of which have been shown to use RGD as their minimal recognition motif (Fig. 4-1 B)[183]. Using pharmacological inhibitors and CRISPR/Cas9-mediated knockout generation, we identified three integrin heterodimers to be important for the transduction of astrocytic cells by rAAV9P1.

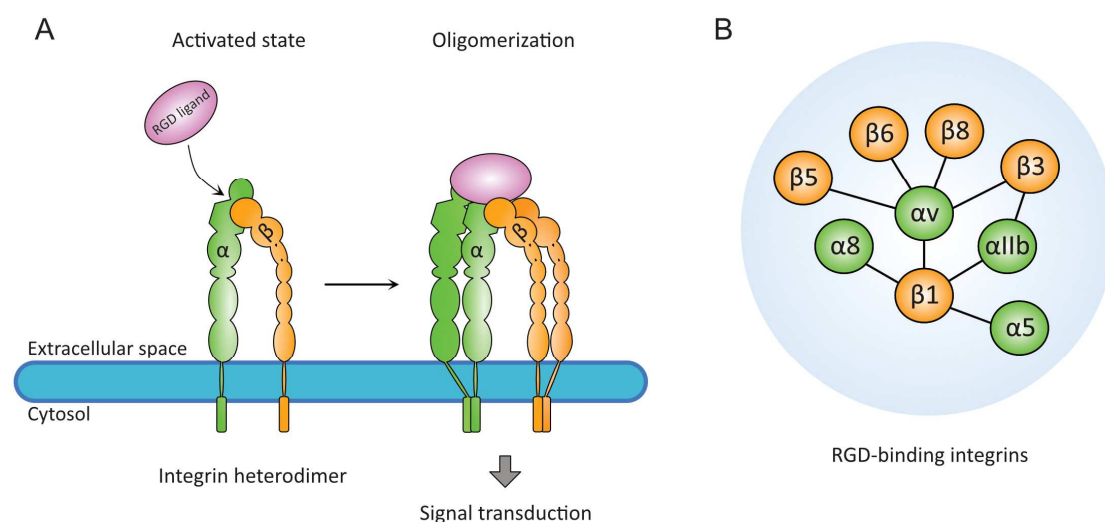


**Figure 4-1 Integrins – an overview.** (A) Schematic representation of an integrin heterodimer anchored in the cellular membrane via its transmembrane domain. Each integrin subunit consists of an extra-cellular, a transmembrane, and an intra-cellular part. A functional integrin is formed by the interaction of an  $\alpha$ - and a  $\beta$ -subunit. In the activated state, specific integrins can bind the RGD motif in proteins of the ECM. Integrins subsequently oligomerize and promote signal transduction via their intra-cellular domains. (B) Combinations of integrin subunits that have been shown to use RGD as their primary interaction motif.

Genetic ablation of the  $\alpha v$  subunit resulted in complete abrogation of effective transduction of U251MG knockout cells by rAAV9P1 as analyzed by flow cytometry. Since lack of the  $\alpha v$  subunits leads to the absence of all integrin heterodimers containing this subunit, this demonstrates the involvement of  $\alpha v$ -containing integrins in rAAV9P1 transduction of astrocytes. Knockout of the *ITGB8* gene showed the same phenotype with drastically reduced levels of cells positive for eYFP transgene expression. Considering that the  $\beta 8$  subunit only pairs with  $\alpha v$ , this leads to the conclusion that the presence of the  $\alpha v\beta 8$  heterodimer on astrocytes is indispensable for transduction by rAAV9P1. Although there are no members of the integrin family that are exclusively expressed on a single cell type in the whole organism, cell-type-specific integrin profiles can be observed [183]. The analysis of RNA sequencing data revealed that in the local environment of the CNS, the *ITGAV* and *ITGB8* genes are expressed considerably higher on mature astrocytes than on neurons. Integrin  $\alpha v\beta 8$  was also shown to be associated with crucial astrocyte functions *in vivo*. Hirota et al. have found that  $\alpha v\beta 8$  is highly expressed on retinal astrocytes and serves as a key regulator of retinal angiogenesis [211]. This

regulatory activity was also described in mouse radial glia in which  $\alpha\beta 8$  promotes stable adhesion of astrocytes to endothelial cells via interaction with its high-affinity ligand latency-associated peptide (LAP) of transforming growth factor  $\beta$  (TGF- $\beta$ ) and supports blood vessel differentiation and stabilization by expressing anti-angiogenic signaling [212]. The binding of  $\alpha\beta 8$  to TGF- $\beta$  LAP is promoted by the interaction with the recognition motif RGDLATI. In this context, the P1 peptide within rAAV9P1 (**RGDLGLS**) mimics the first part of this motif, with RGD being identical and the following amino acid G being a conservative substitution from A [213, 214]. Ablation of  $\alpha\beta 8$  and its subunits have been investigated in many studies, and their effects were summarized by McCarty in 2020 [215]. Overall, these studies have revealed an essential role for astrocytic  $\alpha\beta 8$  in neurovascular development by induction of the TGF- $\beta$  pathway [215]. Given the high importance of abundant expression of  $\alpha\beta 8$  on astrocytes, this molecule qualifies as a receptor to promote astrocyte-selective transduction behavior in the human CNS.

Besides  $\alpha\beta 8$ , there were also two other  $\alpha$  containing integrin heterodimers found to be involved in efficient astrocyte transduction by rAAV9P1. Treatment with the selective  $\alpha\beta 3/\alpha\beta 5$  inhibitor CGT resulted in a dose-dependent reduction of rAAV9P1 transduction efficiency. These results were confirmed by introducing *ITGB3/B5*<sup>-/-</sup> double knockouts in U251MG cells, although transduction efficiency and surface binding were not reduced as drastically as in *ITGB8*<sup>-/-</sup> or *ITGAV*<sup>-/-</sup> cells. Pharmacological inhibition of  $\alpha\beta 3$  alone or single knockouts of the  $\beta 3$ - or  $\beta 5$ -subunit did not influence transduction by rAAV9P1. Both integrin heterodimers  $\alpha\beta 3$  and  $\alpha\beta 5$  have been shown to be involved in astrocytes functioning. Integrin  $\alpha\beta 3$  interacts with the neuronal protein thymocyte differentiation antigen 1 (Thy-1) and thereby induces morphological changes, adhesion, and migration of astrocytes. It is hypothesized that astrocytes react to pro-inflammatory environments and stimulation with tumor necrosis factor after brain injury with higher expression of  $\alpha\beta 3$ , leading to enhanced astrocyte responsiveness and induction of repair mechanisms [216–219]. The  $\alpha\beta 3$ -Thy-1 interaction acts in a bi-directional fashion which triggers the retraction of neural processes and inhibits neurite growth [220]. Interestingly, no strong or differentially regulated expression of  $\alpha\beta 3$  in astrocytes or neurons was detected in RNA sequencing data. In contrast, *ITGB5* expression was increased approximately 2-fold in mature astrocytes compared to neurons, although expression levels remained far below *ITGB8* and *ITGAV* on both cell types. The main function of  $\alpha\beta 5$  on astrocytes has been described to be adhesion. Milner and Sheppard found that primary astrocytes deficient in  $\beta 5$  were unable to adhere to vitronectin coated surfaces, while migration in vitronectin seemed to be more dependent on the presence of  $\alpha\beta 8$  [221]. This could also be observed in the knockout experiments in which U251MG *ITGB5*<sup>-/-</sup> failed to adhere to regular tissue culture flasks but only adhered to surfaces pre-treated with collagen.

These results propose that the efficient transduction of astrocytes by rAAV9P1 requires the interaction with  $\alpha\beta 8$  as an indispensable receptor and with  $\alpha\beta 3$  or  $\alpha\beta 5$ , indicating that the latter two integrins can be used as secondary receptors in a redundant fashion. Indeed,  $\alpha\beta 3$  and  $\alpha\beta 5$  do show similarities that increase the likelihood for their redundant use. Both integrins bind to vitronectin in an RGD-dependent manner [222, 223]. Analysis of the crystal structure of ligand-bound  $\alpha\beta 3$  and subsequent homology modeling of the  $\alpha\beta 5$  structure revealed that their subunits assemble in a similar way, creating comparable requirements for sequence and conformation of ligands [224, 225]. Most integrin inhibitors with nanomolar activities for  $\alpha\beta 3$  inhibition also show inhibiting activity for  $\alpha\beta 5$  in the nanomolar range [186]. This is likely based on the close phylogenetic relationship of the  $\beta 3$ - and the  $\beta 5$ -subunit [226].

Integrins have been shown or proposed to be involved in rAAV transduction in several studies. Most data is available for the best-investigated serotype AAV2. Summerford et al. discovered the interaction of rAAV2 with  $\alpha\beta 5$  by virus overlay assay, and the usage of  $\alpha\beta 5$  as co-receptor was corroborated in later studies [107, 227]. Further studies showed that rAAV2 could utilize other integrins such as  $\alpha 5\beta 1$  as co-receptors for efficient internalization in  $\alpha\beta 5$ -deficient cells via a putative, non-RGD integrin-binding site. This binding site was found to be conserved across several AAV serotypes, including AAV9. One study by Shen et al. showed that in specifically de-sialylated cell lines, transduction by rAAV9 could be reduced by competition with  $\alpha\beta 3$  or  $\alpha\beta 1$  specific antibodies, indicating an involvement of this interaction in rAAV9 transduction [104, 228]. Besides naturally occurring serotypes, studies have investigated the involvement of integrins in the transduction of cells by novel rAAV variants. Here, two variants based on rAAV2 modified by peptide display were described to interact with integrins for cell transduction. Integration of an RGD peptide-containing four additional C residues resulted in interaction with  $\alpha\beta 3$ , while the presence of the peptide PRGDLAP leads to a dependency on  $\alpha\beta 8$  expression on the target cells [229, 230]. Given the abundant expression of integrins throughout the human body and the comparably low cell-type-specific transduction efficiency of naturally occurring serotypes, integrins do not seem suitable for promoting selective transduction. However, the introduction of strong integrin-binding motifs such as RGD might be able to induce an interaction of the rAAV variant capsid with a specific surface integrin that is significantly stronger than the interaction of WT serotypes. If the integrin acts as a primary receptor, cell-selective transduction might be primarily driven by the abundance of the respective integrin on the cell surface. Although stringent specificity for one cell type in the human body might not be achieved by targeting integrins, differential expression of the target integrin in individual compartments might induce selective transduction. Since integrin  $\alpha\beta 8$  expression is not very abundant in the human organism, it might be a suitable candidate for promoting selective transduction. This hypothesis is corroborated by the  $\alpha\beta 8$ -targeting rAAV

Kera2, which efficiently discriminates between human keratinocytes and co-cultured feeder cell lines [230]. The high selectivity of rAAV9P1 might also originate in the dependency on a second integrin co-receptor since high transduction efficiency requires the expression of two independent types of integrin heterodimers on the target cell. This might be a novel strategy for designing highly selective rAAV variants, even outside of the CNS. Future experiments will investigate the physical interaction between AAV9P1 and its integrin receptors by virus overlay assay or cryo-electron microscopy. Further, detailed time-resolved studies should uncover whether the rAAV9P1 binds to both integrin subtypes simultaneously and whether one integrin heterodimer acts as a co-receptor as described for rAAV2.

#### **4.4 rAAV9P1 requires the AAV9 receptors AAVR, LamR, and N-terminal GAL for efficient transduction**

While the interaction of the P1 peptide with cell surface integrins is most likely a prominent feature of efficient and selective transduction of astrocytes by rAAV9P1, this interaction is evidently insufficient to promote the transduction. This was proven by the inability of four rAAV variants carrying the P1 peptide at the same position as rAAV9P1 to efficiently transduce HNSC.100 cells. It was also shown before that insertion of P1 in rAAV2 did not result in increased transduction of astrocytes but instead strongly decreased the transduction of HNSC.100 compared to the WT rAAV2 [147]. This suggests that the capsid of serotype 9, in which the peptide is inserted, plays a significant role in efficient astrocyte transduction. This is in line with several studies that have shown that the effects of peptide insertion on rAAV tropism are dependent on the serotype used and cannot be transferred easily between serotypes [126, 128, 231, 232]. As mentioned earlier, integrin heterodimers can discriminate between different RGD-containing ligands based on the surrounding amino acids and the secondary structure of the RGD region. Therefore, the P1 peptide might adopt a particular conformation within the VP3<sub>AAV9P1</sub> monomer and the fully assembled capsid that renders the peptide favorable for binding to certain integrins and cannot be achieved within a different serotype. Cryo-electron microscopy analysis of rAAV9P1 compared to rAAV2P1 might shed light on potential structural differences within the P1 peptide.

Sequence comparisons of AAV9 with three other serotypes AAV2, 4, and 8 revealed that the P1 insertion site is located within a highly variable region VR-VIII (aa 581-593). While this region has been reported to be involved in HSPG binding by rAAV2 and SIA recognition by rAAV5, no direct involvement in receptor binding has been proposed for VR-VIII in rAAV9 transduction [189, 233, 234]. Several studies using sequence comparisons and domain swapping linked this region to efficient transduction of cardiac and skeletal muscle cells, liver, and pancreatic tissue, as well as slow blood clearance of rAAV9 particles after systemic injection [138, 153, 154, 156, 235, 236]. One of the major obstacles for

using rAAV vectors to target specific cell populations in *in vivo* experiments or gene therapy is off-target transduction and the retention of a substantial amount of injected vectors in organs such as the lung or the liver [237]. Insertion of P1 in VR-VIII of rAAV9 might have the potential to de-target rAAV9P1 from peripheral organs and derived cell types and increase the possibility to reach the CNS even after systemic administration. Weinmann et al. could show that rAAV9P1 (therein called AAVMYO) transduced mouse liver tissue significantly less efficiently than WT rAAV9 after i.v. injection, which indicates that peptide insertion at this position can lead to de-targeting. However, they also observed increased transduction of several musculature groups compared to rAAV9, highlighting again that rAAV9P1 is not a completely astrocyte-specific rAAV variant [203]. In this context, it should be mentioned that rAAV9P1 did transduce cell lines derived from lung and liver carcinomas at good efficiencies in cell culture experiments performed for the targeted mutagenesis studies. The transferability of these *in vitro* results to *in vivo* usage needs to be further investigated but possible *in vivo* off-target transduction by rAAV9P1 should be considered as probable.

The capsid binding sites for the primary receptors of rAAV9 have been mapped by directed mutagenesis studies (GAL binding pocket) or analysis of sequence identity to the receptor binding sites of the closely related rAAV8 (LamR binding footprint). In rAAV9P1, none of the currently identified receptor binding sites in the VP3<sub>AAV9P1</sub> protein is compromised by the P1 insertion. The second part of the laminin receptor binding footprint, which was predicted from sequence homology to AAV8, is located at aa 591-621 and, therefore, in close proximity to the P1 insertion site. However, the sequence alignment in Figure 3-3 A shows that the structure of VP3<sub>AAV9P1</sub> is not severely altered by the P1 insertion in this region. This introduces the possibility that receptor binding promoted by the P1 peptide adds to the pre-existing receptor binding profile of AAV9 rather than replacing existing capsid-cell interactions, which results in a gain-of-function in the new capsid variant. This is a fundamental advantage over peptide insertions into AAV2 at the same position, in which a substantial part of the HSPG binding site is destroyed and replaced by a novel receptor binding site. Using CRISPR/Cas9 mediated knockout generation and modulation of the glycan landscape in U251MG cells, it was proven that all described receptors for AAV9, namely LamR, AAVR, and GAL, are required for efficient astrocyte transduction by rAAV9P1.

In this context, GAL does not occur as an isolated molecule on the cell surface but as the terminal component of N-linked glycans (N-glycans). N-glycans consist of a variety of different monosaccharides linked together by glycosidic bonds that are synthesized in the ER and can be covalently connected to proteins and lipids. These glycoconjugates on glycoproteins and glycolipids are further trimmed and expanded in the ER or the Golgi apparatus by glycosidases and glycosyltransferases resulting in several classes and a plethora of individually constructed N-glycans. In general, trans-membrane and secreted

proteins are targets of intense glycosylation which leads to the establishment of a thick and heavily interlinked layer on the cellular surface, called glycocalyx [238–240]. The glycocalyx shows high variability between cell types and even individual cells of a tissue and has been shown to take active contribution in a broad spectrum of cellular functions, reviewed by Varki in 2017 [240]. In the CNS, the glycan landscape has been correlated with neural development, especially with changes in signal transduction and differentiation, but also cell adhesion and molecular trafficking [241]. Due to limited availability of sensitive and accurate analysis methods, the exact distribution of individual N-glycans on different CNS cells remains elusive. However, it has become more and more evident that major changes in the glycan profile can be associated with pathologies of the CNS, including neurodegenerative and psychological disorders, as well as glioma- and neuroblastoma, highlighting the importance of tightly regulated glycosylation (reviewed in [241]). Neuronal cells seem to carry an increased number of di-, or poly-sialylated glycoconjugates and use this pattern for efficient communication with glial and immune cells. Poly-sialylation is a prominent feature of neurons in different stages of neuronal differentiation, but also on several populations of post-mitotic neurons which was reviewed in great detail by Schnaar et al. [242]. It was shown in this thesis that de-sialylation of U251MG cells leads to an increased transduction by rAAV9P1, indicating that terminal SIA is detrimental for efficient astrocyte transduction. This higher expression of N-glycans with terminal SIA on neurons might be an explanation for the favored transduction of non-neuronal cells by rAAV9P1. This also leads to the hypothesis that local applications of de-sialylating agents such as Neu *in vivo* might increase the general transduction efficiency of rAAV9P1, as it already has been proposed by Shen et al. [118]. While this approach might be beneficial for general transduction, it has to be considered that de-sialylation of all CNS cells might favor targeting of neurons and therefore decrease the astrocyte-selectivity of rAAV9P1. These considerations should be addressed in future *in vivo* studies. While de-sialylation of target cells ubiquitously removes terminal SIA and exposes underlying sugar moieties, the identity of this terminal monosaccharide was identified as GAL since treatment with the GAL-binding lectin ECL strongly decreased transduction efficiency. So far, no detailed studies have been conducted on the differential expression of N-linked glycans with terminal GAL on glial cells and neurons in the CNS. Further studies need to analyze the distribution of N-glycans on different CNS cell types by lectin staining or mass spectrometry analyses to confirm these hypotheses.

For the other identified receptors, the analysis of the online available RNA sequencing dataset revealed that AAVR is expressed on astrocytes without a highly variable expression between mature astrocytes and neurons. LamR expression levels were comparably low in mature astrocytes and neurons in the RNA sequencing dataset. However, LamR expression seems to be considerably higher in fetal astrocytes and decreases with differentiation [185]. This could partially explain why rAAV9P1 transduces astrocyte enriched, differentiated HNSC.100 cells less efficiently than progenitor-like,

proliferating HNSC.100 cells. Both molecules have been shown in knockdown/knockout experiments to be necessary for transduction of a specific cell line, but the roles of LamR and AAVR in cell binding and effective transduction by rAAV9 vectors are still elusive.

Pillay et al. have investigated the contribution of AAVR to rAAV2 infectivity and have proposed the model that AAVR is a prerequisite for efficient AAV endocytosis (reviewed by Summerford et al in [243]). Cryo-electron tomography of rAAV2 complexed with a truncated AAVR construct showed that VR-I and VR-III of rAAV2 are most likely to interact with AAVR and that, among others, S262 is a contact residue of VP1<sub>AAV2</sub> and AAVR [181]. Comparing the sequence of VP1<sub>AAV9P1</sub> with VP1<sub>AAVD20P1</sub> and VP1<sub>AAVS1P1</sub>, the least efficient representatives of the P1 variants on HNSC.100 cells, revealed an amino acid replacement of S263G in VR-I. Mutation of this amino acid in VP1<sub>AAV9P1</sub> led to complete abrogation of transduction of astrocytes and also of other cell lines. TEM analysis confirmed that AAV9P1<sub>S263G</sub> could still form particles with AAV-typical morphology (data not shown), indicating that capsid assembly and particle production are not hindered by this mutation. Further, P1 variants carrying the S263G mutation (rAAVS1P1, rAAVD20P1) did not show significantly reduced binding to HNSC.100 cells compared to the other variants (rAAVS10P1, rAAVH15P1), however, successful transduction (indicated by transgene expression in the flow cytometry analysis) was decreased substantially. A possible explanation could be that AAVR is involved in efficient endocytosis of rAAV particles and not in initial cell surface binding. Although these results need further investigation and confirmation, it might indicate the involvement of rAAV9 VR-I in receptor binding, supposedly interaction with AAVR. Further detailed studies are necessary to investigate the interaction of rAAV9 and rAAV9P1 with the universal AAVR and are beyond the scope of this study.

#### **4.5 The unique rAAV9P1 receptor profile of human astrocytes**

From these results, a detailed profile of the astrocyte target molecules for efficient rAAV9P1 transduction could be constructed (Fig. 4-2). This profile consists of the main receptors N-linked glycans with terminal GAL, the integrin  $\alpha\beta 8$ , and the universal AAVR. LamR and the integrins  $\alpha\beta 3$  and  $\alpha\beta 5$  could be identified as auxiliary receptors. It could be shown that availability of HSPG on human astrocytes is not a determining factor for efficient transduction by rAAV9P1. Noticeably, this profile is distinct from the rAAV2 receptor profile. Although rAAV2 can also efficiently transduce human astrocytes it does so in a HSPG and AAVR dependent fashion without the contribution of any of the rAAV9P1 main receptors. These results show that the described rAAV9P1 receptor profile is a complementation of the rAAV9 receptors that have been published already.

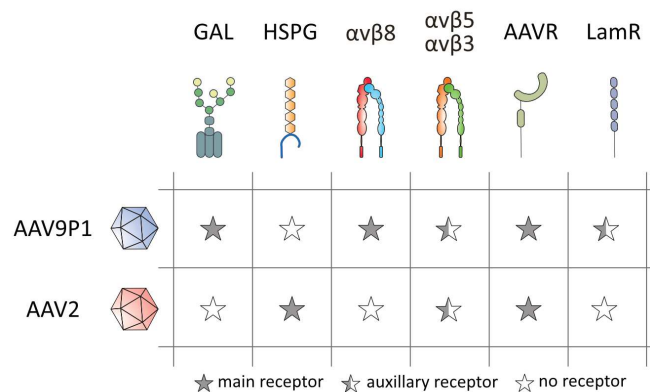


**Figure 4-2 Comparison of the receptor profile of rAAV9P1 and rAAV2 for human astrocytes.** rAAV9P1 uses terminal N-linked galactose (GAL), integrin  $\alpha\beta 8$ , and AAVR as its primary receptors while the integrins  $\alpha\beta 3$  and  $\alpha\beta 5$  as well as LamR function as auxiliary receptors. rAAV9P1 transduction is independent from HSPG. In contrast, rAAV2 transduction is promoted by the main receptors HSPG and AAVR and to a lesser extent by the secondary receptors integrins  $\alpha\beta 3$  and  $\alpha\beta 5$ .

So far, it can only be speculated how rAAV9P1 interacts with these main and auxiliary receptors and how these interaction events are spatially and temporally separated. With information from published data on rAAV9 interaction with surface receptors, it can be hypothesized that rAAV9P1 interacts with GAL residues and  $\alpha\beta 8$  for initial binding and cell recognition and subsequently connects to LamR and the auxiliary integrins  $\alpha\beta 3$  and  $\alpha\beta 5$  via un-occupied P1 peptide residues or a putative, non-RGD integrin binding site to increase rAAV particle capture at the cell surface. Bound rAAV9P1 particles might later interact with AAVR in a so far undetermined fashion for efficient endocytosis and uptake into the cell. This proposed cell surface binding model needs to undergo thorough validation.

#### 4.6 A CRISPR/Cas9 knockout screen reveals involvement of intra-cellular pathways for astrocyte transduction by rAAV9P1

The investigation of receptors for novel rAAV variants is crucial for their advance into clinical settings. Genome-wide CRISPR/Cas9 knockout screens are a powerful tool to study the effects of mutations in every cellular protein-coding gene in an experimental setting. After the first CRISPR/Cas9 screens were conducted in 2014 by two independent labs, this technique has been applied in many studies as an unbiased approach to identify key players and pathways in virus infections such as influenza A virus, Zika virus, Ebola virus, Dengue virus, and SARS-CoV2, among others [244–250]. This technique has been used in AAV research to discover two key factors in rAAV vector transduction, namely AAVR in haploid human cells (HAP1) and G Protein-Coupled Receptor 108 (GPR108) in Huh7 AAVR<sup>-/-</sup> cells [102, 251]. Here, we have performed the first genome-wide CRISPR/Cas9 screen in a human glioblastoma cell line U251MG to investigate factors required for transduction by rAAV9P1. Our results revealed a

substantial number of genes enriched in the eYFP negative sorted population compared to the unsorted control.

Since target molecules on the surface of astrocytes have already been investigated in our hypothesis-driven approach, the eYFP-negative dataset of 1326 genes FGL-1326 was analyzed for enrichment of intra-cellular canonical and associated pathways, as well as biological processes. An upfront analysis of GL-2715 and FGL-1326 for tissue association and MeSH-terms revealed a strong representation of brain tissue or brain diseases, respectively, and served as proof of principle for the tissue association of the gene set.

We found that four out of nine enriched pathways had p-values of 0.0060 and lower and showed a strong physiological relevance for astrocytes. Activity of the Shh canonical pathways was reported to be exclusive to a certain subpopulation of astrocytes in the adult brain and seems to be activated by the expression of Shh in neurons, thereby contributing to bidirectional astrocyte-neuron communication. Shh signaling and subsequent gene expression mediates the ability of astrocytes to regulate the extracellular synaptic environment and therefore synaptic transmission. In addition, Shh activity in astrocytes is associated with neuroprotection by lowering the BBB permeability and exerting anti-inflammatory actions (reviewed in [252]). G-CSF is involved in neuroprotection via angiogenesis which is promoted by vascular endothelial growth factor produced by G-CSF stimulated astrocytes, among others, and in strengthening of the BBB in rats, although this could not be precisely linked to astrocytes (reviewed in [253, 254]). Inositol-1,4,5-trisphosphate (IP3) is an important second messenger in astrocytes that leads to calcium efflux from the ER via the IP3 receptors which is associated with a broad variety of astrocytic functions [255]. EGFR has manifold responsibilities in astrocytes. It plays a role in astrocyte differentiation, maturation, and morphology which influences proper axonal development in neurons. EGF-stimulation of astrocytes promotes axonal growth of neurons and neuroprotection by production of neurotrophic factors. It was suggested that EGFR is involved in astrocyte activation and glial scar formation after CNS injury (reviewed in [256]). SST is also involved in astrocyte-neuronal communication where firing of SST producing interneurons leads to activation of calcium signaling in astrocytes thereby increasing inhibitory transmission by these neurons (reviewed in [257]).

Two of the nine enriched pathways detected in this screen have been described in relation to rAAV transduction. Molecules of the inositol metabolism pathway are generally involved in standard physiological processes such as vesicle trafficking, migration, cytoskeleton reorganization or proliferation [258]. Especially changes in the vesicle trafficking or cell proliferation are prone to negatively affect rAAV transduction. As an example, activation of the phosphatidylinositol-3 kinase (PI3K), an important member of the inositol phosphate metabolism pathway, has been implicated to

be required after endocytosis to guide rAAV2-containing vesicles to the nucleus alongside the microfilaments and microtubules of the cytoskeleton [227]. It is still up for discussion whether different AAV serotypes use different intra-cellular pathways to reach the nucleus, but it is possible that rAAV9P1 transport is facilitated by a highly active PI3K in astrocytes. The second pathway with a connection to AAV transduction is the EGFR pathway. EGFR has been described as a direct co-receptor for rAAV6 transduction and internalization, but not for rAAV2 or rAAV5 [116]. In contrast, an active EGFR protein tyrosine kinase (EGFR-PTK) has been shown to phosphorylate rAAV2 capsids after escape from the endosome and mark virus particles for ubiquitination and subsequent proteasomal degradation. Inhibition of this tyrosine kinase leads to increased transduction efficiency of rAAV2 in different cell types. The tyrosine, serine, and threonine residues that are most important for reduced transduction efficiency upon phosphorylation have been closely mapped by targeted mutagenesis studies [193, 259–261]. So far there is no evidence that rAAV9 or rAAV9P1 are also negatively influenced by EGFR-PTK activity. Comparison between the sequences of VP1<sub>rAAV2</sub> and VP1<sub>rAAV9P1</sub> revealed that one of the mapped tyrosine and several of the serine and threonine residues are substituted with other amino acids in rAAV9P1 indicating that it might not be target of intense phosphorylation by EGFR-PTK and subsequent degradation. Interestingly, the two pathways with AAV association were also determined to be astrocyte-relevant in an independent analysis of the nine enriched pathways as mentioned above.

It should be mentioned that FGL-1326 contained several genes associated with TGF- $\beta$  pathways although individual TGF- $\beta$  pathways were not significantly enriched. Among these genes were major transcription factors and key regulators of the TGF- $\beta$  receptor pathway. The activation of the TGF- $\beta$  by the interaction of  $\alpha$ v $\beta$ 8 with TGF- $\beta$  LAP is common in astrocytes and is responsible for most  $\alpha$ v $\beta$ 8-induced functions of astrocytes such as regulation of angiogenesis. Therefore, it is possible that rAAV9P1 not only utilizes  $\alpha$ v $\beta$ 8 for efficient cell surface binding but may also depend on a functional, intra-cellular TGF- $\beta$  signaling cascade.

Taken together, the results of this screen strongly suggest the involvement of intra-cellular pathways in efficient transduction of astrocytes by rAAV9P1. Since four of the enriched pathways were identified as astrocyte-relevant, it is possible to assume that members of these pathways might contribute to the astrocyte selectivity of rAAV9P1. The relevance of this screen is further supported by the observation that two of detected pathways have already been associated with rAAV vector transduction.

The exact contribution of how members of these pathway influence the intracellular processing of rAAV9P1 still needs to be investigated. Further studies will have to dissect these relationships by CRISPR/Cas9 mediated target validation, pharmacological inhibition, or investigation of the interaction

between rAAV9P1 and key elements of the detected pathways by immunoprecipitation and immunoblot.

#### 4.7 Future perspectives for rAAV9P1

In this study, the broad receptor profile of the novel rAAV vector variant rAAV9P1 on astrocytes was described. It was shown that the astrocyte targeting is very likely to be based on the combinatorial interaction of this modified capsid with several cellular molecules. While the individual molecules are not exclusively expressed by astrocytes, together they enable an astrocyte-selective transduction behavior in the closed compartment of the CNS. In this aspect, rAAV9P1 clearly differs from vectors derived from the naturally occurring serotype AAV2 that efficiently transduces astrocytes via interaction with the ubiquitous surface molecule HSPG, but therefore lacks cell type selectivity. These findings might encourage a new strategy in the development of cell type-selective rAAV vectors that takes into account that the AAV capsid utilizes several receptor molecules for efficient transduction and that cell type selectivity does not need to depend on the availability of one highly cell-type-specific molecule.

The insertion of the P1 peptide into the AAV9 capsid enables rAAV9P1 to use  $\alpha\beta8$  and  $\alpha\beta3/\alpha\beta5$  as additional receptors for efficient transduction of astrocytes. While resting astrocytes usually express  $\alpha\beta8$  and  $\alpha\beta5$  at relatively high levels,  $\alpha\beta3$  was shown to be upregulated upon neurotrauma and promotes reactivity of astrocytes. This enables the possibility of rAAV9P1 to transduce both resting and reactive astrocytes by the alternate use of the two redundant receptors  $\alpha\beta3$  and  $\alpha\beta5$  in *in vivo* models. Current methods for astrocyte-selective transduction usually rely on the usage of GFAP or similar promoters for astrocyte-specific expression of the delivered transgene [142, 143]. However, GFAP is strongly upregulated in reactive astrocytes and, therefore, this approach induces a bias towards the transduction of activated astrocytes. Furthermore, implementation of cell-specific expression strategies affects only expression of the delivered gene but does not change the targeting behavior of the vector particle. *In vivo* studies need to verify this hypothesis and analyze the transduction behavior and distribution of rAAV9P1. Analysis of an RNA sequencing dataset from mouse CNS cells revealed that the  $\alpha$ ,  $\beta8$ , and  $\beta5$  subunits are also stronger expressed on astrocytes than on neurons, indicating that astrocyte selectivity might also be achieved in the mouse brain [262]. Preliminary studies on astrocyte-selective transduction after systemic injection in the mouse model have revealed good BBB penetrance and mainly targeting of astrocytes by rAAV9P1, although these results need further validation (unpublished data generated in collaboration with Prof. Magdalena Götz and Matteo Puglisi). Therefore, rAAV9P1 might present a valuable tool for studying neural

differentiation, basic astrocyte functions, and even neuro-protective astrocyte reprogramming in the mouse model.

As already mentioned above, the cell surface integrin expression profile can be highly variable between cell types and promote selectivity within a certain compartment in the organism. However, due to the ubiquitous integrin expression in the human body, a systemic injection will inevitably lead to off-target transduction. This was observable in our preliminary mouse experiments as well as in experiments conducted by Weinmann et al. [203]. By performing RNA sequencing studies or analyzing online available RNA sequencing and protein expression datasets, the integrin distribution in certain tissues or cell types can be investigated, enabling the evaluation of possible off-target organs before the start of animal experiments. To increase the astrocyte selectivity of rAAV9P1 after systemic administration, further development of the vector is necessary to de-target rAAV9P1 from off-target tissues. One possibility is the usage of cell-type-specific microRNAs. The incorporation of microRNA binding sites in the proximity of the transgene leads to complex formation and subsequent degradation of the transcript by the microRNA-induced silencing complex (miRISC). Several tissue-specific or enriched microRNAs have been described so far and have been proven to be efficient in restricting transgene expression (reviewed in [263]). In the context of rAAV9P1, microRNAs for muscle de-targeting could increase astrocyte selectivity and lead to improved usability in possible *in vivo* settings.

rAAV9P1 might also be well suited for selective targeting of glioblastoma. Studies have shown that  $\alpha$  integrins are upregulated in glioblastoma samples and that their expression correlates with the severity of the GBM [264]. Among these,  $\alpha\beta3$ ,  $\alpha\beta8$ , and  $\alpha\beta5$  are upregulated in glioblastoma tissue and especially the expression of  $\alpha\beta3$  and  $\alpha\beta8$  correlates with malignancy of the tumor and poor survival rate of the patient [265]. Higher integrin expression favors proliferation, invasion, and vascularization of the glioblastoma tissue, which even lead to the development and Phase III clinical testing of the integrin inhibitor CGT as a glioblastoma drug (reviewed in [266]). This specific integrin expression profile on glioblastoma cells might favor them for efficient transduction by rAAV9P1 since many (co-)receptors are expressed in high quantity. This is in line with the observation that the glioblastoma cell line U251MG is transduced by rAAV9P1 with generally higher efficiencies than the astrocyte cell line HNSC.100. It must be considered that integrin subtype expression varies between glioblastoma subtypes and cell types, and further studies are needed to investigate the performance of rAAV9P1 in glioblastoma mouse models.

## 5 Summary

Astrocytes are among the most abundant cell types in the human central nervous system (CNS). They have critical functions in the brain, including the maintenance of neuronal homeostasis and active contribution to the formation, regulation, and maintenance of synapses and synaptic transmission. Further, astrocytes react to CNS damage with proliferation and have been shown to adapt neuronal functions in mice after the artificial expression of neurogenic factors. Astrocytic dysregulation is associated with a variety of neuropathologies, including psychological and neurodegenerative diseases. Treatment strategies for these diseases that rely on modifying the astrocytic gene or protein expression are subject of current research. The main obstacle in this pursuit is the lack of efficient and specific vectors for targeted astrocyte transduction. Adeno-associated virus (AAV) vectors are considered the gold standard for gene therapy due to their favorable biological characteristic. The variant rAAV9P1 has been described to efficiently transduce astrocytes *in vivo* and discriminate between astrocytes and neurons. However, the molecular base of this transduction behavior is still elusive.

In this work, we have investigated the underlying molecular profile that enables efficient and selective transduction of astrocytes by rAAV9P1. We could show that rAAV9P1 transduces astrocytic cell lines more efficiently than vectors derived from its parental serotype AAV9 and with higher selectivity than vectors carrying a capsid from the well-investigated serotype AAV2. It was found that rAAV9P1 follows a transduction mechanism that is distinctly different from the HSPG-dependent, ubiquitous transduction of rAAV2. On the molecular level, rAAV9P1 engages with  $\alpha$ v-containing integrins, likely via the RGD-sequence in the inserted P1 peptide. These integrins include  $\alpha$ v $\beta$ 8 as a central receptor and  $\alpha$ v $\beta$ 3/ $\alpha$ v $\beta$ 5 as potential redundant auxiliary receptors. Besides, rAAV9P1 transduction is dependent on classical AAV9 receptors such as terminal galactose on N-linked cell surface glycans, the 37/67 kDa laminin receptor (LamR), and the essential AAV receptor KIA00319L (AAVR). Furthermore, a genome-wide CRISPR/Cas9 screening in a human glioblastoma cell line revealed that intra-cellular pathways with astrocyte-relevance might be involved in efficient and selective transduction of astrocytes by rAAV9P1.

Taken together, this work presents the detailed receptor profile of rAAV9P1, which achieves high efficiency and cell-type selectivity by combining the binding to new receptors through capsid modifications with pre-existing receptors of the parental serotype. This multi-factorial binding might pave the road for the future development of more cell-type-selective rAAV vectors, but also refining of rAAV9P1 for future *in vivo* and gene therapy approaches.

## 6 Appendix

### 6.1 Supplementary information

**Table 6-1 Canonical pathways enriched in FGL-1326.** The list shows canonical pathways enriched in the analysis of the FGL-1326 gene list with the Gene Ranker tool. Pathways are sorted and assigned ranks according to their p-value. The relation of the expected number of genes belonging to this pathway and the actual observed number of genes in FGL-1326 serves as a measure of enrichment. *Astro-relevance* indicates relevance of this pathway in astrocytes according to literature review; *AAV-related* indicated involvement in AAV transduction according to literature review.

Rank	Pathway	P-value	#[genes expected]/ #[genes observed]	Astro-relevance	AAV-related
1	Signaling events mediated by the Hedgehog family	2,95E-03	1.498/6	✓	
2	Inositol phosphate metabolism	3,39E-03	3.120/9	✓	✓
3	Formyltetrahydroformate biosynthesis	4,19E-03	0.374/3		
4	Nicotine pharmacodynamics pathway	6,67E-03	1.747/6		

**Table 6-2 Associated pathways enriched in FGL-1326.** The list shows associated pathways enriched in the analysis of the FGL-1326 gene list with the Gene Ranker tool. Pathways are sorted and assigned ranks according to their p-value. The relation of the expected number of genes belonging to this pathway and the actual observed number of genes in FGL-1326 serves as a measure of enrichment. *Astro-relevance* indicates relevance of this pathway in astrocytes according to literature review; *AAV-related* indicated involvement in AAV transduction according to literature review.

Rank	Pathway	P-value	#[genes expected]/ #[genes observed]	Astro-relevance	AAV related
1	Interleukin 5 (colony stimulating factor, eosinophil)	5,12E-04	3.958/12		
2	Granulocyte colony stimulating factor	1,44E-03	3.850/11	✓	
3	B cell receptor	2,50E-03	10.031/20		
4	Epidermal growth factor receptor	6,00E-03	28.953/43	✓	✓
5	FMS-like receptor tyrosine kinase 3	7,02E-03	4.066/10		

## 6.2 Equipment

Equipment	Manufacturer
Accu-jet® pro	Brand, Wertheim, GER
Agarose gel chamber model B1A and B2	Peqlab, Erlangen, GER
Bacteria shaker – Minitron	Waters, Eschborn, GER
Biological safety cabinet HERAsafe Heraeus™	Thermo Fisher Scientific, Waltham, MA, USA
Centrifuge Hettich® Rotana 460 R	Hettich, Westfalen, GER
Centrifuge Jouan CR3i	DJB Labcare, Buckinghamshire, UK
ChemiDoc™ XRS	Bio-Rad Laboratories Inc., Hercules, CA, USA
CO2 Incubator HERAccl™ 150i	Thermo Fisher Scientific, Waltham, MA, USA
FACSria III	BD Biosciences, Franklin Lakes, TN, USA
FACSCanto II	BD Biosciences, Franklin Lakes, TN, USA
Fluorescence microscope EVOS FL Cell Imaging System	Thermo Fisher Scientific, Waltham, MA, USA
Fridge 4 °C	Liebherr, Ulm, GER
Freezer -20 °C	Liebherr, Ulm, GER
Freezer -80 °C	Thermo Fisher Scientific, Waltham, MA, USA
Fusion FX	Vilber, Eberhardzell, GER
HandyStep® electronic	Brand, Wertheim, GER
High precision scale	Mettler Toledo, Columbus, OH, USA
Invitrogen Qubit 2.0	Thermo Fisher Scientific, Waltham, MA, USA
Labarotory scale L310	Sartorius, Göttingen, GER
Laboson 200 water and sonication bath	Bender & Hobein AG, Zurich, SUI
Light cycler® 480II 96	Roche, Basel, SUI
Magnetic stirrer with heating unit Combimag REO	IKA, Staufen, GER
Microplate reader Infinite® M200	Tecan, Männedorf, SUI
Mini-Protean® Tetra cell gel electrophoresis chamber	Bio-Rad Laboratories Inc., Hercules, CA, USA
Mr. Frosty™ Freezing Container	Thermo Fisher Scientific, Waltham, MA, USA
Multi-channel pipet Research Plus (100 µl)	Eppendorf, Hamburg, GER
NanoRop™ 2000 Spectrophotometer	Thermo Fisher Scientific, Waltham, MA, USA

Pipets Research Plus	Eppendorf, Hamburg, GER
PowerPac™ Basic	Bio-Rad Laboratories Inc., Hercules, CA, USA
Preparative ultracentrifuge Beckman Optima L-60	Beckman Coulter, Brea, CA, USA
Primovert light microscope	Carl-Zeiss, Jena, GER
Protean® Gel casting system	Bio-Rad Laboratories Inc., Hercules, CA, USA
Qubit™ Fluorometer	Thermo Fisher Scientific, Waltham, MA, USA
Shaker IKA® MS3 basic	IKA, Staufen, GER
Tabletop centrifuge Minifuge Sprout	HeathrowScientific, Nottingham, UK
Tetra Blotting Module	Bio-Rad Laboratories Inc., Hercules, CA, USA
Thermocycler peqSTAR 96 universal gradient	VWR, Radnor, PA, USA
Thermomixer 5436	Eppendorf, Hamburg, GER
Vacuum pump VACUSAFE Comfort	Integra Biosciences GmbH, Biebertal, GER
Vortex Orbit 300	Labnet international inc., Edison, NJ, USA
Water bath	GFL, Hannover, GER

## 7 Abbreviations

∅	diameter
αβγ	Integrin with α-subunit x and β-subunit y
aa	amino acid
AAV (1-11)	Adeno-associated virus (Serotype 1-11)
AAP	Assembly activating protein
AAVR	Adeno-associated virus receptor
Aldh1l1	Aldehyde dehydrogenase 1 family member L1
APS	Ammoniumpersulfate
AQP4	Aquaporine 4
b	Base
BBB	Blood brain barrier
BCA	Bicistronic acid
bp	Base pair
BSA	Bovine serum albumin
C1q	Complement component 1q
CaCl <sub>2</sub>	Calcium chloride
Cap	Capsid gene of AAV
Cas9	Clustered regulatory interspersed small palindromic repeats associated 9
CD4	Cluster of differentiation 4
CD9	Cluster of differentiation 9
CGT	Cilengitide
Ch.5	Chimpanzee AAV variant 5
CMV	Cytomegalo virus
CNS	Central nervous system
CO <sub>2</sub>	Carbon dioxide
Cre	Causes recombination
CRISPR	Clustered regulatory interspersed small palindromic repeats
Ct	Cycle threshold
CTB	Cell titer blue
DMEM	Dulbecco's modified eagles medium
DMSO	Dimethyl sulfoxide
DNA	Desoxyribonucleic acid
dNTPs	Deoxy-nucleoside triphosphate
DPAGT1	UDP-N-acetylglucosamine-dolichyl-phosphate N-acetylglucosamine-phospho-transferase
ds	Double-stranded
dsDNA	Double-stranded DNA
E1A	Early-region 1A
E1b55K	Early-region 1B 55 kilodalton
E2A	Early-region 2A
E4orf6	Early-region 4, open reading frame 6

ECL	<i>Erythrina cristagalli</i> lectin
ECM	Extra cellular matrix
EDTA	Ethylenediaminetetraacetic acid
EGF	Epithelial growth factor
EGFR	Epithelial growth factor receptor
EGFR-PTK	Epithelial growth factor receptor protein tyrosine kinase
ER	Endoplasmic reticulum
ERT2	Estrogen receptor 2
eYFP	Enhanced yellow fluorescent protein
FACS	Fluorescence activated cell sorting
FCS	Fetal calf serum
FGFR1	Fibroblast growth factor receptor 1
Fig.	Figure
FITC	Fluorescein
FGF-2	Fibroblast growth factor 2
FPKM	Fragments per kilo base per million mapped reads
FSC	Forward scatter
g	Gravitation
GAL	Galactose
G-CSF	Granulocyte colony stimulating factor
gDNA	Genomic DNA
Gfa2	2.2 kb minimal glial fibrillary acidic protein promoter
gfaABC1D	600 bp truncated minimal glial fibrillary acidic protein promoter
GFAP	Glial fibrillary acidic protein
Gjb6	Gap junction protein beta 6
GLAST	Glutamate aspartate Transporter 1
GLT1	Glutamate transporter 1
GO	Gene ontology
GOI	Gene of interest
GPR108	G Protein-Coupled Receptor 108
H <sub>2</sub> O	Milli-Q water
HCl	Hydrochloric acid
HEPACAM	Hepatic and glial cell adhesion molecule
HEPES	4-(2-hydroxyethyl)-1-piperazineethanesulfonic acid
HGFR	Hepatocyte growth factor
HIV-1	Human immunodeficiency virus type 1
HNSC.100 prol	Proliferating HNSC.100 cells
HNSC.100 diff	Differentiated HNSC.100 cells
HPLC	High performance liquid chromatography
HSPG	Heparan sulfate proteoglycan
IgG	Immunoglobulin G
IP3	Inositol 1,4,5-trisphosphate

ITR	Inverted terminal repeat
Kb	Kilo bases
KCl	Potassium chloride
kDa	Kilo dalton
KH <sub>2</sub> PO <sub>4</sub>	Monopotassium phosphate
KIAA0319L	Dyslexia associated protein KIAA0319 like
LAP	Latency-associated peptide
LamR	37/67 kDa laminin receptor
LB-medium	Lysogeny broth medium
LIC	Ligation independent cloning
LV	Lentiviral vectors
μ	Micro
MeSH	Medical subject headings
MFI	Median fluorescence intensity
MgCl <sub>2</sub>	Magnesium chloride
miRISC	MicroRNA-induced silencing complex
MOI	Multiplicity of infection
mRNA	Messenger RNA
NaCl	Sodium chloride
Na <sub>2</sub> HPO <sub>4</sub>	Di sodium phosphate
Na/K-ATPase	Sodium/Potassium-Adenosintriphosphatase
NaOH	Sodium hydroxide
Nef	Negative regulatory factor
Neu	Neuraminidase
NG-2 glia	Nerve/glial antigen 2
NGS	Next generation sequencing
NP40	Nonidet P40
nt	Nucleotides
OPC	Oligodendrocyte progenitor cells
Opti-MEM	Optimal Eagle's Minimal Essential Medium
ORF	Open reading frame
p5	AAV promoter 5
p19	AAV promoter 19
p40	AAV promoter 40
PAGE	Polyacrylamide gel electrophoresis
PBS(-T)	Phosphate buffered saline (with Tween)
PCR	Polymerase chain reaction
PDB	Protein data bank
PDGFR	Platelet derived growth factor receptor
PI3K	Phosphatidylinositol 3-kinase
PLA2	Phospholipase A2
qRT-PCR	Quantitative real-time PCR

rAAV	Recombinant adeno-associated virus
rABA	<i>In vitro</i> rAAV-Binding assay
RBE	Rep binding elements
Rep	Replication gene of AAV
Rep40	40 kilo Dalton non-structural proteins of AAV
Rep52	52 kilo Dalton non-structural proteins of AAV
Rep68	68 kilo Dalton non-structural proteins of AAV
Rep78	78 kilo Dalton non-structural proteins of AAV
RGD	Arginine-glycine-aspartic acid
Rh.8	Rhesus monkey AAV variant 8
RNA	Ribonucleic acid
RPII	RNA Polymerase II
RPE	Retinal pigment epithelium
RT	Room temperature
scAAV	Self-complementary AAV
SDS	Sodium dodecylsulfate
SEM	Standard error of the mean
sgRNA	Single guide RNA
Shh	Sonic hedgehog
SIA	Sialic acid
siRNA	Small interfering RNA
Slc1a3	Solute carrier family 1 member 3
SNA	<i>Sambucus nigra</i> lectin
S.O.C.	Super optimal broth
Sox9	Sex-determining region Y (SRY) box transcription factor 9
ss	Single-stranded
ssAAV	Single-stranded AAV
SSC	Side Scatter
ssDNA	Single-stranded DNA
SST	Somatostatin
Tat	Trans-activator of transcription
TEMED	Tetramethylethylenediamine
TGF- $\beta$	Tumor growth factor $\beta$
Thy-1	Thymocyte differentiation antigen 1
TRS	Terminal resolution site
TUN	Tunicamycin
U	Unit
VA-RNA	Virus-associated ribonucleic acid
vg	Vector genome
VP1/2/3	Structural proteins of AAV
VR	Variable region
VSV-G	Vesicular stomatitis virus glycoprotein

(v/v)	Volume per volume
VWMD	Vanishing white matter disease
WT	Wildtype
(w/v)	Weight per volume

## 8 References

1. Virchow R (1871) Vorlesungen über Pathologie, Erster Band: Die Cellularpathologie in ihrer Begründung auf physiologische und pathologische Gewebelehre, 4th ed. Verlag von August Hirschwald
2. Allen NJ, Lyons DA (2018) Glia as architects of central nervous system formation and function. *Science* (80- ) 362:181–185
3. Bass NH, Hess HH, Pope A, Thalheimer C (1971) Quantitative cytoarchitectonic distribution of neurons, glia, and DNA in rat cerebral cortex. *J Comp Neurol* 143:481–490
4. Vasile F, Dossi E, Rouach N (2017) Human astrocytes: structure and functions in the healthy brain. *Brain Struct Funct* 222:2017–2029
5. Leuba G, Garey LJ (1989) Comparison of neuronal and glial numerical density in primary and secondary visual cortex of man. *Exp Brain Res* 77:31–38
6. Tabata H (2015) Diverse subtypes of astrocytes and their development during corticogenesis. *Front Neurosci* 9:114
7. Miller RH, Raff MC (1984) Fibrous and protoplasmic astrocytes are biochemically and developmentally distinct. *J Neurosci* 4:585–92
8. Halassa MM, Fellin T, Takano H, et al (2007) Synaptic islands defined by the territory of a single astrocyte. *J Neurosci* 27:6473–7
9. Ogata K, Kosaka T (2002) Structural and quantitative analysis of astrocytes in the mouse hippocampus. *Neuroscience* 113:221–33
10. Bushong EA, Martone ME, Jones YZ, Ellisman MH (2002) Protoplasmic astrocytes in CA1 stratum radiatum occupy separate anatomical domains. *J Neurosci* 22:183–92
11. Oberheim NA, Takano T, Han X, et al (2009) Uniquely hominid features of adult human astrocytes. *J Neurosci* 29:3276–87
12. Sofroniew M V., Vinters H V. (2010) Astrocytes: Biology and pathology. *Acta Neuropathol* 119:7–35
13. Araque A, Parpura V, Sanzgiri RP, Haydon PG (1999) Tripartite synapses: Glia, the unacknowledged partner. *Trends Neurosci* 22:208–215
14. Haydon PG, Blendy J, Moss SJ, Rob Jackson F (2009) Astrocytic control of synaptic transmission and plasticity: a target for drugs of abuse? *Neuropharmacology* 56 Suppl 1:83–90
15. Allen NJ (2014) Astrocyte regulation of synaptic behavior. *Annu Rev Cell Dev Biol* 30:439–463
16. Navarrete M, Perea G, Maglio L, et al (2013) Astrocyte calcium signal and gliotransmission in human brain tissue. *Cereb Cortex* 23:1240–6
17. Allen NJ, Eroglu C (2017) Cell Biology of Astrocyte-Synapse Interactions. *Neuron* 96:697–708
18. Farhy-Tselnicker I, Allen NJ (2018) Astrocytes, neurons, synapses: A tripartite view on cortical circuit development. *Neural Dev* 13:7
19. Bialas AR, Stevens B (2013) TGF- $\beta$  signaling regulates neuronal C1q expression and developmental synaptic refinement. *Nat Neurosci* 16:1773–82
20. Chung WS, Clarke LE, Wang GX, et al (2013) Astrocytes mediate synapse elimination through MEGF10 and MERTK pathways. *Nature* 504:394–400
21. Schafer DP, Lehrman EK, Kautzman AG, et al (2012) Microglia Sculpt Postnatal Neural Circuits

- in an Activity and Complement-Dependent Manner. *Neuron* 74:691–705
22. Han X, Chen M, Wang F, et al (2013) Forebrain engraftment by human glial progenitor cells enhances synaptic plasticity and learning in adult mice. *Cell Stem Cell* 12:342–53
  23. Pekny M, Pekna M (2016) Reactive gliosis in the pathogenesis of CNS diseases. *Biochim Biophys Acta - Mol Basis Dis* 1862:483–491
  24. Demetrius LA, Magistretti PJ, Pellerin L (2015) Alzheimer’s disease: The amyloid hypothesis and the Inverse Warburg effect. *Front Physiol* 5:522
  25. Chung WS, Allen NJ, Eroglu C (2015) Astrocytes control synapse formation, function, and elimination. *Cold Spring Harb Perspect Biol* 7:a020370
  26. Chung WS, Welsh CA, Barres BA, Stevens B (2015) Do glia drive synaptic and cognitive impairment in disease? *Nat Neurosci* 18:1539–1545
  27. Middeldorp J, Hol EM (2011) GFAP in health and disease. *Prog Neurobiol* 93:421–443
  28. Dietrich J, Lacagnina M, Gass D, et al (2005) EIF2B5 mutations compromise GFAP+ astrocyte generation in vanishing white matter leukodystrophy. *Nat Med* 11:277–283
  29. Bugiani M, Boor I, Van Kollenburg B, et al (2011) Defective glial maturation in vanishing white matter disease. *J Neuropathol Exp Neurol* 70:69–82
  30. Eng LF, Ghirnikar RS, Lee YL (2000) Glial Fibrillary Acidic Protein: GFAP-Thirty-One Years (1969–2000). *Neurochem Res* 25:1439–51
  31. Todd AC, Hardingham GE (2020) The regulation of astrocytic glutamate transporters in health and neurodegenerative diseases. *Int J Mol Sci* 21:1–32
  32. Capendeguy O, Horisberger JD (2004) Functional effects of Na<sup>+</sup>,K<sup>+</sup>-ATPase gene mutations linked to familial hemiplegic migraine. *NeuroMolecular Med* 6:105–116
  33. Moseley AE, Williams MT, Schaefer TL, et al (2007) Deficiency in Na,K-ATPase  $\alpha$  isoform genes alters spatial learning, motor activity, and anxiety in mice. *J Neurosci* 27:616–26
  34. Szymocha R, Akaoka H, Dutuit M, et al (2000) Human T-Cell Lymphotropic Virus Type 1-Infected T Lymphocytes Impair Catabolism and Uptake of Glutamate by Astrocytes via Tax-1 and Tumor Necrosis Factor Alpha. *J Virol* 74:6433–6441
  35. Stefanik M, Formanova P, Bily T, et al (2018) Characterisation of Zika virus infection in primary human astrocytes. *BMC Neurosci* 19:5
  36. Sher AA, Glover KKM, Coombs KM (2019) Zika virus infection disrupts astrocytic proteins involved in synapse control and axon guidance. *Front Microbiol* 10:596
  37. Yoshikawa T (2003) Significance of human herpesviruses to transplant recipients. *Curr Opin Infect Dis* 16:601–6
  38. Donati D, Martinelli E, Cassiani-Ingoni R, et al (2005) Variant-Specific Tropism of Human Herpesvirus 6 in Human Astrocytes. *J Virol* 79:9439–9448
  39. Schneider M, Tigges B, Meggendorfer M, et al (2015) A new model for post-integration latency in macroglial cells to study HIV-1 reservoirs of the brain. *AIDS* 29:1147–59
  40. Lutgen V, Narasipura SD, Barbian HJ, et al (2020) HIV infects astrocytes in vivo and egresses from the brain to the periphery. *PLOS Pathog* 16:e1008381
  41. Brack-Werner R (1999) Astrocytes: HIV cellular reservoirs and important participants in neuropathogenesis. *AIDS* 13:1–22

42. Pekny M, Pekna M, Messing A, et al (2016) Astrocytes: a central element in neurological diseases. *Acta Neuropathol* 131:323–345
43. Zhang Y, Barres BA (2010) Astrocyte heterogeneity: An underappreciated topic in neurobiology. *Curr Opin Neurobiol* 20:588–94
44. Kery R, Chen A, Kirschen G (2020) Genetic targeting of astrocytes to combat neurodegenerative disease. *Neural Regen Res* 15:199–211
45. Merienne N, Le Douce J, Faivre E, et al (2013) Efficient gene delivery and selective transduction of astrocytes in the mammalian brain using viral vectors. *Front Cell Neurosci* 7:106
46. Fassler M, Weissberg I, Levy N, et al (2013) Preferential Lentiviral Targeting of Astrocytes in the Central Nervous System. *PLoS One* 8:e76092
47. Park F (2007) Lentiviral vectors: Are they the future of animal transgenesis? *Physiol Genomics* 31:159–173
48. Thomas CE, Ehrhardt A, Kay MA (2003) Progress and problems with the use of viral vectors for gene therapy. *Nat Rev Genet* 4:346–58
49. Atchison RW, Casto BC, Hammon WMD (1965) Adenovirus-associated defective virus particles. *Science (80- )* 149:754–6
50. Berns KI, Giraud C (1996) Biology of adeno-associated virus. *Curr Top Microbiol Immunol* 218:1–23
51. Weitzman MD, Linden RM (2011) Adeno-associated virus biology. *Methods Mol Biol* 807:1–23
52. Li W, Asokan A, Wu Z, et al (2008) Engineering and selection of shuffled AAV genomes: A new strategy for producing targeted biological nanoparticles. *Mol Ther* 16:1252–1260
53. Gao G, Vandenberghe LH, Alvira MR, et al (2004) Clades of Adeno-Associated Viruses Are Widely Disseminated in Human Tissues. *J Virol* 78:6381–8
54. Samulski RJ, Berns KI, Tan M, Muzyczka N (1982) Cloning of adeno-associated virus into pBR322: Rescue of intact virus from the recombinant plasmid in human cells. *Proc Natl Acad Sci U S A* 79:2077–81
55. Srivastava A, Lusby EW, Berns KI (1983) Nucleotide sequence and organization of the adeno-associated virus 2 genome. *J Virol* 45:555–64
56. Sonntag F, Schmidt K, Kleinschmidt JA (2010) A viral assembly factor promotes AAV2 capsid formation in the nucleolus. *Proc Natl Acad Sci U S A* 107:10220–5
57. Naso MF, Tomkowicz B, Perry WL, Strohl WR (2017) Adeno-Associated Virus (AAV) as a Vector for Gene Therapy. *BioDrugs* 31:317–334
58. Maurer AC, Pacouret S, Cepeda Diaz AK, et al (2018) The Assembly-Activating Protein Promotes Stability and Interactions between AAV's Viral Proteins to Nucleate Capsid Assembly. *Cell Rep* 23:1817–1830
59. Wang D, Tai PWL, Gao G (2019) Adeno-associated virus vector as a platform for gene therapy delivery. *Nat Rev Drug Discov* 18:358–378
60. Bartlett JS, Wilcher R, Samulski RJ (2000) Infectious Entry Pathway of Adeno-Associated Virus and Adeno-Associated Virus Vectors. *J Virol* 74:2777–85
61. Wang D, Tai PWL, Gao G (2019) Adeno-associated virus vector as a platform for gene therapy delivery. *Nat Rev Drug Discov* 18:358–378
62. Xiao W, Warrington KH, Hearing P, et al (2002) Adenovirus-Facilitated Nuclear Translocation of

- Adeno-Associated Virus Type 2. *J Virol* 76:11505–17
63. Samulski RJ, Zhu X, Xiao X, et al (1991) Targeted integration of adeno-associated virus (AAV) into human chromosome 19. *EMBO J* 10:3941–50
  64. Schnepf BC, Jensen RL, Chen C-L, et al (2005) Characterization of Adeno-Associated Virus Genomes Isolated from Human Tissues. *J Virol* 79:14793–803
  65. Berns KI (1990) Parvovirus replication. *Microbiol Rev* 54:316–29
  66. Gonçalves MAFV (2005) Adeno-associated virus: From defective virus to effective vector. *Virol J* 2:43
  67. Im DS, Muzyczka N (1990) The AAV origin binding protein Rep68 is an ATP-dependent site-specific endonuclease with DNA helicase activity. *Cell* 61:447–57
  68. Wu Z, Asokan A, Samulski RJ (2006) Adeno-associated Virus Serotypes: Vector Toolkit for Human Gene Therapy. *Mol Ther* 14:316–27
  69. Trempe JP, Carter BJ (1988) Alternate mRNA splicing is required for synthesis of adeno-associated virus VP1 capsid protein. *J Virol* 62:3356–63
  70. Stutika C, Gogol-Döring A, Botschen L, et al (2016) A Comprehensive RNA Sequencing Analysis of the Adeno-Associated Virus (AAV) Type 2 Transcriptome Reveals Novel AAV Transcripts, Splice Variants, and Derived Proteins. *J Virol* 90:1278–89
  71. King JA, Dubielzig R, Grimm D, Kleinschmidt JA (2001) DNA helicase-mediated packaging of adeno-associated virus type 2 genomes into preformed capsids. *EMBO J* 20:3282–91
  72. Van Vliet KM, Blouin V, Brument N, et al (2008) The role of the adeno-associated virus capsid in gene transfer. *Methods Mol Biol* 437:51–91
  73. Girod A, Wobus CE, Zádori Z, et al (2002) The VP1 capsid protein of adeno-associated virus type 2 is carrying a phospholipase A2 domain required for virus infectivity. *J Gen Virol* 83:973–978
  74. Hermonat PL, Labow MA, Wright R, et al (1984) Genetics of adeno-associated virus: isolation and preliminary characterization of adeno-associated virus type 2 mutants. *J Virol* 51:329–39
  75. Warrington KH, Gorbatyuk OS, Harrison JK, et al (2004) Adeno-Associated Virus Type 2 VP2 Capsid Protein Is Nonessential and Can Tolerate Large Peptide Insertions at Its N Terminus. *J Virol* 78:6595–609
  76. Vance MA, Mitchell A, Samulski RJ (2015) AAV Biology, Infectivity and Therapeutic Use from Bench to Clinic. In: *Gene Therapy - Principles and Challenges*. pp 119–143
  77. Gao G, Alvira MR, Somanathan S, et al (2003) Adeno-associated viruses undergo substantial evolution in primates during natural infections. *Proc Natl Acad Sci U S A* 100:6081–6
  78. Jooss K, Yang Y, Fisher KJ, Wilson JM (1998) Transduction of Dendritic Cells by DNA Viral Vectors Directs the Immune Response to Transgene Products in Muscle Fibers. *J Virol* 72:4212–23
  79. Naso MF, Tomkowicz B, Perry WL, Strohl WR (2017) Adeno-Associated Virus (AAV) as a Vector for Gene Therapy. *BioDrugs* 31:317–334
  80. Choi VW, McCarty DM, Samulski RJ (2006) Host Cell DNA Repair Pathways in Adeno-Associated Viral Genome Processing. *J Virol* 80:10346–56
  81. Grimm D, Kay M (2005) From Virus Evolution to Vector Revolution: Use of Naturally Occurring Serotypes of Adeno-associated Virus (AAV) as Novel Vectors for Human Gene Therapy. *Curr Gene Ther* 3:281–304
  82. Ferrari FK, Samulski T, Shenk T, Samulski RJ (1996) Second-strand synthesis is a rate-limiting

- step for efficient transduction by recombinant adeno-associated virus vectors. *J Virol* 70:3227–34
83. McCarty DM (2008) Self-complementary AAV vectors; advances and applications. *Mol Ther* 16:1648–56
  84. McCarty DM, Fu H, Monahan PE, et al (2003) Adeno-associated virus terminal repeat (TR) mutant generates self-complementary vectors to overcome the rate-limiting step to transduction in vivo. *Gene Ther* 16:2112–8
  85. Wang Z, Ma HI, Li J, et al (2003) Rapid and highly efficient transduction by double-stranded adeno-associated virus vectors in vitro and in vivo. *Gene Ther* 10:2105–11
  86. dos Santos Coura R, Nardi NB (2008) A role for adeno-associated viral vectors in gene therapy. *Genet Mol Biol* 31:1–11
  87. Davidson BL, Breakefield XO (2003) Viral vectors for gene delivery to the nervous system. *Nat Rev Neurosci* 4:353–64
  88. Nakai H, Yant SR, Storm TA, et al (2001) Extrachromosomal Recombinant Adeno-Associated Virus Vector Genomes Are Primarily Responsible for Stable Liver Transduction In Vivo. *J Virol* 75:6969–6976
  89. Samulski RJ, Muzyczka N (2014) AAV-mediated gene therapy for research and therapeutic purposes. *Annu Rev Virol* 1:427–51
  90. El Andari J, Grimm D (2021) Production, Processing, and Characterization of Synthetic AAV Gene Therapy Vectors. *Biotechnol J* 16:2000025
  91. Thomas CE, Storm TA, Huang Z, Kay MA (2004) Rapid Uncoating of Vector Genomes Is the Key to Efficient Liver Transduction with Pseudotyped Adeno-Associated Virus Vectors. *J Virol* 78:3110–22
  92. Wang AY, Peng PD, Ehrhardt A, et al (2004) Comparison of adenoviral and adeno-associated viral vectors for pancreatic gene delivery in vivo. *Hum Gene Ther* 15:405–13
  93. Rabinowitz JE, Rolling F, Li C, et al (2002) Cross-Packaging of a Single Adeno-Associated Virus (AAV) Type 2 Vector Genome into Multiple AAV Serotypes Enables Transduction with Broad Specificity. *J Virol* 76:791–801
  94. Halbert CL, Rutledge EA, Allen JM, et al (2000) Repeat Transduction in the Mouse Lung by Using Adeno-Associated Virus Vectors with Different Serotypes. *J Virol* 74:1524–1532
  95. Summerford C, Samulski RJ (1998) Membrane-Associated Heparan Sulfate Proteoglycan Is a Receptor for Adeno-Associated Virus Type 2 Virions. *J Virol* 72:1438–45
  96. Simon Davis DA, Parish CR (2013) Heparan sulfate: A ubiquitous glycosaminoglycan with multiple roles in immunity. *Front Immunol* 4:470
  97. Srivastava A (2016) In vivo tissue-tropism of adeno-associated viral vectors. *Curr Opin Virol* 21:75–80
  98. Ellis BL, Hirsch ML, Barker JC, et al (2013) A survey of ex vivo/in vitro transduction efficiency of mammalian primary cells and cell lines with Nine natural adeno-associated virus (AAV1-9) and one engineered adeno-associated virus serotype. *Virol J* 10:74
  99. Mingozzi F, High KA (2011) Therapeutic in vivo gene transfer for genetic disease using AAV: Progress and challenges. *Nat Rev Genet* 12:341–355
  100. Wu Z, Miller E, Agbandje-McKenna M, Samulski RJ (2006)  $\alpha$ 2,3 and  $\alpha$ 2,6 N-Linked Sialic Acids Facilitate Efficient Binding and Transduction by Adeno-Associated Virus Types 1 and 6. *J Virol* 80:9093–103

101. Chen S, Kapturczak M, Loiler SA, et al (2005) Efficient transduction of vascular endothelial cells with recombinant adeno-associated virus serotype 1 and 5 vectors. *Hum Gene Ther* 16:235–47
102. Pillay S, Meyer NL, Puschnik AS, et al (2016) An essential receptor for adeno-associated virus infection. *Nature* 530:108–12
103. Akache B, Grimm D, Pandey K, et al (2006) The 37/67-Kilodalton Laminin Receptor Is a Receptor for Adeno-Associated Virus Serotypes 8, 2, 3, and 9. *J Virol* 80:9831–9836
104. Asokan A, Hamra JB, Govindasamy L, et al (2006) Adeno-Associated Virus Type 2 Contains an Integrin  $\alpha 5\beta 1$  Binding Domain Essential for Viral Cell Entry. *J Virol* 80:8961–9
105. Kashiwakura Y, Tamayose K, Iwabuchi K, et al (2005) Hepatocyte Growth Factor Receptor Is a Coreceptor for Adeno-Associated Virus Type 2 Infection. *J Virol* 79:609–14
106. Qing K, Mah C, Hansen J, et al (1999) Human fibroblast growth factor receptor 1 is a co-receptor for infection by adeno-associated virus 2. *Nat Med* 5:71–77
107. Summerford C, Bartlett JS, Samulski RJ (1999)  $\alpha V\beta 5$  integrin: A co-receptor for adeno-associated virus type 2 infection. *Nat Med* 5:78–82
108. Handa A, Muramatsu S-I, Qiu J, et al (2000) Printed in Great Britain Adeno-associated virus (AAV)-3-based vectors transduce haematopoietic cells not susceptible to transduction with AAV-2-based vectors
109. Kurzeder C, Koppold B, Sauer G, et al (2007) CD9 promotes adeno-associated virus type 2 infection of mammary carcinoma cells with low cell surface expression of heparan sulphate proteoglycans. *Int J Mol Med* 19:325–33
110. Blackburn SD, Steadman RA, Johnson FB (2006) Attachment of adeno-associated virus type 3H to fibroblast growth factor receptor 1. *Arch Virol* 151:617–23
111. Ling C, Lu Y, Kalsi JK, et al (2010) Human hepatocyte growth factor receptor is a cellular coreceptor for adeno-associated virus serotype 3. *Hum Gene Ther* 21:1741–1747
112. Walters RW, Yi SMP, Keshavjee S, et al (2001) Binding of Adeno-associated Virus Type 5 to 2,3-Linked Sialic Acid is Required for Gene Transfer. *J Biol Chem* 276:20610–6
113. Walters RW, Pilewski JM, Chiorini JA, Zabner J (2002) Secreted and transmembrane mucins inhibit gene transfer with AAV4 more efficiently than AAV5. *J Biol Chem* 277:23709–23713
114. Kaludov N, Handelman B, Chiorini JA (2002) Scalable purification of adeno-associated virus type 2, 4, or 5 using ion-exchange chromatography. *Hum Gene Ther* 13:1235–1243
115. Di Pasquale G, Davidson BL, Stein CS, et al (2003) Identification of PDGFR as a receptor for AAV-5 transduction. *Nat Med* 9:1306–12
116. Weller ML, Amornphimoltham P, Schmidt M, et al (2010) Epidermal growth factor receptor is a co-receptor for adeno-associated virus serotype 6. *Nat Med* 16:662–4
117. Seiler MP, Miller AD, Zabner J, Halbert CL (2006) Adeno-associated virus types 5 and 6 use distinct receptors for cell entry. *Hum Gene Ther* 17:10–9
118. Shen S, Bryant KD, Brown SM, et al (2011) Terminal n-linked galactose is the primary receptor for adeno-associated virus. *J Biol Chem* 286:13532–40
119. Grimm D, Lee JS, Wang L, et al (2008) In Vitro and In Vivo Gene Therapy Vector Evolution via Multispecies Interbreeding and Retargeting of Adeno-Associated Viruses. *J Virol* 82:5887–911
120. Grimm D, Zolotukhin S (2015) E Pluribus Unum: 50 Years of Research, Millions of Viruses, and One Goal-Tailored Acceleration of AAV Evolution. *Mol Ther* 23:1819–1831

121. Perabo L, Goldnau D, White K, et al (2006) Heparan Sulfate Proteoglycan Binding Properties of Adeno-Associated Virus Retargeting Mutants and Consequences for Their In Vivo Tropism. *J Virol* 80:7265–9
122. Michelfelder S, Kohlschütter J, Skorupa A, et al (2009) Successful expansion but not complete restriction of tropism of adeno-associated virus by in vivo biopanning of random virus display peptide libraries. *PLoS One* 4:e5122
123. Jang JH, Koerber JT, Kim JS, et al (2011) An evolved adeno-associated viral variant enhances gene delivery and gene targeting in neural stem cells. *Mol Ther* 19:667–75
124. Sayroo R, Nolasco D, Yin Z, et al (2016) Development of novel AAV serotype 6 based vectors with selective tropism for human cancer cells. *Gene Ther* 23:18–25
125. Stachler MD, Bartlett JS (2006) Mosaic vectors comprised of modified AAV1 capsid proteins for efficient vector purification and targeting to vascular endothelial cells. *Gene Ther* 13:926–31
126. Michelfelder S, Varadi K, Raupp C, et al (2011) Peptide ligands incorporated into the threefold spike capsid domain to re-direct gene transduction of AAV8 and AAV9 in vivo. *PLoS One* 6:e23101
127. Deverman BE, Pravdo PL, Simpson BP, et al (2016) Cre-dependent selection yields AAV variants for widespread gene transfer to the adult brain. *Nat Biotechnol* 34:204–9
128. Varadi K, Michelfelder S, Korff T, et al (2012) Novel random peptide libraries displayed on AAV serotype 9 for selection of endothelial cell-directed gene transfer vectors. *Gene Ther* 19:800–9
129. Bartlett JS, Samulski RJ, McCown TJ (1998) Selective and rapid uptake of adeno-associated virus type 2 in brain. *Hum Gene Ther* 9:1181–6
130. Mandel RJ, Snyder RO, Leff SE (1999) Recombinant adeno-associated viral vector-mediated glial cell line- derived neurotrophic factor gene transfer protects nigral dopamine neurons after onset of progressive degeneration in a rat model of Parkinson's disease. *Exp Neurol* 160:205–14
131. Davidson BL, Stein CS, Heth JA, et al (2000) Recombinant adeno-associated virus type 2, 4, and 5 vectors: Transduction of variant cell types and regions in the mammalian central nervous system. *Proc Natl Acad Sci U S A* 97:3428–32
132. Liu G, Martins IH, Chiorini JA, Davidson BL (2005) Adeno-associated virus type 4 (AAV4) targets ependyma and astrocytes in the subventricular zone and RMS. *Gene Ther* 12:1503–8
133. Wang C, Wang CM, Clark KR, Sferra TJ (2003) Recombinant AAV serotype 1 transduction efficiency and tropism in the murine brain. *Gene Ther* 10:1528–34
134. Cearley CN, Wolfe JH (2006) Transduction characteristics of adeno-associated virus vectors expressing cap serotypes 7, 8, 9, and Rh10 in the mouse brain. *Mol Ther* 13:528–37
135. Hammond SL, Leek AN, Richman EH, Tjalkens RB (2017) Cellular selectivity of AAV serotypes for gene delivery in neurons and astrocytes by neonatal intracerebroventricular injection. *PLoS One* 12:e0188830
136. Pignataro D, Sucunza D, Vanrell L, et al (2017) Adeno-associated viral vectors serotype 8 for cell-specific delivery of therapeutic genes in the central nervous system. *Front Neuroanat* 11:2
137. Foust KD, Nurre E, Montgomery CL, et al (2009) Intravascular AAV9 preferentially targets neonatal neurons and adult astrocytes. *Nat Biotechnol* 27:59–65
138. Pulicherla N, Shen S, Yadav S, et al (2011) Engineering liver-detargeted AAV9 vectors for cardiac and musculoskeletal gene transfer. *Mol Ther* 19:1070–8
139. Brenner M, Kisseberth WC, Su Y, et al (1994) GFAP promoter directs astrocyte-specific

- expression in transgenic mice. *J Neurosci* 14:1030–7
140. Lee Y, Messing A, Su M, Brenner M (2008) GFAP promoter elements required for region-specific and astrocyte-specific expression. *Glia* 56:481–93
  141. Merienne N, Le Douce J, Faivre E, et al (2013) Efficient gene delivery and selective transduction of astrocytes in the mammalian brain using viral vectors. *Front Cell Neurosci* 7:106
  142. Yu X, Nagai J, Khakh BS (2020) Improved tools to study astrocytes. *Nat Rev Neurosci* 21:121–138
  143. Cahoy JD, Emery B, Kaushal A, et al (2008) A transcriptome database for astrocytes, neurons, and oligodendrocytes: A new resource for understanding brain development and function. *J Neurosci* 28:264–78
  144. Gerstein MB, Kundaje A, Hariharan M, et al (2012) Architecture of the human regulatory network derived from ENCODE data. *Nature* 489:91–100
  145. Whiteld TW, Wang J, Collins PJ, et al (2012) Functional analysis of transcription factor binding sites in human promoters. *Genome Biol* 13:R50
  146. De Leeuw CN, Korecki AJ, Berry GE, et al (2016) RAAV-compatible MiniPromoters for restricted expression in the brain and eye. *Mol Brain* 9:52
  147. Kunze C, Börner K, Kienle E, et al (2018) Synthetic AAV/CRISPR vectors for blocking HIV-1 expression in persistently infected astrocytes. *Glia* 66:413–427
  148. Kunze C (2017) Strategien zur Inhibierung der HIV-Reaktivierung in latent infizierten Astrozyten
  149. Xie J, Xie Q, Zhang H, et al (2011) MicroRNA-regulated, systemically delivered rAAV9: A step closer to CNS-restricted transgene expression. *Mol Ther* 19:526–35
  150. DiMattia MA, Nam H-J, Van Vliet K, et al (2012) Structural Insight into the Unique Properties of Adeno-Associated Virus Serotype 9. *J Virol* 86:6947–58
  151. Fechner H, Sipo I, Westermann D, et al (2008) Cardiac-targeted RNA interference mediated by an AAV9 vector improves cardiac function in coxsackievirus B3 cardiomyopathy. *J Mol Med* 86:987–97
  152. Inagaki K, Fuess S, Storm TA, et al (2006) Robust systemic transduction with AAV9 vectors in mice: efficient global cardiac gene transfer superior to that of AAV8. *Mol Ther* 14:45–53
  153. Pacak CA, Byrne BJ (2011) AAV vectors for cardiac gene transfer: Experimental tools and clinical opportunities. *Mol Ther* 19:1582–90
  154. Pacak CA, Mah CS, Thattaliyath BD, et al (2006) Recombinant adeno-associated virus serotype 9 leads to preferential cardiac transduction in vivo. *Circ Res* 99:e3-9
  155. Suckau L, Fechner H, Chemaly E, et al (2009) Long-term cardiac-targeted RNA interference for the treatment of heart failure restores cardiac function and reduces pathological hypertrophy. *Circulation* 119:1241–52
  156. Sun B, Young SP, Li P, et al (2008) Correction of multiple striated muscles in murine pompe disease through adeno-associated virus-mediated gene therapy. *Mol Ther* 16:1366–71
  157. Kaya Z, Katus HA, Rose NR (2010) Cardiac troponins and autoimmunity: Their role in the pathogenesis of myocarditis and of heart failure. *Clin Immunol* 134:80–8
  158. Duque S, Joussemet B, Riviere C, et al (2009) Intravenous administration of self-complementary AAV9 enables transgene delivery to adult motor neurons. *Mol Ther* 17:1187–96
  159. Bell CL, Gurda BL, Van Vliet K, et al (2012) Identification of the Galactose Binding Domain of the

- Adeno-Associated Virus Serotype 9 Capsid. *J Virol* 86:7326–33
160. Boutin S, Monteilhet V, Veron P, et al (2010) Prevalence of serum IgG and neutralizing factors against adeno-associated virus (AAV) types 1, 2, 5, 6, 8, and 9 in the healthy population: Implications for gene therapy using AAV vectors. *Hum Gene Ther* 21:704–12
  161. Kuzmin DA, Shutova M V., Johnston NR, et al (2021) The clinical landscape for AAV gene therapies. *Nat Rev Drug Discov* 20:173–174
  162. Reichart F, Maltsev O V, Kapp TG, et al (2019) Selective Targeting of Integrin  $\alpha\beta 8$  by a Highly Active Cyclic Peptide. *62:2024–2037*
  163. Grimm D, Streetz KL, Jopling CL, et al (2006) Fatality in mice due to oversaturation of cellular microRNA/short hairpin RNA pathways. *Nature* 441:537–541
  164. Sanjana NE, Shalem O, Zhang F (2014) Improved vectors and genome-wide libraries for CRISPR screening. *Nat Methods* 11:783–784
  165. Villa A, Snyder EY, Vescovi A, Martínez-Serrano A (2000) Establishment and properties of a growth factor-dependent, perpetual neural stem cell line from the human CNS. *Exp Neurol* 161:67–84
  166. Rothenaigner I, Kramer S, Meggendorfer M, et al (2009) Transduction of human neural progenitor cells with foamy virus vectors for differentiation-dependent gene expression. *Gene Ther* 16:349–358
  167. Rothenaigner I, Kramer S, Ziegler M, et al (2007) Long-term HIV-1 infection of neural progenitor populations. *AIDS* 21:2271–2281
  168. Kumar S, Stecher G, Tamura K (2016) MEGA7: Molecular Evolutionary Genetics Analysis Version 7.0 for Bigger Datasets. *Mol Biol Evol* 33:1870–1874
  169. Schmid-Burgk JL, Schmidt T, Gaidt MM, et al (2014) OutKnocker: A web tool for rapid and simple genotyping of designer nuclease edited cell lines. *Genome Res* 24:1719–1723
  170. Kelley LA, Mezulis S, Yates CM, et al (2015) The Phyre2 web portal for protein modeling, prediction and analysis. *Nat Protoc* 10:845–858
  171. Waterhouse A, Bertoni M, Bienert S, et al (2018) SWISS-MODEL: Homology modelling of protein structures and complexes. *Nucleic Acids Res* 46:W296–W303
  172. Bertoni M, Kiefer F, Biasini M, et al (2017) Modeling protein quaternary structure of homo- and hetero-oligomers beyond binary interactions by homology. *Sci Rep* 7:1–15
  173. Notredame C, Higgins DG, Heringa J (2000) T-coffee: A novel method for fast and accurate multiple sequence alignment. *J Mol Biol* 302:205–217
  174. Pettersen EF, Goddard TD, Huang CC, et al (2021) <scp>UCSF ChimeraX</scp> : Structure visualization for researchers, educators, and developers. *Protein Sci* 30:70–82
  175. Goddard TD, Huang CC, Meng EC, et al (2018) UCSF ChimeraX: Meeting modern challenges in visualization and analysis. *Protein Sci* 27:14–25
  176. Riss TL, Moravec RA, Niles AL, et al (2004) Cell Viability Assays. In: *Assay Guidance Manual*. Eli Lilly & Company and the National Center for Advancing Translational Sciences
  177. Guo P, Zhang J, Chrzanowski M, et al (2019) Rapid AAV-Neutralizing Antibody Determination with a Cell-Binding Assay. *Mol Ther - Methods Clin Dev* 13:40–46
  178. Doench JG, Fusi N, Sullender M, et al (2016) Optimized sgRNA design to maximize activity and minimize off-target effects of CRISPR-Cas9. *Nat Biotechnol* 34:184–191

179. Schmid-Burgk JL, Xie Z, Frank S, et al (2012) Rapid hierarchical assembly of medium-size DNA cassettes. *Nucleic Acids Res* 40:
180. Kaletta J, Pickl C, Griebler C, et al (2020) A rigorous assessment and comparison of enumeration methods for environmental viruses. *Sci Rep* 10:
181. Meyer NL, Hu G, Davulcu O, et al (2019) Structure of the gene therapy vector, adeno-associated virus with its cell receptor, aavr. *Elife* 8:e44707
182. Pierschbacher MD, Ruoslahti E (1984) Cell attachment activity of fibronectin can be duplicated by small synthetic fragments of the molecule. *Nature* 309:30–33
183. Y Takada XYSS (2007) The integrins. *Genome Biol* 8:215
184. Sun CC, Qu XJ, Gao ZH (2016) Arginine-Glycine-Aspartate Binding Integrins as Therapeutic and Diagnostic Targets. *Am J Ther* 23:e198–e207
185. Zhang Y, Sloan SA, Clarke LE, et al (2016) Purification and Characterization of Progenitor and Mature Human Astrocytes Reveals Transcriptional and Functional Differences with Mouse. *Neuron* 89:37–53
186. Kapp TG, Rechenmacher F, Neubauer S, et al (2017) A comprehensive evaluation of the activity and selectivity profile of ligands for RGD-binding integrins. *Sci Rep* 7:1–13
187. Mas-Moruno C, Rechenmacher F, Kessler H (2011) Cilengitide: The First Anti-Angiogenic Small Molecule Drug Candidate. Design, Synthesis and Clinical Evaluation. *Anticancer Agents Med Chem* 10:753–768
188. Choi Y, Kim E, Lee Y, et al (2010) Site-specific inhibition of integrin  $\alpha\beta 3$ -vitronectin association by a ser-asp-val sequence through an Arg-Gly-Asp-binding site of the integrin. *Proteomics* 10:72–80
189. Opie SR, Warrington, KH, Agbandje-McKenna M, et al (2003) Identification of Amino Acid Residues in the Capsid Proteins of Adeno-Associated Virus Type 2 That Contribute to Heparan Sulfate Proteoglycan Binding. *J Virol* 77:6995–7006
190. Sarrazin S, Lamanna WC, Esko JD (2011) Heparan sulfate proteoglycans. *Cold Spring Harb Perspect Biol* 3:1–33
191. Heifetz A, Keenan RW, Elbein AD (1979) Mechanism of Action of Tunicamycin on the UDP-GlcNAc:Dolichyl-Phosphate GlcNAc-1 -Phosphate Transferase. *Biochemistry* 18:2186–2192
192. Pillay S, Meyer NL, Puschnik AS, et al (2016) An essential receptor for adeno-associated virus infection. *Nature* 530:108–112
193. Riyad JM, Weber T (2021) Intracellular trafficking of adeno-associated virus (AAV) vectors: challenges and future directions. *Gene Ther*
194. Li C, Samulski RJ (2020) Engineering adeno-associated virus vectors for gene therapy. *Nat Rev Genet* 21:255–272
195. Ylä-Herttua S (2015) Glybera's second act: The curtain rises on the high cost of therapy. *Mol Ther* 23:217–218
196. Hoy SM (2019) Onasemnogene Apeparvovec: First Global Approval. *Drugs* 79:1255–1262
197. Gao J, Hussain RM, Weng CY (2020) Voretigene Neparvovec in Retinal Diseases: A Review of the Current Clinical Evidence. *14:3855–3869*
198. Girod A, Ried M, Wobus C, et al (1999) Genetic capsid modifications allow efficient re-targeting of adeno-associated virus type 2. *Nat Med* 5:1052–1056

199. O'Donnell J, Taylor KA, Chapman MS (2009) Adeno-associated virus-2 and its primary cellular receptor-Cryo-EM structure of a heparin complex. *Virology* 385:434–443
200. Heparin-Binding Proteins - H. Edward Conrad - Google Books. [https://books.google.de/books?hl=de&lr=&id=UzYE6FKy6O4C&oi=fnd&pg=PP2&ots=By\\_OSwy7CC&sig=6VKG8ZoJGON5p5LMZel6y-RwJhk&redir\\_esc=y#v=onepage&q&f=false](https://books.google.de/books?hl=de&lr=&id=UzYE6FKy6O4C&oi=fnd&pg=PP2&ots=By_OSwy7CC&sig=6VKG8ZoJGON5p5LMZel6y-RwJhk&redir_esc=y#v=onepage&q&f=false). Accessed 31 Mar 2021
201. Rossi A, Dupaty L, Aillot L, et al (2019) Vector uncoating limits adeno-associated viral vector-mediated transduction of human dendritic cells and vector immunogenicity. *Sci Rep* 9:1–14
202. Adachi K, Nakai H (2010) A new recombinant adeno-associated virus (AAV)-based random peptide display library system: Infection-defective AAV1.9-3 as a novel detargeted platform for vector evolution. In: *Gene Therapy and Regulation*. World Scientific Publishing Co. Pte Ltd, pp 31–55
203. Weinmann J, Weis S, Sippel J, et al (2020) Identification of a myotropic AAV by massively parallel in vivo evaluation of barcoded capsid variants. *Nat Commun* 11:1–12
204. Börner K, Kienle E, Huang LY, et al (2020) Pre-arrayed Pan-AAV Peptide Display Libraries for Rapid Single-Round Screening. *Mol Ther* 28:1016–1032
205. Davidsson M, Wang G, Aldrin-Kirk P, et al (2019) A systematic capsid evolution approach performed in vivo for the design of AAV vectors with tailored properties and tropism. *Proc Natl Acad Sci U S A* 116:27053–27062
206. Venkatakrisnan B, Yarbrough J, Domsic J, et al (2013) Structure and Dynamics of Adeno-Associated Virus Serotype 1 VP1-Unique N-Terminal Domain and Its Role in Capsid Trafficking. *J Virol* 87:4974–4984
207. Govindasamy L, DiMattia MA, Gurda BL, et al (2013) Structural Insights into Adeno-Associated Virus Serotype 5. *J Virol* 87:11187–11199
208. Xie Q, Bu W, Bhatia S, et al (2002) The atomic structure of adeno-associated virus (AAV-2), a vector for human gene therapy. *Proc Natl Acad Sci U S A* 99:10405–10410
209. Fang J, Haasl RJ, Dong Y, Lushington GH (2005) Discover protein sequence signatures from protein-protein interaction data. *BMC Bioinformatics* 6:277
210. Hanahan D, Weinberg RA (2000) The hallmarks of cancer. *Cell* 100:57–70
211. Hirota S, Liu Q, Lee HS, et al (2011) The astrocyte-expressed integrin  $\alpha\beta 8$  governs blood vessel sprouting in the developing retina. *Development* 138:5157–5166
212. Cambier S, Gline S, Mu D, et al (2005) Integrin  $\alpha\beta 8$ -mediated activation of transforming growth factor- $\beta$  by perivascular astrocytes: An angiogenic control switch. *Am J Pathol* 166:1883–1894
213. Jackson T, Clark S, Berryman S, et al (2004) Integrin  $\alpha\beta 8$  Functions as a Receptor for Foot-and-Mouth Disease Virus: Role of the  $\beta$ -Chain Cytodomain in Integrin-Mediated Infection. *J Virol* 78:4533–4540
214. Mu D, Cambier S, Fjellbirkeland L, et al (2002) The integrin  $\alpha\beta 8$  mediates epithelial homeostasis through MT1-MMP-dependent activation of TGF- $\beta 1$ . *J Cell Biol* 157:493–507
215. Mccarty JH (2020) REVIEW SUBJECT COLLECTION: ADHESION  $\alpha\beta 8$  integrin adhesion and signaling pathways in development, physiology and disease. 133:jcs239434
216. Lagos-Cabré R, Alvarez A, Kong M, et al (2017)  $\alpha\beta 3$  Integrin regulates astrocyte reactivity. *J Neuroinflammation* 14:194
217. Avalos AM, Arthur WT, Schneider P, et al (2004) Aggregation of integrins and RhoA activation are required for Thy-1-induced morphological changes in astrocytes. *J Biol Chem* 279:39139–

39145

218. Kong M, Muñoz N, Valdivia A, et al (2013) Thy-1-mediated cell-cell contact induces astrocyte migration through the engagement of  $\alpha V\beta 3$  integrin and syndecan-4. *Biochim Biophys Acta - Mol Cell Res* 1833:1409–1420
219. Avalos AM, Valdivia AD, Muñoz N, et al (2009) Neuronal Thy-1 induces astrocyte adhesion by engaging syndecan-4 in a cooperative interaction with  $\alpha V\beta 3$  integrin that activates PKC $\alpha$  and RhoA. *J Cell Sci* 122:3462–3471
220. Herrera-Molina R, Frischknecht R, Maldonado H, et al (2012) Astrocytic  $\alpha V\beta 3$  Integrin Inhibits Neurite Outgrowth and Promotes Retraction of Neuronal Processes by Clustering Thy-1. *J Cell Sci* 125:e34295
221. Milner R, Huang X, Wu J, et al (1999) Distinct roles for astrocyte  $\alpha V\beta 5$  and  $\alpha V\beta 8$  integrins in adhesion and migration. *J Cell Sci* 112 ( Pt 2):4271–4279
222. Memmo LM, McKeown-Longo P (1998) The  $\alpha V\beta 5$  integrin functions as an endocytic receptor for vitronectin | *Journal of Cell Science*. *J Cell Sci* 111:425–433
223. Horton MA (1997) The  $\alpha V\beta 3$  integrin “vitronectin receptor.” *Int J Biochem Cell Biol* 29:721–725
224. Marinelli L, Gottschalk KE, Meyer A, et al (2004) Human integrin  $\alpha V\beta 5$ : Homology modeling and ligand binding. *J Med Chem* 47:4166–4177
225. Xiong JP, Stehle T, Zhang R, et al (2002) Crystal structure of the extracellular segment of integrin  $\alpha V\beta 3$  in complex with an Arg-Gly-Asp ligand. *Science* (80- ) 296:151–155
226. Brower DL, Brower SM, Hayward DC, Ball EE (1997) Molecular evolution of integrins: Genes encoding integrin subunits from a coral and a sponge
227. Sanlioglu S, Benson PK, Yang J, et al (2000) Endocytosis and Nuclear Trafficking of Adeno-Associated Virus Type 2 Are Controlled by Rac1 and Phosphatidylinositol-3 Kinase Activation. *J Virol* 74:9184–9196
228. Shen S, Berry GE, Castellanos Rivera RM, et al (2014) Functional Analysis of the Putative Integrin Recognition Motif on Adeno-associated Virus 9 \*. *J Virol* 88:290:1496–504
229. Shi W, Bartlett JS (2003) RGD inclusion in VP3 provides adeno-associated virus type 2 (AAV2)-based vectors with a heparan sulfate-independent cell entry mechanism. *Mol Ther* 7:515–525
230. Sallach J, Di Pasquale G, Larcher F, et al (2014) Tropism-modified AAV vectors overcome barriers to successful cutaneous therapy. *Mol Ther* 22:929–939
231. Khabou H, Desrosiers M, Winckler C, et al (2016) Insight into the mechanisms of enhanced retinal transduction by the engineered AAV2 capsid variant -7m8. *Biotechnol Bioeng* 113:2712–2724
232. Ying Y, Müller OJ, Goehring C, et al (2010) Heart-targeted adeno-associated viral vectors selected by in vivo biopanning of a random viral display peptide library. *Gene Ther* 17:980–990
233. Excoffon KJDA, Koerber JT, Dickey DD, et al (2009) Directed evolution of adeno-associated virus to an infectious respiratory virus. *Proc Natl Acad Sci U S A* 106:3865–3870
234. Kern A, Schmidt K, Leder C, et al (2003) Identification of a Heparin-Binding Motif on Adeno-Associated Virus Type 2 Capsids. *J Virol* 77:11072–11081
235. Inagaki K, Fuess S, Storm TA, et al (2006) Robust systemic transduction with AAV9 vectors in mice: efficient global cardiac gene transfer superior to that of AAV8. *Mol Ther* 14:45–53
236. Kotchey NM, Adachi K, Zahid M, et al (2011) A potential role of distinctively delayed blood clearance of recombinant adeno-associated virus serotype 9 in robust cardiac transduction.

- Mol Ther 19:1079–1089
237. Duan D (2016) Systemic delivery of adeno-associated viral vectors. *Curr Opin Virol* 21:16–25
  238. Moremen KW, Tiemeyer M, Nairn A V. (2012) Vertebrate protein glycosylation: Diversity, synthesis and function. *Nat. Rev. Mol. Cell Biol.* 13:448–462
  239. Stanley P, Taniguchi N AM (2017) N-glycans. In: Varki A, Cummings RD, Esko JD et al. (ed) *Essentials of Glycobiology*. Cold Spring Harbor Laboratory Press, p Chapter 9
  240. Varki A (2017) Biological roles of glycans. *Glycobiology* 27:3–49
  241. Iqbal S, Fard MG, Everest-Dass A, et al (2018) Understanding cellular glycan surfaces in the central nervous system. *Biochem Soc Trans* 47:89–100
  242. Schnaar RL, Gerardy-Schahn R, Hildebrandt H (2014) Sialic acids in the brain: Gangliosides and polysialic acid in nervous system development, stability, disease, and regeneration. *Physiol Rev* 94:461–518
  243. Summerford C, Jude Samulski R AAVR: A Multi-Serotype Receptor for AAV. *YMTHE* 24:663–666
  244. Wang T, Wei JJ, Sabatini DM, Lander ES (2014) Genetic screens in human cells using the CRISPR-Cas9 system. *Science* (80- ) 343:80–84
  245. Shalem O, Sanjana NE, Hartenian E, et al (2014) Genome-scale CRISPR-Cas9 knockout screening in human cells. *Science* (80- ) 343:84–87
  246. Daniloski Z, Jordan TX, Wessels HH, et al (2021) Identification of Required Host Factors for SARS-CoV-2 Infection in Human Cells. *Cell* 184:92-105.e16
  247. Li B, Clohisey SM, Chia BS, et al (2020) Genome-wide CRISPR screen identifies host dependency factors for influenza A virus infection. *Nat Commun* 11:
  248. Li Y, Muffat J, Javed AO, et al (2019) Genome-wide CRISPR screen for Zika virus resistance in human neural cells. *Proc Natl Acad Sci U S A* 116:9527–9532
  249. Flint M, Chatterjee P, Lin DL, et al (2019) A genome-wide CRISPR screen identifies N-acetylglucosamine-1-phosphate transferase as a potential antiviral target for Ebola virus. *Nat Commun* 10:285
  250. Labeau A, Simon-Loriere E, Hafirassou M-L, et al (2020) A Genome-Wide CRISPR-Cas9 Screen Identifies the Dolichol-Phosphate Mannose Synthase Complex as a Host Dependency Factor for Dengue Virus Infection. *J Virol* 94:e01751-19
  251. Dudek AM, Zabaleta N, Zinn E, et al (2020) GPR108 Is a Highly Conserved AAV Entry Factor. *Mol Ther* 28:367–381
  252. Hill SA, Fu M, Garcia ADR (2021) Sonic hedgehog signaling in astrocytes. *Cell Mol Life Sci* 78:1393–1403
  253. Xiao BG, Lu CZ, Link H (2007) Cell biology and clinical promise of G-CSF: Immunomodulation and neuroprotection: Cellular Medicine. *J Cell Mol Med* 11:1272–1290
  254. Li L, McBride DW, Doycheva D, et al (2015) G-CSF attenuates neuroinflammation and stabilizes the blood-brain barrier via the PI3K/Akt/GSK-3 $\beta$  signaling pathway following neonatal hypoxia-ischemia in rats. *Exp Neurol* 272:135–144
  255. Okubo Y (2020) Astrocytic Ca<sup>2+</sup> signaling mediated by the endoplasmic reticulum in health and disease. *J. Pharmacol. Sci.* 144:83–88
  256. Romano R, Bucci C (2020) Role of EGFR in the Nervous System. *Cells* 9:1887

257. Mederos S, Perea G (2019) GABAergic-astrocyte signaling: A refinement of inhibitory brain networks. *Glia* 67:1842–1851
258. Hakim S, Bertucci MC, Conduit SE, et al (2012) Inositol polyphosphate phosphatases in human disease. *Curr Top Microbiol Immunol* 362:247–314
259. Zhong L, Zhao W, Wu J, et al (2007) A dual role of EGFR protein tyrosine kinase signaling in ubiquitination of AAV2 capsids and viral second-strand DNA synthesis. *Mol Ther* 15:1323–1330
260. Büning H, Srivastava A (2019) Capsid Modifications for Targeting and Improving the Efficacy of AAV Vectors. *Mol. Ther. - Methods Clin. Dev.* 12:248–265
261. Zhong L, Li B, Mah CS, et al (2008) Next generation of adeno-associated virus 2 vectors: Point mutations in tyrosines lead to high-efficiency transduction at lower doses. *Proc Natl Acad Sci U S A* 105:7827–7832
262. Zhang Y, Chen K, Sloan SA, et al (2014) An RNA-sequencing transcriptome and splicing database of glia, neurons, and vascular cells of the cerebral cortex. *J Neurosci* 34:11929–11947
263. Domenger C, Grimm D (2019) Next-generation AAV vectors-do not judge a virus (only) by its cover. *Hum. Mol. Genet.* 28:R3–R14
264. Ellert-Miklaszewska A, Poleszak K, Pasierbinska M, Kaminska B (2020) Integrin signaling in glioma pathogenesis: From biology to therapy. *Int J Mol Sci* 21:888
265. Schittenhelm J, Schwab EI, Sperveslage J, et al (2013) Longitudinal Expression Analysis of  $\alpha$ v Integrins in Human Gliomas Reveals Upregulation of Integrin  $\alpha$ v $\beta$ 3 as a Negative Prognostic Factor. *J Neuropathol Exp Neurol* 72:194–210
266. Malric L, Monferran S, Gilhodes J, et al (2017) Interest of integrins targeting in glioblastoma according to tumor heterogeneity and cancer stem cell paradigm: An update. *Oncotarget* 8:86947–86968

## 9 Acknowledgements

First and foremost, I want to thank my doctoral supervisor Ruth for giving me the opportunity to work in her research group and on this exciting research project. Under her supervision, I had the possibility to incorporate my own visions and ideas into the project but could always rely on her guidance and expertise to ensure the growth and development of our research.

A huge thank you goes to Johanna, who literally was my whole research group for the last 1.5 years. Thank you very much for your help in the lab, but beyond this, for all the laughter and silliness that helped me stay motivated. Of course, I also thank Alex, Vidya, and Van for being my lab-buddies, for great and fruitful discussions, but even more for all the joyful moments that made my doctoral time worthwhile. I also want to thank Christine whose work was the foundation of my project and who introduced me to the wondrous world of AAVs.

I also want to thank all the members of the Institute of Virology in Neuherberg, in particular Regina, Jutta, and Ute, for being the organizational backbone of everything.

Special thank goes to Prof. Dirk Grimm and his whole research group at the BioQuant (University of Heidelberg). Without this cooperation, this project would not have been possible. Particularly, I want to thank Ellen Wiedtke, who taught me in the high arts of AAV production and helped me when I struggled to live up to her standards.

I also would like to thank Dr. Bettina Kempkes, Dr. Benedikt Grothe, and Dr. Michelle Vincendeau for participating in my Thesis Advisory Committee and for their constructive comments and questions, which helped in progressing this project.

Thank you to Dr. Veit Hornung and Dennis Nagl, who shared their expertise and a substantial amount of practical help for the knockout generation. Thank you to Dr. Joel Anton Schick and Dr. Kamyar Hadian for their help with the experimental conduction and analysis of the CRISPR/Cas9 knockout screen. Thank you very much to Dr. Thomas Werner who performed the gene enrichment analysis of the screen sequencing data. Thank you to Dr. Elfriede Nössner and Dr. Thomas Hofer for their expertise and practical help with cell sorting and to Dr. Andreas Klingl, who contributed to this work by performing the electron microscopy analysis of the vector particles. Thank you to Prof. Horst Kessler for providing the  $\alpha\beta 8$ -ligand 2a for inhibition experiments.

An dieser Stelle möchte ich mich bei meinen Eltern und meinen Schwestern bedanken. Danke, dass ihr mich immer und bedingungslos unterstützt und ich in jeder Situation zu euch kommen kann. Euch stolz zu machen ist mein größter Antrieb.

And most importantly, I want to thank Dennis, who has carried me in my whole academic and personal way until this very moment. Your support, confidence, and patience were essential for me to reach this milestone. Thank you for being my biggest supporter; I am so grateful to have you in my life.

## 10 Publications

### Poster presentations and conference talks

- 03/2021                    30<sup>th</sup> Annual Meeting of the Society of Virology (oral presentation)  
Titel: Profiling cell surface molecules for gene delivery to astrocytes by the AAV  
vector AAV9P1
- 02/2020                    <interact< 2020 (poster)  
Titel: Characterization of the transduction behavior of a novel Adeno-  
associated virus vector variant AAV9P1

### Paper

**Bauer A.**, Brack-Werner R. (in press). „Modelling HIV latency in astrocytes with the human neural progenitor cell line HNSC.100.“ In: Poli G., Romerio F., Vincenzi E. (eds) HIV reservoirs: Modelling, Quantification and Approaches to a Cure. Methods in Molecular Biology.

Herrmann A., Roesner M., Werner T., Hauck SM., Koch A., **Bauer A.**, Schneider M, Brack-Werner R. (2020). “Potent inhibition of HIV replication in primary human cells by novel synthetic polyketides inspired by Aureothin.” Scientific Reports. Volume 10. Issue 1.

Kunze C., Hermann A., **Bauer A.**, Brack-Werner R. (2018). “Gibt es Strategien gegen die latente Infektion?” MMW – Fortschritte der Medizin. Volume 160. Issue Suppl 2.

## 11 Eidesstattliche Erklärung

Ich versichere hiermit an Eides statt, dass die vorgelegte Dissertation von mir selbständig und ohne unerlaubte Hilfe angefertigt ist.

München, den ..... 12.01.2022 ..... Amelie Bauer .....  
(Unterschrift)

### Erklärung

Hiermit erkläre ich,

dass die Dissertation nicht ganz oder in wesentlichen Teilen einer anderen Prüfungskommission vorgelegt worden ist.

dass ich mich anderweitig einer Doktorprüfung ohne Erfolg **nicht** unterzogen habe.

München, den..... 12.01.2022 ..... Amelie Bauer .....  
(Unterschrift)